Structural Insights Obtained for Homodimeric Full-length LRRK2/LRRK1 Protein Complexes and Liposomal Preparation as a tool to Study Membrane Proteins under Buffer Gradients by Cryo-EM

Inauguraldissertation

zur

Erlangung der Würde eines Doktors der Philosophie

vorgelegt der

Philosophisch-Naturwissenschaftlichen Fakultät

der Universität Basel

von

Kushal Sejwal

aus Neu Delhi, Indien

Basel, Schweiz, 2017

Genehmigt von der Philosophisch-Naturwissenschaftlichen Fakultät

der Universität Basel

auf Antrag von

Prof. Dr. Henning Stahlberg (Biozentrum, Universität Basel),
Fakultätsverantwortlicher

Prof. Dr. Timm Maier (Biozentrum, Universität Basel), Koreferent

Basel, 21.06.2016

Prof. Dr. Jörg Schibler
Dekan der PhilosophischNaturwissenschaftlichen
Fakultät

Acknowledgements

With a deep sense of gratitude, I wish to express my sincere thanks to my supervisor Henning Stahlberg, for his meticulous guidance and encouragement throughout my Ph.D. He helped me to think independently, develop ideas and to apply scientific attitude towards solving a problem.

I would like to convey special thanks to my co-supervisors Timm Maier and Marek Basler for supporting me with scientific advice and feedback at different levels of my research. Also, Jan Pieter Abrahams for kindly chairing the PhD Defense committee.

Also, I am thankful to Jean-Marc Taymans for collaborating with our lab and giving me the opportunity to work in their projects. It has been a very fruitful collaboration and I have learnt a lot from all our discussions and interactions.

My PhD wouldn't have been possible without Mohamed Chami for his unconditional support, training and encouragement. I would like to give special thanks to all the CINA's past and present lab members for being kind and helpful. They provided a very lively environment to work.

The acknowledgment cannot be complete without thanking my loving wife Prerna, who has been my pillar of support from the very first day, also my mother and in-laws who showered upon me their constant blessings. I would like to share this moment of happiness with my beloved sister Pritika. She rendered me enormous support during the whole tenure of my PhD. Above all, I thank the Almighty for His divine grace.

Contents

List of Figures

List of Tables

Dedicated to my late father, who unfortunately didn't stay in this world long enough to see his son finish his doctorate ...

Chapter 1

Abstract

Parkinson's (PD) is one the most common neurodegenerative movement disorder. The complex etiology of the disease makes treatment difficult and although the past decades of research have substantially increased our understanding of the disease, a completely cure is still missing. Originally considered a sporadic disease, extensive genome wide studies of PD patients has identified various genes which are now linked to PD. Out of all the genes, the most prevalent is the leucine rich repeat kinase 2 (LRRK2). Mutations in LRRK2 are now believed to cause the most common familial forms, and some sporadic forms, of Parkinson's. LRRK2 gene encodes for a large multidomain protein complex LRRK2. Structurally LRRK2 is characterized by an unique modular architecture which contains a GTPase and a kinase domain in the same complex and further surrounded by several protein-protein interaction domains. Most of the pathologically important LRRK2 mutations are clustered in the catalytic core of the protein, hinting that altered GTPase and kinase activities play a crucial role in pathogenesis. There is a need to unravel the structural mechanism that drive and modulate LRRK2 GTPase and kinase activities for a better understanding of the disease mechanism and developing advanced therapeutic strategies.

Another related but less scrutinized protein is LRRK1, the closest paralogue of LRRK2. The domain organization of LRRK1 is very similar to LRRK2 and the expression profile and cellular organization of both the proteins are also overlapping. However, irrespective of these similarities, mutations in LRRK1 have not been genetically associated with PD. This difference has stimulated various studies to understand the functional roles of LRRK2 and LRRK1 and the link between the two. Structural and functional studies on LRRK1 are not yet fully explored as LRRK2.

So far, it has been a challenge to isolate a sufficient quantity of intact, full-length LRRK2 and LRRK1 protein for structure determination. The available structural insights for

LRRK2 come indirectly from the study of related proteins from the same family in lower organisms. Crystal structures for the human LRRK2 ROC domain and bacterial ROC-COR and kinase domain have been published so far. Although, these structures have advanced our understanding of LRRK2 functions but are insufficient to fully address their physiological relevance. Similarly, structural information about LRRK1 is minimal with no 3D structures reported, neither of full-length protein nor of any of its domains. In addition to continued effort to solve atomic models of individual catalytic domains of LRRK2 and LRRK1 by X-ray crystallography, there is a need to elucidate structure of full-length protein complex to delve deeper into the molecular functioning of the whole protein, given that fact that surrounding the catalytic core, LRRK2 and LRRK1 has a number of protein-interaction domains which impart high degree of conformational flexibility in order to accommodate different substrate to carry out the diverse functions.

The goal of this thesis is to solve the three dimensional structures of the homodimeric complexes formed by full-length LRRK2 and LRRK1, respectively, analyzed by cryo-electron microscopy (cryo-EM) imaging and computational single particle image analysis. This will enable for the first time to unveil the tertiary structure of the protein complex. To realise the aim, the primary goal was to standardise the expression and purification of full length LRRK2 and LRRK1 to produce adequate quantity and quality of proteins for structural determination. Constructs for the mammalian expression of 3xflag tagged LRRK2 and 3flag tagged LRRK1 were expressed in human embryonic kidney (HEK) 293 cells and subsequently used for affinity purification. Further, extensive optimization of the purified protein for cryo-EM sample preparation was carried out with the final aim to prepare homogenous sample for data collection by cryo-EM. Chapter 3 includes the methods used for the expression and purification of LRRK2, sample optimization for cryo-EM, data collection and single particle image processing. Chapter 2 gives a general introduction to Parkinson's, its various aspects and the role of LRRK2 in Parkinson's disease, followed by an introduction to LRRK2 and LRRK1.

In a second project, a novel method development is proposed to use liposomes as a tool to study membrane proteins under buffer gradients by cryo-EM. Methods are described on how to embed membrane proteins, such as voltage-gated potassium channels, into lipid vesicles (liposomes), while altering the buffer conditions inside and the outside of the buffer differently. This allows setting up a gradient such as pH, salt, ligands or membrane potential across the liposome bilayer membrane. Chapter 4, describes these methods to prepare liposomes, establish gradient, verify the presence of different buffers inside and outside of the liposomes. The goal of the project is the provide a proof of concept for the methods to be suitable for vitrification and image collection by cryo-EM. By optimising different lipid of protein ratios, well ordered 2D crystalline liposomes reconstituted with membrane protein were generated. These proteoliposomes can be processed by using

a combination of electron crystallography and single particle processing routines. Alternatively, for larger membrane proteins, tomography and subtomogram averaging can also be utilised. Chapter 2 covers an introduction to electron microscopy, cryo-EM and image processing, which is the common methodological tool used in both the projects.

Chapter 2

Introduction

2.1 Parkinson's Disease

The history of Parkinson's disease to be documented in literature dates back to 1817, when British physician, James Parkinson (1755-1824) first described about this deadly disease in his landmark article An Essay on the Shaking Palsy(Donaldson 2015). Later, it was French neurologist Jean Martin Charcot (1825-1893), who made further contribution to the understanding of the disease and named it after James Parkinson as an honor. Today nearly 200 years later, we know Parkinson's' disease as a progressive and chronic neurodegenerative disorder of the central nervous system (CNS) that affects control of voluntary movement. It is one the leading neurodegenerative disorders, second to Alzheimer disease and affects nearly ∼1% of the population over 55 years of age and 10% for those over 80 years of age. Of all these cases, nearly 90% are sporadic, where there is no known cause, while 10% are genetically linked either in an autosomal recessive or autosomal dominant manner(Dauer and Przedborski 2003). PD is prevalent all over the globe; however, the occurrence of disease is slightly lower in women than in men(Shulman 2007). According to the statistics in Europe, the estimated prevalence and incidence rates of Parkinson‘s Disease was approximately 108 to 257/100,000 and 11 to 19/100,000 per year, respectively. Though a lot of progress is made in understanding the neurobiology of PD, the diagnosis of PD still remains a major challenge. There are treatments available to lessen the symptoms but at present PD is incurable.

2.1.1 Symptoms of Parkinson's disease

The symptoms of Parkinson's disease can be broadly divided into two types: motor symptoms and non-motor symptoms. The fundamental motor symptoms in PD are

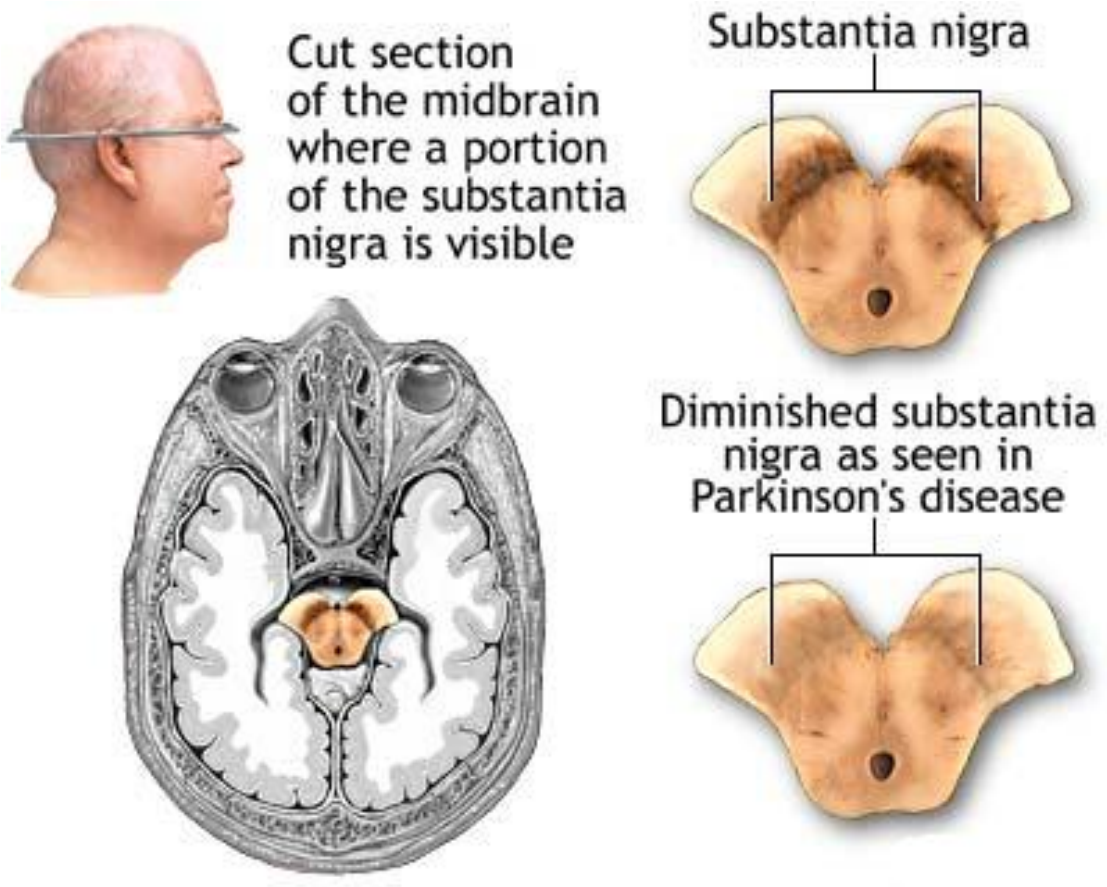

FIGURE 2.1: Loss in Substantia Nigra. (Image source: A.D.A.M Inc, 2011)

rigidity, bradykinesia and postural instability. Regardless of the etiology, they are all caused by the loss of dopaminergic neurons in the substantia nigra (Figure 2.1). The most evident of the motor symptom in PD is tremor, which has a characteristic appearance in PD patients. It is one of the most common symptoms found in 70% of the PD patients. The tremor starts with the hands, with a back and forth motion of the thumb and the forefingers(Jankovic 2008). The second most common symptom in PD patients is Rigidity, which results from the stiffness and lack of movement in a body part such as ankles, hips, knee, shoulders and neck. Bradykinesia denotes slowness in movement or in some patients can also turn into akinesia that means complete absence of movement. This is also a common symptom and a characteristic clinical feature of PD. Over time patients lose the ability to execute rapid, multi-step movements. The last common motor symptom of PD is postural instability that occurs due to the loss of postural reflexes. The patients suffer from impaired balances, unsteady posture and frequent falls(Dauer and Przedborski 2003). Apart from these major symptoms, other motor dysfunctions are also common in PD. These include feet shuffling, reduced arm swing, and abnormal forward-flexed posture. Abnormal muscle contractions are also common in PD patients that can cause severe fatigue and reported in estimated 50%

of patients. Speech disorder are also routinely observed and characterised by facial laryngeal bradykinesia and rigidity which causes difficulty in finding words(Matison et al. 1982; Critchley 1981). Complications related to respiratory abnormalities are also seen in PD patients(Biousse et al. 2004). In addition to motor symptoms, usually in the later stages of the disease, PD patients suffer from a variety of non-motor symptoms. These non-motor symptoms are predominantly a result of the loss of non-dopaminergic neurons. These include problems with sleep cycles, cognition abilities and behaviour. These symptoms affect the quality of life of the PD patients and are most troublesome(Hely et al. 2005). Among these the most prevalent non-motor symptom is sleep disturbance, which occurs in nearly all PD patients(Jahan et al. 2009). Sleep disturbances include other related symptoms like insomnia, rapid eye movement, sleep deprivation, sleep apnea and parasomnias. It has been suggested, sleep disorders in patients could hint to be a precursor of early onset PD(Schenck et al. 1996; Plazzi et al. 1997). Cognition disabilities and neuropsychiatric disorders like depression and anxiety are also common PD symptoms(Aarsland et al. 2007). There is a propensity of a quarter of all PD patients progressing to dementia in the advance stages of the disease, which involves slowing of thoughts and memory difficulty and behavioral regulation. Delusions, paranoia and hallucinations may also develop in severe PD cases(Frank 2005);(Frank 2005; Levin and Katzen 2005). Mental disorders, anxiety and mood disorders are also linked to PD. These have been related to a affected dopamine metabolism(Leentjens 2004; Nuti et al. 2004).

2.1.2 Etiology

Etiology is a branch of medical science concerned with the causes and origins of a disease. Parkinson's disease is a very complex disease and its etiology is still unclear. Most PD patients have idiopathic Parkinson's disease i.e. having no specific known cause for the disease. However, recently many cases have been attributed to have genetic factors involved. There are other risk factors such as age, environmental toxins and pesticides that have been linked with the risk of developing PD.

2.1.2.1 Aging

Age is the major risk factor for PD. Aging can cause irreversible damage to the cells, weaken repairing capacity of the cells and predispose people to neurodegenerative diseases(Hindle 2010). Within a population, the percentage of affected individuals rises from 1% (65 years of age) to 5% (85 years of age). Though, there is not a clear known reason for a gender factor involved in the PD but the occurrence of PD patients in males

is slightly more than the females. One study suggested the protection of dopaminergic neurons by female hormone estrogen(Shulman 2007). Geographic distribution too does not play a big role in PD, although PD cases in Hispanic and non-Hispanic American people is slightly higher than in African Americans and Asians(Van Den Eeden et al. 2003). The age also plays a role at onset of PD, which has a wide distribution. Although, the mean age at onset is 55 years, disease onset can also occur at what is termed as a juvenile onset which happen before 21 years of age; or an early onset occurring between 21 and 50 years of age; or lastly as late onset which is beyond 50 years(Dauer and Przedborski 2003).

2.1.2.2 Environment

Environmental factors have been for decades thought to be the most prominent cause of PD. Several years of research have identified specific environment agents like neurotoxins and viruses responsible for PD. In the early 1980's, one such environmental agent was discovered, methyl-4-phenyl-1,2,3,6- tetrahydropyridine or MPTP for short. MPTP is a prodrug to the neurotoxin MPP+, which have been known to cause permanent symptoms of PD. While MPTP itself has no psychoactive effects, the compound may be accidentally produced during the 1-methyl-4-phenyl-4- propionoxypiperidine (MPPP) synthesis. MPPP is a synthetic opioid drug with effects similar to those of morphine and pethidine(Langston et al. 1983). MPTP has been demonstrated for the toxicity of dopaminergic neurons in mouse models that further confirmed its specific toxicity to PD(Teismann and Ferger 2001). MPTP has been since actively used to study disease models in various animal studies.

Another chemical that has been linked to induce a toxic model in PD is Rotenone. Rotenone is a widely used insecticide and fish poison which is highly lipophilic and readily gains access to all organs(Talpade et al. 2000). Like MPP+, Rotenone can bind to the same site of mitochondrial complex I and can inhibit the electron transport chain(Betarbet et al. 2000). Other heavy metals and industrial toxins have also been examined for their role as a potential environmental causes of PD but no causal link has been identified. In addition to chemical environmental factors linked to PD as inducing agents, viruses have also been identified to cause PD. In 1918 influenza outbreak caused post-encephalitis PD in a large population. A recent study reported that certain strains of H5N1 avian flu virus infection can cause higher susceptibility to PD(Jang et al. 2009).

2.1.2.3 Genetics

A lot of early research on PD identified these environmental factors associated and helped cracking the mystery of the disease Etiology, however, recent research interests have now been shifted to the genetics factors involved in PD. The shift is a result of improvements in the molecular and genetic research technologies in recent decades. Today, it is estimated that 5-15% of all PD cases have a genetic component involved, showing both autosomal recessive and dominant modes of inheritance. If the age of disease onset, family history of PD and special ethnic origin are considered as well, then the percentage can go as high as 75%(Klein and Schlossmacher 2006; Lcking et al. 2000). Several studies have repeatedly given evidence to support that genetics risk factors play an important role in PD. For instance, after age; as the first predictor for high risk of PD, family history of PD is the second best predictor(Semchuk et al. 1993). These reports which study the family history of PD patients reveals that for idiopathic PD patients, it is very likely they will have a positive family history and there are double chances for the individuals to develop the disease that have a first degree relative with PD(Marder et al. 1996; Lazzarini et al. 1994). More insights on the genetic link between PD patients comes from the large cross-sectional twin studies, which have identified major differences in concordance rates between the monozygotic twins and the dizygotic twins in early onset PD but absent in late onset PD(Wirdefeldt et al. 2004). These studies has shed more light on the genetic risk factors involved in PD but they been proven incapable to detect the incomplete penetrant mutations(Simon et al. 2002). Results from another longitudinal study that used 18F-dopa positron emission tomography (PET) to study dopaminergic functions in twins found 75% disease concordance to occur in monozygotic twins, while for dizygotic twins, it was 22%, regardless of age at onset(Piccini et al. 1999). Together, these data suggests that the genetics susceptibility in PD is much greater than previously anticipated. These genetic contributions might not be detected straightway because sometime patients do not have clear family history or the mutated gene has low penetration. Other factors like environment exposure and genetic predisposition can also play a role.

2.1.3 Pathology

There are two pathological conditions in PD that are considered hallmark. First is the loss of nigrostriatal dopaminergic neurons in the midbrain and the second is the formation of intraneuronal cytoplasmic inclusions in the remaining dopaminergic neurons located in substantia nigra pars compacta (SNpc), these are termed as Lewy bodies (Figure 2.2)(Dauer and Przedborski 2003). There are four major dopamine pathways

located in the brain, nigrostriatal pathway is one of them and is primarily involved in the control and production of voluntary response. This pathway comprises of dopaminergic neurons and their cell bodies are located in SNpc region of the brain. The SNpc contains large amount of a substance called neuromelanin, which gives the region its characteristic pigmented appearance. Macroscopic alterations can be noticed on cut surfaces of the brainstem, where neuronal loss can be inferred from a depigmentation in the SNpc. At the start of the disease symptoms, around 60% of the dopaminergic neurons in the SNpc region have already started degenerating(Marsden 1983). Frederic Lewy (1885-1950) was the first neurologist to observe Lewy bodies in 1912. Lewy bodies are considered characteristic indicator of PD but they are also well known pathological features in other neurological disease such as dementia with Lewy bodies (DLB), Hallervorden-Spatz syndrome, Alzheimer's disease and Down's syndrome(Neumann et al. 2000; Giasson et al. 2000; Spillantini et al. 1998). Even in 10-15 % of patients over the age of 65, dying without any clinical or pathological neurological illness, Lewy bodies are found in the autopsy of neurons of the SNpc(Gibb and Lees 1988; Braak et al. 2003).

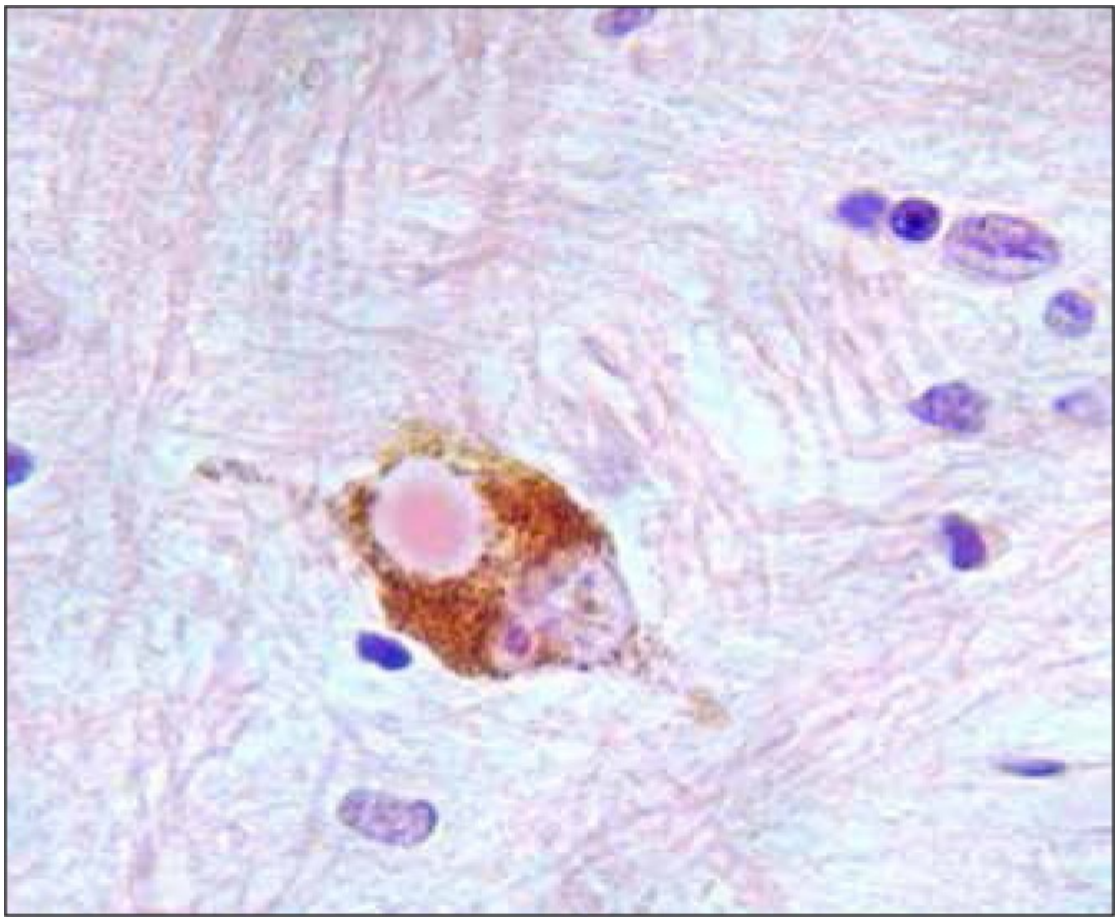

FIGURE 2.2: A single Lewy Body present in a pigmented neuron from the substantia nigra Cunningham et al., 2015)

Lewy bodies are spherical, intraneuronal masses containing a variety of proteins including α-synuclein, synphilin-1, ubiquitin proteasome system (UPS), heat shock proteins and tau proteins(Ishizawa et al. 2003; Olanow et al. 2004). Lewy bodies have been divided into two morphological types: classical (brainstem) Lewy bodies and cortical Lewy bodies.

Classical Lewy bodies are primarily composed of α-synuclein and are characterised by 10um wide dense core which is surrounded by a halo looking appearance. While, cortical Lewy bodies have a more homogenous appearance without having a distinctive core and halo around them(Forno 1996). The formation of Lewy bodies is still unclear, though there are several hypotheses to explain the mechanism. Recent findings suggest Lewy bodies are related to aggresomes and functions as a cellular scrapyard of degraded ubiquitinated proteins in response of proteolytic stress. It is still not fully understood whether Lewy bodies have a detrimental role in causing neuronal death or are simply a byproduct of neurodegeneration.

Braak's staging system was recently created by Braak and colleagues. They created a neuropathological staging procedure that allows differentiating between initial, intermediate, and final stages of PD-related lesions. The early changes are defined in the Braak stage 1 and Braak stage 2 and they are generally pre-symptomatic, seen mostly in medulla oblongata and olfactory bulb. In Braak stages 3 and 4, cell death and inclusion formation begins and protein aggregation is noticed in areas of the midbrain and basal forebrain. The final stages 5 and 6 are characterized by progressive neurodegeneration in the cerebral cortex and in the other affected regions of the brain(Davie 2008; Braak et al. 2006). Among all the Braak's stages, the manifestation of clinical features of PD occurs during stage 3. In PD patients, the percentage of dopamine depletion in putamen region is 80%, while the neuronal loss in substantia nigra pars compacta at disease onset is 60%(Lang and Lozano 1998). This loss of neurons is responsible for the depigmentation in substantia nigra pars compacta, which is the classic neuropathological hallmark in PD(Marsden 1983). The depletion of dopaminergic neurons within the caudate and SNpc neighbouring projection sites are comparatively less(Uhl et al. 1985; Price et al. 1978). Parkinsonism is a term used very often in PD pathology to denote the broader other PD like neurological disorders like dementia with Lewy bodies (DLB), progressive supranuclear palsy (PSP) and multiple system atrophy (MSA). These account for more than 80% of cases and share similar clinical symptoms of PD but not necessarily the neuropathological features of PD.

2.1.4 Diagnosis

Diagnosis of Parkinson's disease is often very difficult. The symptoms of PD overlap with symptoms of other neurological disorders, especially at the early stages. This makes PD difficult to diagnose and physicians are required to have broad experience in neurological disorders. Early detection of PD is very difficult and most of the times early signs and symptoms of the disease are dismissed as the normal effects of aging or other disease conditions. It is estimated that around 40% of patients may not be diagnosed for PD at all and a quarter of patients are often misdiagnosed.(Gelb et al. 1999). At present, there are no laboratory tests that could be used to diagnose PD, so the only diagnosis possible is typically based on the medical history, interviews, counseling and neurological examination of the patients together with regular laboratory tests like electroencephalogram (EEG), computed tomography (CT), magnetic resonance imaging (MRI) and blood tests. These techniques are not used to directly diagnose PD but more useful to rule out other diseases that can be secondary causes of parkinsonism, such as vascular pathology, basal ganglia tumors, and hydrocephalus(Brooks 2010). There are two common clinical tools that are used in the diagnosis of PD and determine its severity: the Hoehn and Yahr Scale and the Unified Parkinson's Disease Rating Scale (UPDRS)(Goetz 2006). During these diagnoses and assessment physicians enquire about characteristic symptoms of PD such as resting tremor, rigidity, bradykinesia and postural instability. The presence of at least two of these motor symptoms confirms the diagnosis of PD. The patient undergoing the examination is also asked to perform a series of behavior test, including walking around and sitting down to confirm diagnosis. Though these test help in the timely detection of the disease, they are often considered not very definitive.

2.1.5 Treatment

There is currently no cure for PD. The medication and treatments available only help to relieve the symptoms and improve the quality of life of PD patients. There has been considerable progress in understanding the etiology, pathogenesis, and pathology of PD which have resulted in the development of numerous treatments for this chronic disorder. Current treatment practices, however, only target the dopaminergic features of the disease to alleviate motor symptoms which prevents these treatments to be proven fully satisfactory. There is yet an absence of any therapeutics that either slow progression or completely stop the neurodegeneration in PD patients.

The most common medication practice in PD is to counteract the depletion of dopamine, therefore most medications function by increasing the dopamine supply in brain. There

are different kinds of drugs known that increase the level of dopamine in the brain, these include: Levodopa (L-dopa), Catechol O-methyltransferase (COMT) inhibitors, MAO-B inhibitors and dopamine agonists. Out of these Levodopa remains the most commonly used drug in PD treatment. Levodopa is a dopamine precursor that was first introduced in 1950s. In contrast to dopamine, Levodopa can cross the blood brain barrier easily and then converted into dopamine by the amino acid decarboxylase (AADC) enzyme also known as dopa- decarboxylase (Figure 2.3). However only a small fraction of levodopa enters dopaminergic neurons, while most of the remaining drug is metabolized to dopamine in the peripheral nervous system. This can cause a wide variety of side effects in PD patients. To curb the unwanted side effects of Levodopa in the peripheral nervous system, it is supplemented with a peripheral dopa-decarboxylase inhibitor (DDCI)(Radad et al. 2005). Another class of drugs that are usually co-administered with Levodopa are Catechol O-methyltransferase (COMT) inhibitors (e.g., entacapone and tolcapone) which functions by blocking the breakdown of Levodopa. The efficacy to these PD medications can be dramatically positive in the early stages of treatment. However, the response of medications starts fading with the progress of disease and eventually patients lose the responsiveness to the medication. So, both DDC and COMT inhibitors aids in increasing the amount of levodopa that brain receives. Once in the brain, there is another problem, the dopamine that is being generated by conversion of Levodopa can further be metabolized and broken down into other compounds. Here, monoamine oxidase-B (MAO-B) inhibitors (e.g., selegiline and rasagiline) comes to rescue and prevents the formation of these inactive dopamine metabolites and hence improving motor function in PD patients. They do this by inhibiting the enzyme MOA-B that catalyse the breakdown of Dopamine. Another class of drugs used in PD treatments is agonists of Dopamine like pramipexole (Mirapex) and ropinirole (Requip), these are capable of mimicking the effect of dopamine on neurons. But these drugs are only used temporarily as they are capable of desensitizing dopamine receptors and can cause long-term problems in patients if taken routinely(Koller and Rueda 1998). Apart from these major drugs for PD treatment, several naturally occurring products are known to be beneficial in reducing PD symptoms. Natural anti-oxidants like vitamin E, vitamin C, Coenzyme Q10 and NADH have been used with some degree of relief in PD patients. Apart from these drugs, which are targeted towards motor symptoms, there are other pharmacological strategies that can be used to treat non-motor symptoms of PD. These include the usage of tricyclics and selective serotonin reuptake inhibitors (SSRIs) to treat depressions that is common in PD patients(Lieberman 2006). Clozapine is routinely known to significantly improve psychosis in patients when used in low doses(Pollak et al. 2004). To treat other non-motor symptoms in PD patients like sleep imbalance, speech problem etc. non-pharmacological strategies and counseling is employed(Freedom 2007). Occupational, speech therapies are often known to improve the overall quality of life for PD

patients(Boelen 2007).

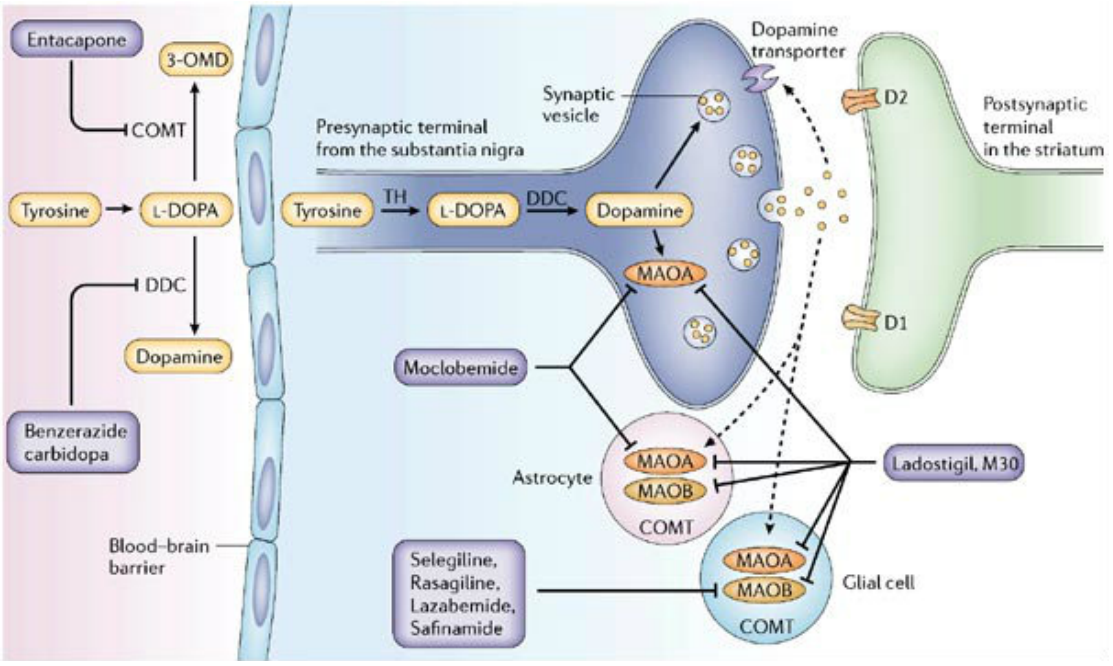

FIGURE 2.3: Dopamine biosynthesis and its regulation by various drugs. (Youdim et al., 2006)

When drugs are not able to control the symptoms or produce harmful side effects in PD patients, surgical treatments are considered. Though surgery is not a cure to treat PD, it can often help in relieving pain and PD symptoms. Of all the known PD related surgeries, the most commonly performed is deep brain stimulation (DBS). DBS uses electrical impulses to stimulate targeted areas in the brain such as subthalamic nucleus (STN) and the globus pallidus interna (GPi)(Plaha et al. 2006; Benabid et al. 2009). In this way, the tissues are not physically destroyed and still inactivated to reduce the PD symptoms. In DBS, patients are implanted with a impulse generator which is connected by wires to the target brain region via electrodes. Once activated, these electrodes can inactivate the tissues by using continuous electrical pulses.(Kern and Kumar 2007; Hammerstad and Hogarth 2001). Owing to these advantages, DBS is the most preferred surgical method used in PD but there are still few side effects that are associated with DBS. These include cognitive disability, hallucination, bleeding in the brain, depression etc.. Nevertheless, DBS has proved to be an effective treatment and helped more than 70% of PD patients to a reduce medications and significantly improved their motor symptoms.

Other surgical methods that are used in PD treatments in early days and not used very often now a day, are both focused on removing the areas in brain which are thought to be involved in PD symptoms. These two areas of brain are globus pallidus and thalamus and the surgeries performed to remove part of these two brain areas are pallidotomy and

thalamotomy, respectively. Globus pallidus is the part of the brain that is believed to become overactive in PD patients and serves to slow body movement, while thalamus is thought to be responsible for the abnormal brain activity that causes tremors(Kern and Kumar 2007; Hammerstad and Hogarth 2001).

Another area of PD treatment that has been very recently proposed and still under active development is gene therapy. The general idea of gene therapy is to create and transplant specialised cells that are capable of producing dopamine in the PD patients. So far the approach is to use adeno-associated viral vector serotype 2 (AAV2) as a vector platform to transfer the genes coding for enzymes such as aromatic L-amino acid decarboxylase (AADC). This therapy can restore the normal levels of AADC in the striatum thereby catalysing more conversion of levodopa to dopamine and reducing levodopa induced dyskinesia in PD patients(Forsayeth et al. 2010). The proposed plans are still in early stages of pharmaceutical trials and viral gene delivery is still not FDA approved due to the overlying safety concerns. Therefore it's a long way for gene therapy to be used widely in PD treatments.

2.1.6 Genes associated with PD

Traditionally, PD has been considered a sporadic disease. However, according to the statistics, around 15% of individuals suffering with PD are reported to have a first-degree relative who already has the disease(Samii et al. 2004). Over the past two decades, advancement in the genetic and molecular techniques has revealed startling genetic link to PD. It is now estimated at least 5% -15% of all known PD cases are caused due to a mutation in one of several specific genes which are transmitted in either an autosomal-dominant or autosomal-recessive pattern(Funayama et al. 2002; Lesage and Brice 2009). Extensive genome wide studies have identified 11 regions of human genome that are linked to PD. Large scale gene mapping of PD affected families have further extended our understanding and identified seven major genes which are responsible for PD. These genes are: SNCA, UCH-L1, MAPT, PRKN, DJ1, PINK1 and LRRK2. Out of these, α-synuclein (SNCA) was the very first to be associated with the autosomal dominant form of PD(Krger et al. 1998; Au and Calne 2005; Polymeropoulos et al. 1997). α-synuclein is a 140 amino acids protein that is primarily found in the human neuronal tissues and also forms the major constituents of Lewy bodies. The α-synuclein gene was the very first gene to be discovered as a causative factor for PD, later it was reported that the occurrence of this gene mutation is very rare(Farrer et al. 1998). Higher levels of α-synuclein due to the genomic multiplication of α-synuclein gene are also believed to be linked to familial PD and there has been studies that show a direct relationship between the gene multiplication and disease onset age, progression and

phenotypic severity(Mueller et al. 2005). The exact role of the α-synuclein mutations in PD and their biochemical mechanism is still not clear. It is generally believed that the aberrant dopamine metabolism, protein degradation dysfunction and ER stress are implications in the pathogenesis of PD linked with α-synuclein mutations(Corti et al. 2005).

TABLE 2.1: List of all known genes, loci and proteins associated with Parkinson's disease.

Locus	**Gene**	**Protein**	**Model**
Park1	SNCA	α-synuclein	Autosomal dominant
Park2	PARK2	Parkin	Autosomal recessive
Park3	Unknown	Unknown	Autosomal dominant
Park4	SNCA	α-synuclein	Autosomal dominant
Park5	UCHL1	Ubiquitin c terminal hydrolase	Autosomal dominant
Park6	PINK1	Pten-induced putative kinase 1	Autosomal recessive
Park7	PARK7	DJ-1	Autosomal recessive
Park8	LRRK2	Leucine-rich repeat kinase 2	Autosomal dominant
Park9	ATP13A2	Lysosomal type 5 ATPase	Autosomal recessive
Park10	Unknown	Unknown	Risk locus
Park11	GIGYF2	GRB interacting GYF protein 2	Autosomal dominant
Park12	Unknown	Unknown	X-linked
Park13	HTRA2	HTRA serine peptidase 2	Autosomal dominant
Park14	PLA2G6	Phospholipase A2	Autosomal recessive
Park15	FBXO7	F-box only protein 7	Autosomal recessive
Park17	VPS35	Vacuolar protein sorting 35	Autosomal dominant
Park18	EIF4G1	Eukaryotic translation initiation factor 4 gamma 1	Autosomal dominant
Park19	DNAJC16	DNAJ/HSP40 homolog subfamily C member 6	Autosomal recessive
-	SNCA	α-synuclein	Risk locus
-	LRRK2	Leucine-rich repeat kinase 2	Risk locus
-	GBA	Glucocerebrocidase	Risk locus

Ubiquitin carboxy-terminal hydrolase L1 (UCH-L1) is another gene that has been linked with PD. It was identified as a single missense mutation (Ile93Met) in a sibling pair with autosomal-dominant PD(Leroy et al. 1998). Later, another polymorphism S18Y was identified in the UCH-L1 gene which was also associated as a PD risk factor mutation(Elbaz et al. 2003). UCH-L1 is highly abundant protein, which is specific to neurons and also found in Lewy bodies of sporadic PD patients and is also known to promote accumulation of α-synuclein(Lowe et al. 1990). This is the reason anti-UCH-L1 antibodies are widely used in staining of Lewy bodies. This protein belongs to the family of deubiquitinating enzymes and functions in the hydrolysis of long ubiquitin polymers(Wilkinson et al. 1989; Rodriguez-Viciana et al. 1997).

Mutations in the parkin gene have been identified as one of the most common cause of early-onset parkinsonism and were reported for the first time in several Japanese families with autosomal recessive juvenile parkinsonism(Kitada et al. 1998). Since then, a number of other mutations have been reported for this gene. It is the second largest

gene known and encodes for the parkin protein on chromosome 6q34. It is a component of the large E3 ubiquitin ligase and responsible for transferring activated ubiquitin molecules to substrate targeted for UPS mediated protein degradation(Schlossmacher and Shimura 2005). Loss of function in parkin is a major cause of early onset PD and many parkin mutations have been reported, which affect the wild type parkin cellular localization, disruption of mitochondrial integrity and cellular homeostasis(Wang et al. 2005; Cookson et al. 2003; Narendra et al. 2008).

Mutations in the DJ-1 gene were identified in 2003 in two families with autosomal recessive PD in the early onset stage(Bonifati et al. 2003). Pathogenic mutations in DJ-1 are rare and known early-onset PD cases are less than 1 percent(Abou-Sleiman et al. 2003). The protein expression is mostly localized in neuronal and glial cells in the brain. Though the precise function of the protein remains elusive, it has been postulated to play a role in oxidative stress response and have also been linked with the mitochondrial impairment(Bandopadhyay et al. 2004).

In a study of three families with early onset autosomal recessive PD, mutations in the PINK1 gene were identified which, were previously linked with the PARK6 locus(Valente et al. 2004). PINK1 is a mitochondrial serine/threonine-protein kinase. Not a lot is known about the protein's cellular functions, but it has been suggested to play a protective role during stress induced mitochondrial dysfunction(Gandhi et al. 2006; Silvestri et al. 2005). There have been few mutations identified for this protein which show impaired protein folding and kinase activity(Beilina et al. 2005). Similar to Parkin, for PNK1 as well, loss of function mutations are believed to be a cause of early onset PD and suggested that PINK1 may act upstream of Parkin in common pathological pathways(Wang et al. 2011).

Another gene that has been linked with PD is the microtubule associated protein tau (MAPT). Protein aggregation resulting from the neurofibrillary tangles consisting mainly of tau proteins has been known to occur in PD. There may be occasional aggregation of α-synuclein as well. MATP mutations have been reported in frontotemporal dementia with Parkinsonism linked to chromosome 17 (FTDP-17) and also in atypical PD without Lewy body formation. LRRK2 is the most recently identified gene for PD and the next section describes it in detail.

2.2 LRRK2

2.2.1 Introduction

In 2004, a locus located on the chromosome 12q12 was linked to autosomal dominant PD in a large Japanese family, the Sagamihara. The identified locus is termed as PARK8 and was further confirmed to be linked with PD by genomic studies of other families belonging to diverse nations like United States, China and European countries(Funayama et al. 2005; Paisan-Ruiz et al. 2005; Shen 2004; Zimprich et al. 2004). The gene that is associated with PARK8 and linked with parkinsonism was identified as LRRK2(Paisan-Ruiz et al. 2004). LRRK2 is also known by another name, dardarin, which comes from dardara (meaning tremor in Basque language). LRRK2 gene comprises of a total of 144 kilobases containing 51 exons. Mutations in the LRRK2 gene have since the time of its discovery proven to be the most common cause of familial PD(Satake et al. 2009). The protein encoded by the gene is also called LRRK2 and has an approximate molecular weight of 286 kDa.

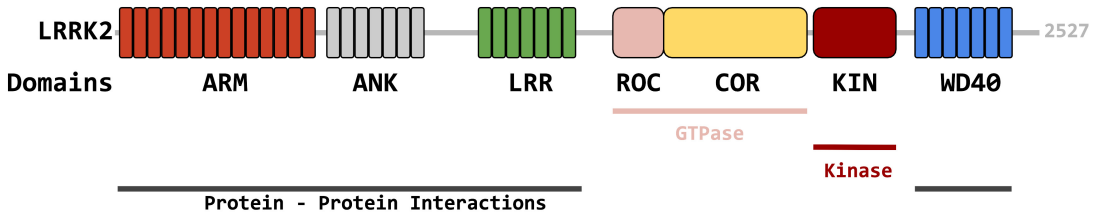

FIGURE 2.4: Domain organization of LRRK2. Predicted domains are depicted with different colors and they are also color coded according to their function. Grey line denotes those protein protein domains which are implicated in protein-protein interactions, which include : armadillo repeats(ARM), ankyrin repeats(ANK), leucine-rich repeats(LRR) and WD40 repeats (WD40). The domains involved in the GTPase function are depicted in pink color and includes the Ras Of Complex proteins (ROC) and C-terminal Of ROC (COR) domains and the red line denotes the Kinase domain (KIN)

2.2.2 Domain structure

LRRK2 is a member of the protein family known as ROCO. This multi-domain protein family is characterised by a unique structural/functional feature, there is a Roc (Ras of complex protein) domain which is immediately followed by a COR (C terminal Roc) domain forming what is termed as a Roc-COR tandem.(Marin et al. 2008; Bosgraaf and Van Haastert 2003). ROCO proteins are found in all forms of living organisms ranging from prokaryotes, metazoans, plants and mammals. To date, at least 40 members of the ROCO protein superfamily has been identified(Bosgraaf and Van Haastert 2003).

Apart from the characteristic Roc-COR domain, LRRK2 comprises several independent domains including a kinase domain, a C-terminal WD30 domain and three protein-protein interaction domains like armadillo (ARM), ankyrin repeats (ANK), leucine-rich repeats (LRR) (Figure 2.4). Most of the pathologically important mutations are clustered in the catalytic core of this protein comprising of Roc-COR and Kinase domain, hinting that LRRK2 might function as a upstream central modulator in various cell signalling pathways which are involved in the proper functioning of brain. The presence of both protein-protein interaction domains together with enzymatic domains in the same protein suggests further that LRRK2 might serve as a scaffolding protein for assembly of other proteins in multiprotein signalling cascades.

2.2.2.1 ARM domain and ANK domain

The N-terminal of LRRK2 begins with three repeat domains. The first one is Armadillo Repeat (ARM) domain and is composed of a repeating 42 amino acids motif organised in typical three α-helixes pattern that was first identified in the Armadillo protein in Drosophila, from which it got its name (Figure 2.5, top). The human homologue of the Drosophila Armadillo protein is β-catenin. The Armadillo domain is known to form a versatile molecular platform and facilities interaction with various proteins(Tewari et al. 2010). All the structures proposed for these repeating domains come from structural modeling and bioinformatics tools and they differ in their claims slightly(Cardona et al. 2014; Mills et al. 2012). The repeat size, number and likely boundaries of these predicted structural domains differ in different studies and therefore, there is still a need to validate the claims unambiguously with real experimental structure.

The next domain in LRRK2 is called Ankyrin (ANK) domain and is composed of seven ankyrin repeats. Each Ankyrin repeat has a characteristic structure, which is composed of two antiparallel helices, which is followed by a β-hairpin loop. The ANK repeats stack together and form a slightly curved structure (Figure 2.5, bottom). Ankyrin repeats are also found in various bacterial as well as other eukaryotic proteins and form functional, structural motifs in signalling proteins, transcription factors, cytoskeletal proteins etc(Mosavi et al. 2004). As with the ARM domain, the structural model for the ANK domain comes from homology modelling, using known protein structures with similar domains for prediction and they differ in the usage of bioinformatics software and tools(Cardona et al. 2014; Mills et al. 2012).

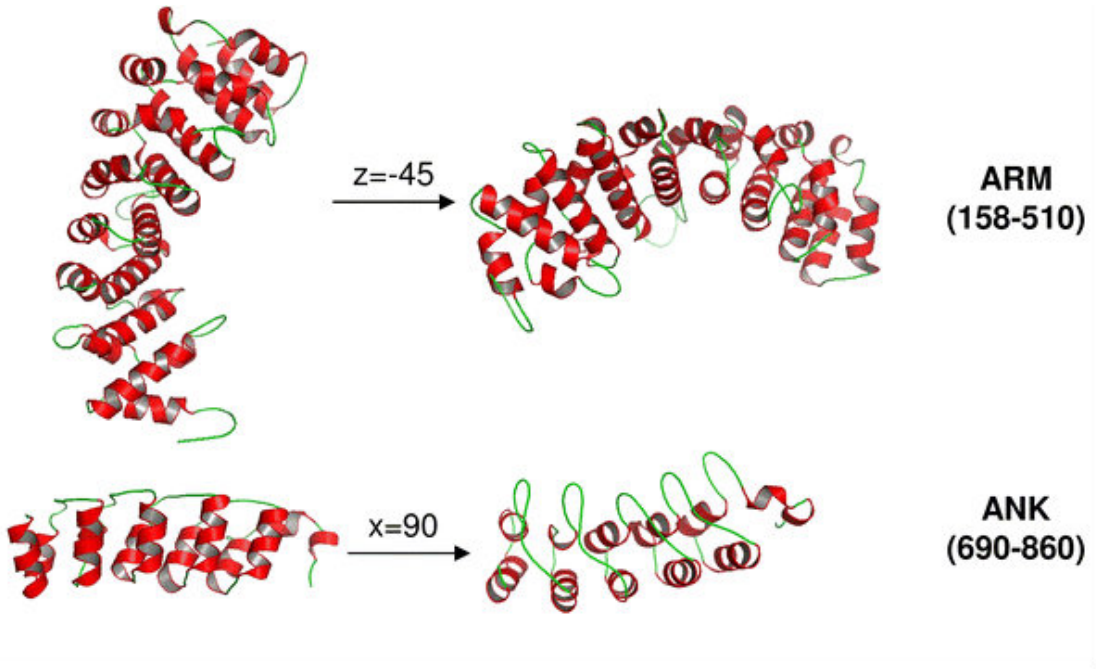

FIGURE 2.5: Predicted model and limit definition of LRRK2's ARM (top) and ANK (bottom) domains. (Cardona et al., 2014)

2.2.2.2 Leucine-rich repeat (LRR) domain

The third repeating domain is the Leucine-rich repeat (LRR) domain. LRRK2 contains 13 of the namesake LRRs. LRR is a very conserved domain that is found in variety of proteins in all organisms responsible for intra and inter cellular protein-protein interactions. These repeats are usually 20-29 amino acids long and usually present in tandem. Individual repeats form a structure of β-α units, each unit comprising of a β-strand and an α-helix, held approximately parallel to each other. Several of such repeats are arranged consecutively and parallel to a common axis, forming an arch-like structure(Kobe and Kajava 2001). There are several mutations in LRR that has been linked to PD, signifying the importance of the LRR domain in the disease pathogenesis. There are several pathogenic mutations (R1067Q, S1096C, and S1228T) and one disease segragating mutation (I1122V) known to be lying within the LRR domain, all these mutations are located at the surface and postulated to be involved in protein binding. Recently, a study by Van Craenenbroeck and colleagues focussed on the structural analysis of LRR by expressing and purifying LRR in bacteria. The study revealed the presence of 18% α-helices and 21% β-sheets (Figure 2.6)(Vancraenenbroeck et al. 2012).

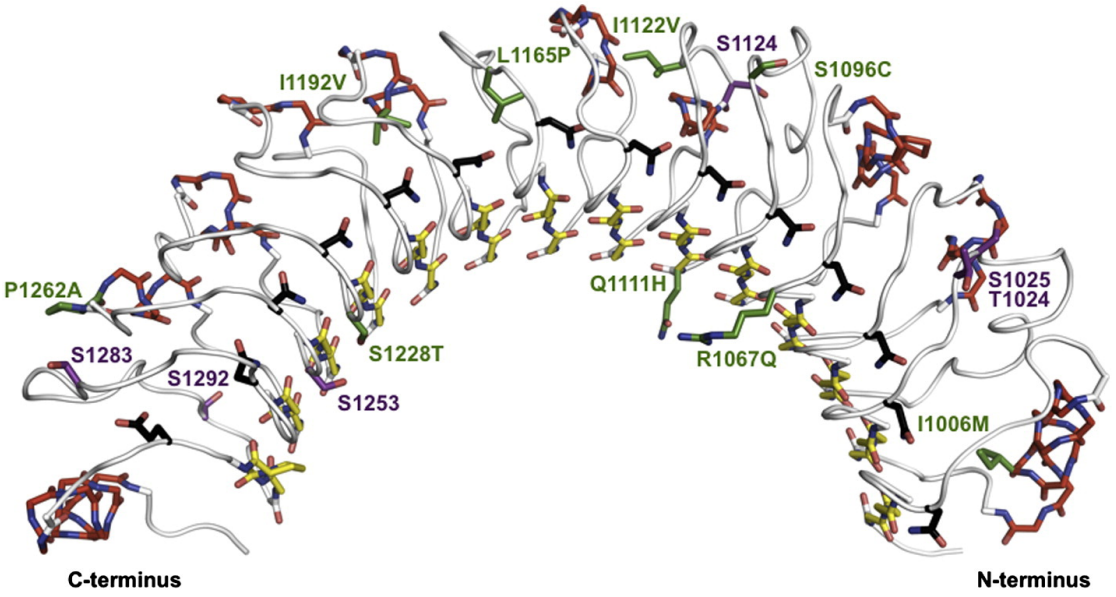

FIGURE 2.6: Ribbon representation of the predicted model of LRR domain of LRRK2 (residues 983 to 1317) (Vancraenenbroeck et al., 2012)

2.2.2.3 Ras of complex protein (Roc) domain

The Roc domain of the ROCO protein family is a characteristic feature of the family and stands out among other members of Ras superfamily of small GTPases(Bosgraaf and Van Haastert 2003). The Ras related small GTPase protein superfamily has five subfamilies within: Ras, Rho, Rab, Sar/Arf and Ran. They play a variety of biological roles. These Ras-related GTPases functions as molecular switches in the cell in order to regulate the diverse function that they perform. They serve by switching between the GTP-bound and GDP-bound conformations. The GTP-bound state is the active conformation where the GTPases are cable of binding to the substrate or another protein, which further evoke downstream reactions. There are additional guanine nucleotide binding proteins which are specific of each GTPase subfamily and regulates to enhance GTP-binding and enhance downstream signaling. An example is of guanine nucleotide exchange factors (GEFs) which facilitate GTP-binding while GTPase activating proteins (GAPs) enhance the rate of GTP hydrolysis to terminate signalling, and there is another class of protein called GDP dissociation inhibitors (GDIs) which are known to inactivate the GDP-bound protein(Takai et al. 2001)

The Roc domain of LRRK2 shares the most sequence homology with the Rab subfamily of Ras-related GTPases. The Rab GTPases are fairly conserved in the entire living organism from yeast to higher eukaryotes. In the human genome, there are a number of genes linked with Rab GTPases. These protein from different organism differ from each other mostly in their C-terminal, which have been implicated to be involved in cell signalling, whereas the residues which are involved in guanine nucleotide binding

are mostly conserved(Chavrier et al. 1991). From X-ray crystallography experiments, we know that the Rab GTPases share a structure that is very similar to the structure of all small GTPases of the Ras superfamily. The general structure is composed of six stranded beta sheets that are surrounded by five alpha helices. The five loops that connect these beta strands and alpha helices are responsible for binding of guanine nucleotide and magnesium ions(Stenmark and Olkkonen 2001). Out of these five loops, four are conserved in Roc domains, including the amino acids residues, which are involved in the binding and hydrolysis of GTP. The catalytic mechanism of Rab proteins is very similar to that of other Ras related GTPases.

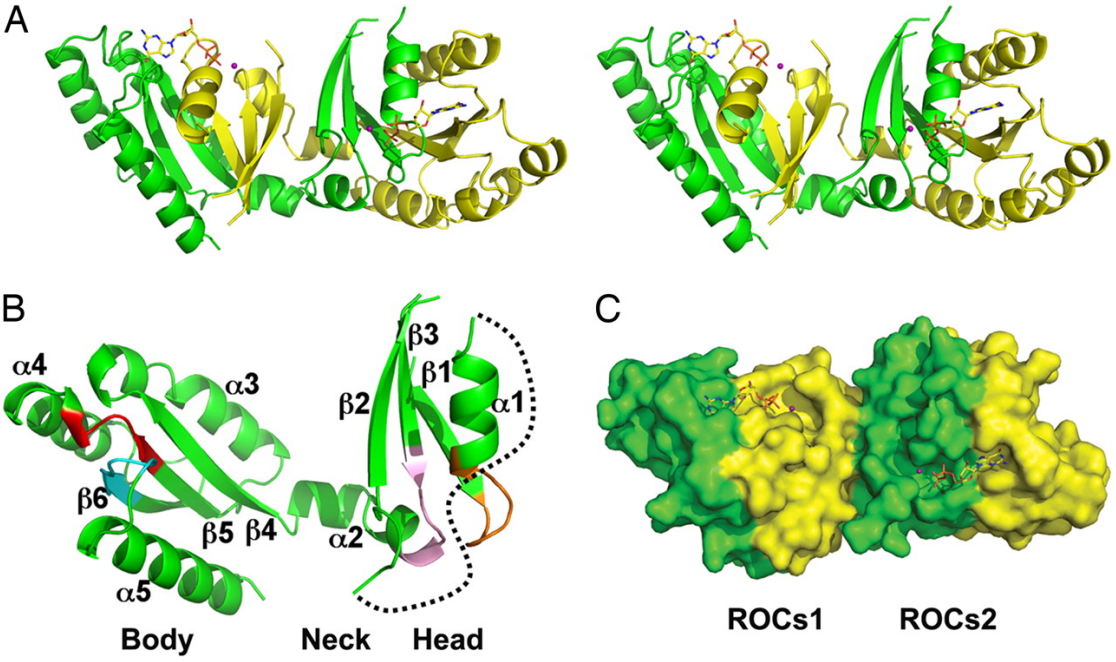

FIGURE 2.7: Atomic structure of ROC GTPase. (A) Stereoview of the domain-swapped dimer. The two individual monomers are shown in yellow and green. (B) Ribbon representation of a single monomer. The three head, neck, and body subdomains are indicated, along with the labeled secondary structures. The P-loop, G3/Switch II, and G4 and G5 loops are indicated in orange, pink, red, and cyan, respectively. The disordered G2 loop is shown as a black dotted curve. (C) Surface representation highlighting the GDP-Mg2+ binding pocket on the surface of the dimer that is contributed from both monomers. The pair of functional units are shown as ROCs1 and ROCs2, respectively. (Deng et al., 2008)

Until now, only the crystal structure that has been solved is that of the human LRRK2 Roc GTPase domain. The Roc domain displays a dimeric structure where the dimeric fold forms an extensive domain swapping at the catalytic core. Each of the Roc domain monomer contains five α-helices and six β-strands. There are other sub domains as well, which forms the head, neck and body and a pair of active sites. The two monomers are arranged in a pseudo two-fold symmetry and are further stabilized by hydrophobic interactions and extensive hydrogen bonding(Deng et al. 2008). Three of the LRRK2 pathogenic mutations lie within the Roc domain at residue R1441 (R1441C, R1441G,

and R1441H). The residue R1441 is located at the end of α-helix 3 that is further linked with the carbonyl oxygen of F1401 residue and the hydroxyl group of T1404 residue, which are located on α-helix 2 from the other peptide chain at the dimer interface via hydrogen bonding. The R1441C mutation is believed to weaken the Roc dimer structure by disrupting the hydrogen bonding thereby destabilizing the dimer formation (Figure 2.7)(Deng et al. 2008). The importance of dimeric formation of the Roc domain and its affect on Roc GTPase activity has been further confirmed by other studies(Guo et al. 2007; Ito et al. 2007). Another putative mutation PD linked mutation I1371V lies near the conserved GTP binding pocket and can alter the catalytic activity of the domain.

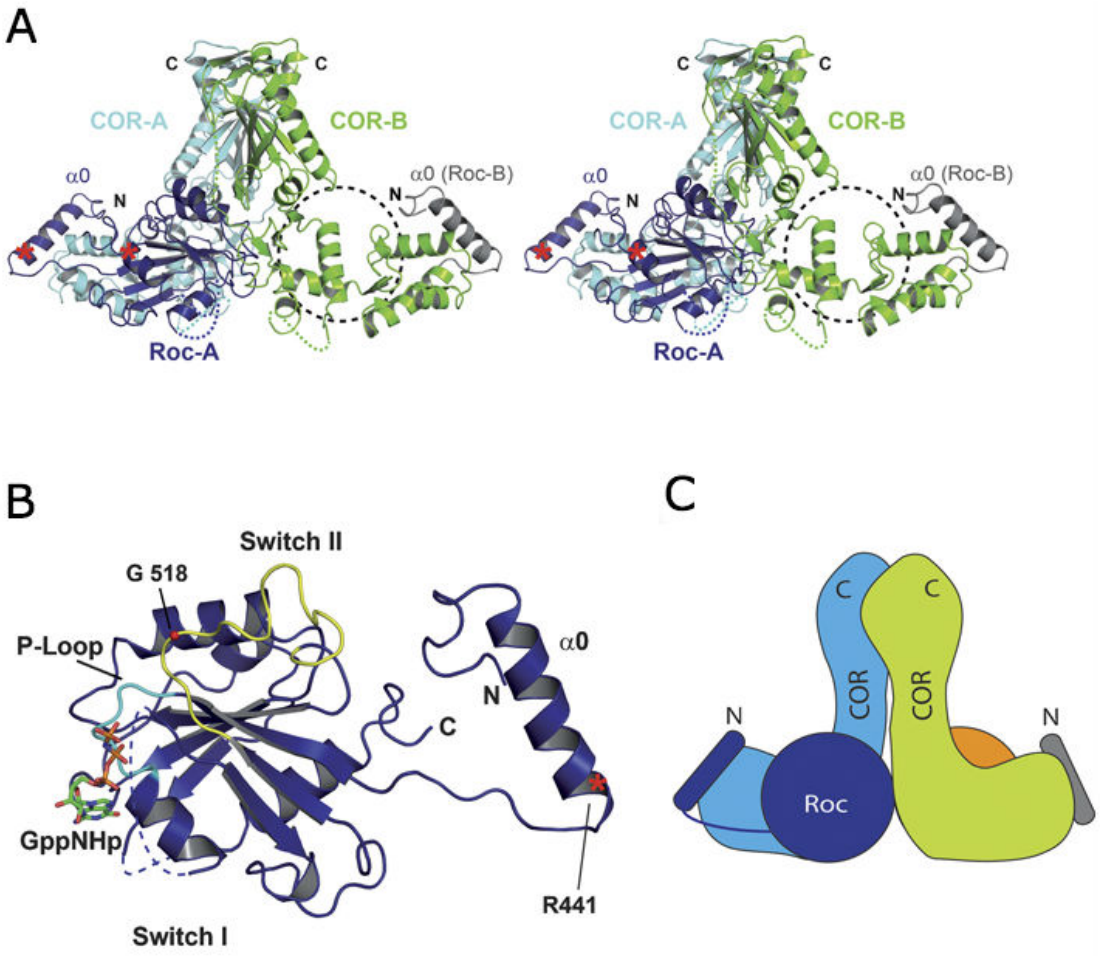

FIGURE 2.8: Structure of the Roc-COR tandem. (A) Stereo-ribbon diagram of the Roc-COR dimer with COR domains A and B, and for Roc domain A and parts of Roc domain B in different shades of blue. (B) Ribbon plot of Roc domain A and helix 0 (E) Schematic view of the complete Roc-COR dimer including the full Roc-B subunit. (Gotthardt et al., 2008)

Another study aimed to gain insight into the human LRRK2 Roc-COR domain by solving the structure of its prokaryotic homologue in C. tepidum(Gotthardt et al. 2008). Roc-COR domain of the homologous ROCO protein in C. tepidum was isolated from

the full-length protein by limited proteolysis method and subject to cystalization and structure determination by X-ray crystallography (Figure 2.8). The COR domain is comprised of two subdomains which are linked by a flexible linker domain. Each subdomain is further made up of mostly α-helical structure with a short N-terminal β-sheet which is antiparallel and have three short strands. Towards the C-terminal, there is a central seven-stranded antiparallel β-sheet flanked by four α-helices and a β-hairpin motif. The two subdomains of the COR forms a dimeric structure (Figure 2.8). The structure has confirmed that the dimerization in the Roc-COR tandem structures occurs at the C-terminal of COR subdomains. The interactions between Roc and the COR domains contributes to the dimer formation. It was reported in the study that the PD linked mutation occur between the Roc and COR domains and involve the α-helix 3 of Roc domain which causes the disruption of the hydrogen bonding and reduce the interaction between Roc-COR tandem and therefore decreasing the GTPase activity(Gotthardt et al. 2008). This study identified the dimerization of Roc-COR to be mediated by the COR domain which contradicts the previous claims from the crystal structure of the Roc dimer, and suggested a Roc mediated dimerization(Deng et al. 2008). These ambiguities further emphasize the need of a full-length structure of LRRK2 at high resolution.

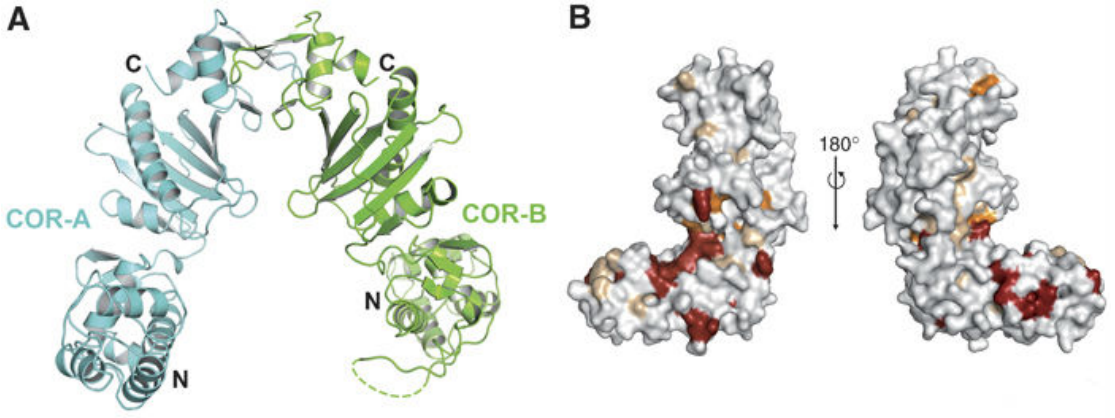

FIGURE 2.9: Structural of the COR domain dimer. (A) Ribbon diagram of one (physiological dimer) of the COR dimers found in the crystal, with different protomers shown in green and cyan. Loops, that are not visible in the structure are indicated as dashed lines. (B) Surface representation of the COR monomer in two different orientations separated by 180°, with residues totally invariant between bacteria and man in red and those highly conserved in orange. (Gotthardt et al., 2008)

2.2.2.4 C-terminal of Roc (COR) domain

Another characteristic domain common to all the ROCO proteins is the COR domain. It always occurs immediately after the Roc Domain. This tandem arrangement of Roc-COR is highly conserved in all organisms and throughout evolution, which suggests the mutual dependence of function between the two main domains of ROCO proteins.

The COR domain comprises of 300-400 residues (Figure 2.9). There have been several bioinformatics studies to understand the sequence homology of the domains but COR domain does not show any significant homology to any known protein domain.

2.2.2.5 Kinase domain

The kinase domain in LRRK2 is also called mitogen-activated protein kinase kinase kinase (MAPKKK) domain. Based on the sequence similarity, the kinase domain of the LRRK2 belongs to the tyrosine kinase-like (TKL) subfamily of human protein kinases. The members of TKL protein kinase family show sequence similarity to both tyrosine kinases as well as serine/threonine kinases(Manning et al. 2002). The kinase domain also bears resemblance to the receptor interacting protein kinases (RIPKs), a class of protein kinases important in sensing cellular stress and activate mitogen-activated protein kinase (MAPK) pathways(Meylan and Tschopp 2005). The atomic structure of the kinase domain of LRRK2 has not yet been solved. By utilising the close homology with human B-Raf for which the atomic structure is already known by X-ray crystallography (Figure 2.10, A), a homology model can be generated for LRRK2 kinase domain. The kinase motif DF/YG that is conserved motif of kinase lies at the interface of the small and the large catalytic lobes. The motif responsible for magnesium ion binding is called the D motif. Magnesium ion binding is required for the ATP phosphotransfer(Guo et al. 2006). For the interaction with the alpha carbon helix via hydrophilic interactions, rest of the motif is responsible and this is found to be critical for the catalytic activity(Nolen et al. 2004). For the activity of the protein kinases, majority of them requires phosphorylations of the activation segment. Once phosphorylated, the activation segment undergoes a conformational change, thereby enabling binding of the substrate and required catalysis can be performed. The PD-associated LRRK2 mutations G2019S and I2020T are placed at the N terminal end of the activation segment, with glycine residue position 2019, which belongs to the conserved DF/YF sequence. Another PD related mutation of LRRK2 I2012T lies within the magnesium binding region of the domain(Mata et al. 2006). These mutations therefore directly affect the kinase catalytic activity.

Recently, a high-resolution structure of the ameba LRRK2 kinase domain homolog has been solved with X-ray crystallography and proposed as a platform for understanding the human LRRK2 kinase domain (Gilsbach et al. 2012). The kinase domain was purified and crystallized from ROCO4, the Roco family protein in Dictyostelium. Roco4 has the same domain architecture as LRRK2 and much more stable biochemically and structurally. The 3D structure of Roco4 kinase is very similar to that of other kinases. It is comprised of two-lobed kinase structure, with an adenine nucleotide bound in the

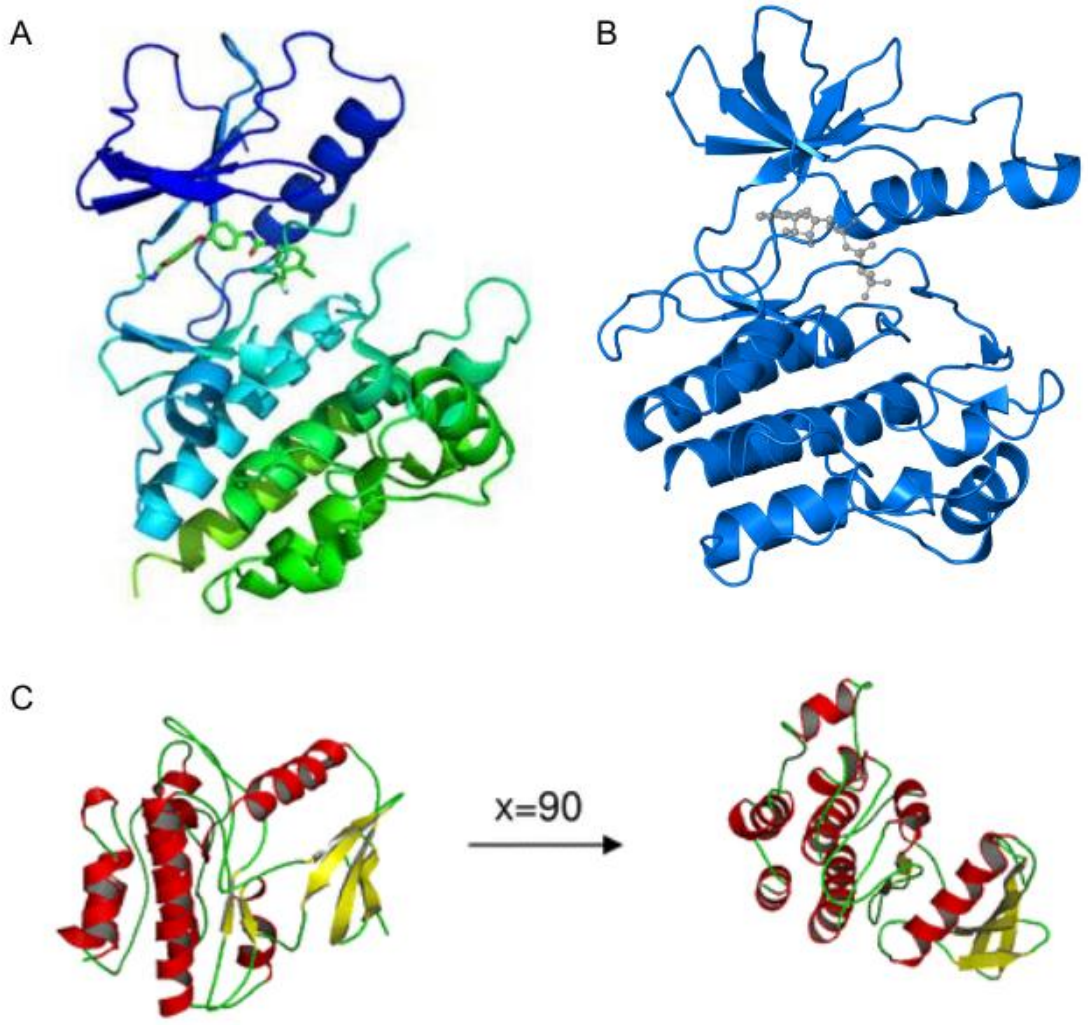

FIGURE 2.10: Atomic models of Kinase domain. (A) PDB model of B-Raf, a known MAPKKK activated by Ras (pdb no. 1UWH). (B) Crystal Structure of the Roco4 Kinase Domain bound to AppCp from D. discoideum (PDB No. 4F0F) (C) Homology model of human LRRK2 Kinase domain, using Discoideum Roco4 Kinase Domain as a template (Cardona et al., 2014)

conventional nucleotide-binding pocket (Figure 2.10, B). The N-terminal lobe is slightly smaller and is mostly comprised of anti-parallel β sheets. It also contains the conserved αC-helix. The other C-terminal lobe is relatively bigger and composed of α-helices and contains the activation loop with the conserved N-terminal DFG motif. The cleft between the two lobes forms the ATP binding site and acts as the catalytic core of the kinase together with αC-helix and the activation loop. The atomic structure also revealed for the correct position of the αC-helix, a polar contact formation is essential between Roco4 Lys 1055 from the β3-strand and Glu1078 from the αC-helix. While for the catalysis, the DFG motif is essential. The Asp residue makes contact with all three ATP phosphates either directly or via coordination of a magnesium ion; the Phe residue makes hydrophobic contacts to the αC-helix and the HxD motif is responsible

for the correct positioning of the DFG motif. Using the atomic model of Roco4 as a template, Cardona and colleagues generated a model for human LRRK2 Kinase domain using homology modelling. The domain is formed by seven α-helices and six β-sheets linked by loops, which are exposed to the solvent (Figure 2.10, C) (Cardona et al. 2014).

2.2.2.6 WD40 domain

There are seven repeats of WD40 in LRRK2. The typical architecture of WD repeat comprises of the N-terminal GG dipeptides of 11-24 residues and the C-terminal WD dipeptide ranging from 40-60 residues. Sandwiched between the C and N terminal is a conserved sequence that forms the core of this domain. Each repeat forms a four-stranded, antiparallel beta pleated sheets and forms a circular propeller-like structure (Figure 2.11)(Mata et al. 2006). Despite the highly conserved motif and sequence similarity between the proteins that contain the WD40 domain, they all posses a high diversity in their function. This is very unusual for a domain where the expected tertiary structure is very similar. There are a number of WD40 containing proteins in eukaryotes and carry out diverse functions like RNA processing, cytoskeleton assembly, cellular trafficking and transcription regulation. In most of these cellular processes, the WD40 domain does not perform any enzymatic function but rather mainly functions to mediate protein-protein interactions. There are special proteins like LRRK2, where WD40 is fused with the kinase domain in the C-terminal(Janda et al. 1996; Smith et al. 1999). In relation to Parkinson's disease there has been two putative pathogenic mutations in LRRK2 WD40 domain. The first mutation, G2385R is located on the surface of one of the propeller blade and postulated to be involved in altering protein-protein interaction. While the second mutation, T2358I is located in the core part of the domain(Mata et al. 2006).

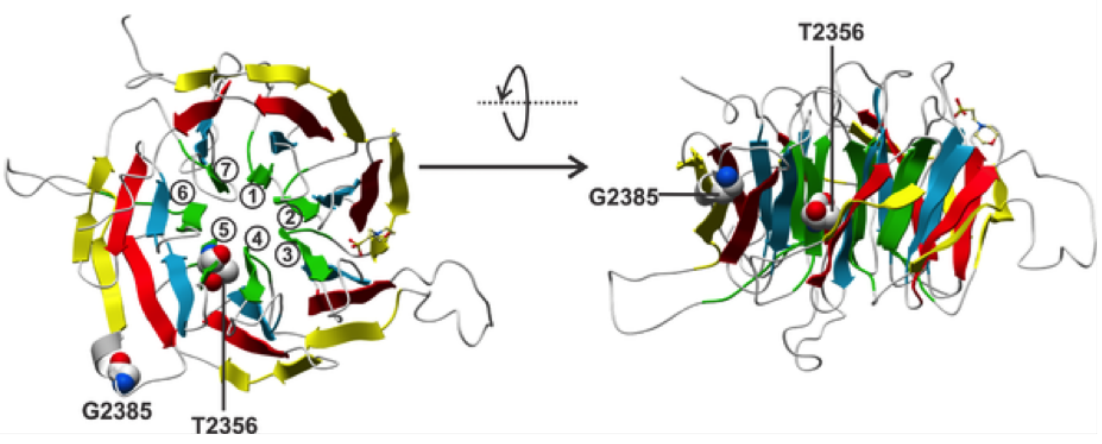

FIGURE 2.11: A model resembling the predicted repeat pattern of the LRRK2 WD-40 repeat domain. (Mills et al., 2014)

2.2.3 Prevalence of LRRK2 mutations in Parkinson's disease

Mutations in the LRRK2 and their link with Parkinson disease have brought widespread public attention to the pathobiology of LRRK2 in PD. In comparison to other genes which are involved in PD, LRRK2 linked PD has two special aspects. Firstly, mutations in LRRK2 gene is found not only in familial form of the disease but for sporadic cases as well and secondly, pathobiological features of the LRRK2 linked PD, both for familial and sporadic cases, are very similar to each other(Bonifati 2006). Of all the known mutations for LRRK2, the G2019S mutation, located in the kinase domain of the protein is the most commonly occurring in both familial and sporadic PD. The G2019S mutation is found in 1-2% of sporadic PD patients while 3-6% of patients with familial PD are known to have this mutation. Although several groups have identified this mutation and linked it with PD, the frequency of the G2019S mutation varies greatly with the geographic population. For example in Europe, the G2019S mutation is present at a comparatively lower frequency 4-18% of familial PD and 1-6% of sporadic PD, with slightly more prevalence in southern European countries than the northern European countries. In contrast the prevalence of G2019S mutation is extremely low in Asian population(Lu et al. 2005; Tan et al. 2005; Fung, Chen, Hardy, Hernandez, et al. 2006; Punia et al. 2006; Tomiyama et al. 2006). However, among patients from the middle east, Arab states, North Africa and Jewish population, extremely high prevalence is observed (30-38% of familial and 15-22% of sporadic cases)(Lesage et al. 2006). The penetration of G2019S mutations in PD patients appears to be dependent on age, increasing from around 20% at the age of 50 to as high as 85% when the patient reaches 70(Kachergus et al. 2005). In recent studies, the lifetime penetration of G2019S mutation in large scale studies in PD patients population from United States and Europe yielded figures between 24 to 33%, this explains the high occurrence of G2019S mutation in sporadic PD case(Goldwurm et al. 2007; Clark et al. 2006). Apart from G2019S, there are other mutations in LRRK2 that are linked to PD in many studies, though the prevalence is generally lower than that of G2019S. Among these other mutations, another common PD related mutation located in the Roc domain are the R1441G and R1441C mutations. The R1441G mutation has been associated with among Spanish and Basque PD patients with a very high prevalence of around 8%.(Paisan-Ruiz et al. 2004). For the other common mutation, R1441C, a prevalence of 3.4 % was reported in a study on 60 European families(Di Fonzo, Wu-Chou, et al. 2006). Apart from the catalytic core of Roc-COR and Kinase domains, another G2385R variant, located in the WD40 domain, has been identified as a common risk factor for sporadic PD in populations of Chinese ethnicity(Di Fonzo, Tassorelli, et al. 2006; Fung, Chen, Hardy, Singleton, et al. 2006; Tan et al. 2007). Other putative mutations, located all along the multi-domain

structure of LRRK2 are known but have been have been reported with a rather low frequency of ¡ 1%(Punia et al. 2006). These include S1228T, R1441H, R1067Q, I1122V,, Y1699C, I2020T and M1869T.

2.2.4 Localization of LRRK2

Studies of mRNA expression pattern in mouse showed that expression pattern of LRRK2 differ significantly from the other PD related genes. For example, mRNA expression levels of other PD related genes like α-synuclein, parkin, UCHL-1, DJ-1, and PINK1 are observed in most of the neurons of the brain including the dopamine neurons located in the midbrain(Galter et al. 2007; Solano et al. 2000). In contrary, LRRK2 mRNA expression is absent in dopamine synthesising neurons of the SNpc and only observed in dopaminergic areas of the brain such as the striatum, olfactory tubercle and cortex(Melrose et al. 2006; Galter et al. 2006; Taymans et al. 2006).
Apart from the brain, LRRK2 is expressed broadly in peripheral organs like liver, lungs, kidneys and spleen(Higashi et al. 2007). Intracellularly, LRRK2 has found to be localized within a number of cellular organelles like Golgi vesicles, plasma membrane, lysosomes, mitochondria, synaptic vesicles and cytoskeleton. These localizations of LRRK2 hints towards a putative role in cellular vesicle trafficking, mitochondrial integrity and protein turnover. There is also substantially higher expression of LRRK2 in the immune system than in the brain cells which implies the emerging role of LRRK2 in the immune regulation(Dzamko and Halliday 2012). Recently, a study has suggested that in additional to the cytosolic monomer LRRK2, membrane associated LRRK2 can exists as dimeric structure and possesses enhanced kinase activity and GTPase activity compared to the soluble counterparts(Sen et al. 2009).
In brain cells of humans, both the LRRK2 mRNA and LRRK2 protein expression are found in the regions of brain like cerebral cortex, SNpc and caudate putamen, which are pathologically relevant in PD(Biskup et al. 2006). There are also studies to support the co-localization of LRRK2 with α-synuclein in the brainstems and lewy bodies(Zhu, Babar, et al. 2006; Zhu, Siedlak, et al. 2006). There has been conflicting evidence regarding the immunostaining of Lewy bodies for LRRK2, when other groups failed to detect any LRRK2 protein in Lewy bodies(Greggio et al. 2006). This reported ambiguity might be a result of utilization of diverse LRRK2 antibodies or variations in preparation of brain tissues for immunohistochemistry.

2.2.5 LRRK2 and Mitochondrial dysfunction

Over the past few years, mitochondrial dysfunction has been increasingly appreciated as a key modulator in neurodegenerative diseases and now recognised as a key feature of both sporadic as well as familial Parkinsonism. Mitochondria are vital organelles of the cell, which are responsible for cellular ATP synthesis, calcium homeostasis, apoptosis initiation and ROS formation. An important aspect of mitochondrial functioning is the fission and fusion dynamics they go through and this key fission-fusion mitochondrial dynamics is essential for integrity, electrical balance and protection of mitochondria(Berman et al. 2008). Moreover, the critical role of cellular respiration in the brain functioning and its impairment has been implicated in PD and several other neurodegenerative diseases. The implication of mitochondrial autophagy in PD linked with LRRK2 came from the study of mutant mouse carrying the human G2019S mutant LRRK2 and it was observed that there was aggregation and accumulation of mitochondria in the brain(Ramonet et al. 2011). In another study, a major reduction in the levels of ATP and altered morphology of mitochondria was identified in fibroblast with the same G2019S LRRK2 mutation of PD patients(Mortiboys et al. 2010). It was later validated that wild type LRRK2 interacts with a number of mitochondrial fission fusion regulators by co-localizing with the regulators in the cytosol as well as the membranes, indicating for the first time a directly regulatory role(Wang et al. 2012; Stafa et al. 2014). Together in the primary neurons of rats and the human neuroblastoma, it has been established that LRRK2 directly interacts with Drp1, the key fission regulator of the mitochondria at the membrane which further activates Drp1 by phosphorylation and increase mitochondrial fission(Niu et al. 2012; Stafa et al. 2014). This fission mechanism of mitochondria via the LRRK2-Drp1 mediated pathway is enhanced by overexpression wild type LRRK2 as well as G2019S mutant LRRK2, however, the process can be rescued by the inhibition of Drp1 or fusion enhancement (Figure 2.12)(Su & Qi 2013). LRRK2 also have been reported to interact with two other key mitochondrial fusion regulators Mfn 1/2 and OPA1 and modulates their activity, as the PD patients carrying the common G2019S mutation showed reduced level of mature OPA1(Stafa et al. 2014). Studies on the LRRK2 orthologue LRK-1 in C. elegans also revealed protective role of LRK-1 in mitochondrial stress by acting antagonistically with PINK-1(Samann et al. 2009). All together, these data demonstrate a close interaction between the mitochondria and LRRK2 but till date, it has been impossible to confirm mitochondrial dysfunction as the primary pathogenic effect of LRRK2 linked PD.

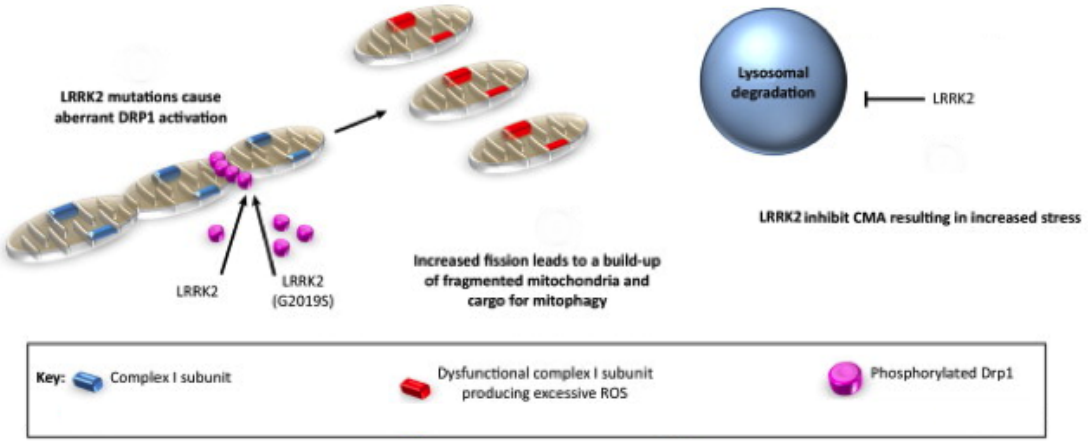

FIGURE 2.12: Overview of the roles of LRRK2 in mitochondrial dysfunction : LRRK2 activates the mitochondrial fission protein dynamin related protein-1 (Drp1) via phosphorylation. Increase in the kinase activity can results in aberrant Drp1 phosphorylation and fission. In G2019S mutated PD associated LRRK2, increased fission and ROS production leads to mitochondrial dysfunction. The increased number of fragmented mitochondria will increase autophagic flux due to the increase in mitophagic cargo. LRRK2 mutations can impair CMA resulting in cellular stress.(Adapted from Ryan et al., 2015)

2.2.6 Enzymatic activity of LRRK2

The catalytic core of LRRK2 that comprises of the Roc-COR domain and the kinase domain has been studied well in the past few years. LRRK2 functions both as a functional GTPase as well as a kinase which can undergo autophosphorylation and substrate phosphorylation(Gloeckner et al. 2006; West et al. 2005).

LRRK2 is identified as a GTP-binding protein as confirmed by the studies using radiolabeled GTP and GTP-agarose(Lewis et al. 2007; Guo et al. 2007). LRRK2 have been shown to have the ability to bind and hydrolyze GTP(Li et al. 2007). Biochemical studies carried out to understand the kinase activity routinely measure the autophosphorylation of LRRK2 itself or phosphorylation of Myelin Basic Protein (MBP) as a generic kinase substrate and phosphorylation of an artificial substrate called LRRKtide(Lewis 2012). Though the status of these proteins as substrates for LRRK2 remains unclear. The most prevalent mutation of LRRK2 G2019S has been found to directly affect the kinase activity and increase it to as much as threefold when compared to the kinase activity in WT LRRK2. As the mutation is located in the catalytic core of the kinase domain, it can likely affect the conformation of the kinase domain and affects its enzymatic action(Smith et al. 2006; Guo et al. 2007; Ito et al. 2007; West et al. 2007). Another common mutation R1441C that occur in the Roc domain has been reported in several studies to decrease the GTPase activity and the GTP turnover rate, without

affecting the GTP binding of the protein (Gloeckner et al. 2006; West et al. 2005; Li et al. 2007).

Other familial PD linked mutations like R1441C, R1441G, I1371V and Y1699C located within the Roc and COR domains are shown to cause increased GTP-binding as measured by binding to GTP-agarose, while mutations outside these domains did not affect GTP-binding compared to wild-type LRRK2(West et al. 2007). In contrast, R1441C mutation also have been demonstrated to enhance GTP binding in LRRK2 with mutation as compared to the wild type in other studies(Lewis et al. 2007; Guo et al. 2007).

There are two types of autophosphorylation that can occur, within the same molecule, which is termed as intramolecular phosphorylation or with other molecules, which is called intermolecular phosphorylation. Luzon and colleagues demonstrated that LRRK2 expressed in bacteria displays intermolecular autophosphorylation targeting T2031 and S2032 residues in the activation segment(Luzon-Toro et al. 2007). There have been other autophosphorylation sites that have been recognised which include those located in the Roc domain like S1403, T1404, T1410, T1491 as well as those located in the kinase domain T1967 and T1969. The kinase domain is shown to influence the GTPase domain as well as other domains(Kamikawaji et al. 2009). This hypothesis has been tested in another study which reported that GTPase activity can be modified by the auto-phosphorylation of the LRRK2 T1503 site located in the GTPase domain(Webber et al. 2011), which further supports the idea that the kinase domain may influence the GTPase domain in LRRK2.

The enzymatic activity of LRRK2 has been demonstrated to be strongly correlated with its dimerization. The most common pathological G2019S mutation in LRRK2 enhances dimerization of the protein and results in enhanced kinase activity. Using kinase inhibitors results in disruption of LRRK2 dimers and higher weight oligomer formation is promoted(Sen et al. 2009).

Several studies have reported the kinase activity of MAPKKK domain of the LRRK2 and the effect of PD related mutations on its enzymatic activity. The G2019S mutation is considered to enhance the kinase activity in LRRK2 in vitro and therefore LRRK2 linked PD is characterised as gain-of-function of protein kinase activity. Mutants of LRRK2 with inactive kinase activity are found to be less toxic both in vitro and in vivo(Greggio et al. 2006; Smith et al. 2006; Zhihua Liu et al. 2011; S. Lee et al. 2010). But there still exists some discrepancies in the literature and there is no clear consensus regarding the affect PD associated mutation has on the kinase activity of LRRK2. For example, there are studies where other common mutations like R1441C, R1441G, R1514Q, Y1699C and I2020T are reported to enhance the kinase activity measured by

autophosphorylation, confirming the gain-of-function mechanism model for the LRRK2-linked PD, in contrast there are other studies that report these mutants either do not influence any kinase activity or even inhibit the kinase activity(Jaleel et al. 2007; Luzn-Toro et al. 2007). According to one in vivo study, it was reported that the inhibition of kinase activity in LRRK2 can also decrease the LRRK2 protein level in mouse kidney and lung, implying that LRRK2 kinase activity may be able to control the protein level as well(Herzig et al. 2011). Another interesting aspect of the kinase activity in LRRK2 is its ability to affect its protein-protein interaction and also cellular localization. The phosphorylation of S910/935 is necessary for the interaction of LRRK2 with other 14-3-3 proteins, confirmed by mutant studies of S910/935 LRRK2, which started to accumulate in the cytoplasm(Nichols et al. 2010; Dzamko et al. 2010).

2.2.7 LRRK2 therapeutic strategy

For the development of therapeutics for LRRK2 related PD, a great understanding of the biological functioning and cellular signaling is very important. The role of LRRK2 to function as a kinase has been well established, which makes it an interesting clinical target. Therefore a specific inhibitor against the kinase core of the protein can be a potential treatment regime in PD. Converging studies directs to the inhibition of LRRK2 kinase activity as a key therapeutic concept and there has been recently a lot of research in this particular area. Several generic kinase inhibitors has been studied against LRRK2 and found to inhibit LRRK2 kinase activity and protect against LRRK2 toxicity both in vitro and in vivo(B. D. Lee et al. 2010). Other kinase inhibitors like GW5074 and sorafenib were also reported to protect against G2019S LRRK2-induced neurodegeneration(Zhaohui Liu et al. 2011). The effect of LRRK2 kinase inhibition can also cause cellular changes for example, LRRK2 kinase inhibitors were found to dephosphorylate LRRK2 at S910/935 mutation, and further restrict the interaction with 14-3-3 and promote formation of inclusion bodies(Dzamko et al. 2010). There is still information lacking to explains the cellular correlations of the protective effect induced by LRRK2 inhibitors. But nonetheless several potent, promising kinase inhibitors are discovered. One such inhibitor is LRRK2-IN1, which unfortunately could not get clinical approval because of the inability to cross the blood brain barrier. The IC50 value of LRRK2-IN1 is 6 mM for G2019S and 13mM for WT LRRK2(Deng et al. 2011). Though kinase inhibitors has proved to be a promising therapeutic drug for LRRK2, there has been some concern on their usage. It has been reported in a study that inhibition of LRRK2 kinase activity can also lead to decrease in LRRK2 protein level in cells and disrupt normal kidney function and lung homeostasis, which can cause organ malfunction(Herzig et al. 2011). To counteract such side effect of kinase inhibitors, more

research on strategies to directly target the inhibitors to the brain might be needed in future.

2.3 LRRK1

Apart from LRRK2, there are three other ROCO family proteins that have been identified in humans. These are Leucine-rich repeat kinase 1 (LRRK1), death-associated kinase 1 (DAPK1) and Malignant fibrous histiocytoma amplified sequence 1 (MFASHI1) (Bosgraaf and Van Haastert 2003). Of these the closest paralogue of LRRK2 is LRRK1. Both the LRRKs shared a conserved domain architecture that is typical of the ROCO family of proteins. LRRK1 is a 2015 amino acids long protein and structurally lacks the ARM and WD40 domains of LRRK2(Taylor et al. 2007; Korr et al. 2006). Apart form the missing domains, the sequence identity and similarity between the common domains of the two proteins varies between 14% and 50% (Figure 2.13)(Civiero et al. 2012). Moreover, both proteins are basally phosphorylated(Greggio et al. 2007) and expressed in the brain(Biskup et al. 2007). However, irrespective of their similar expression profile and close homology, mutations in LRRK1 have not been genetically associated with PD(Taylor et al. 2007). Although in a recent exome sequencing in a German family with autosomal dominant late-onset PD, LRRK1 along with EEF1D were identified as the best candidate, hinting at a possible role of LRRK1 in addition to LRRK2 in the genetic foundation of PD(Schulte et al. 2014). But more conclusive studies are required to find LRRK1 variants as causative agents of PD. A study induced PD linked mutations in both LRRK2 and LRRK1 at equivalent residues to determine the comparative toxicity level and it was found that mutations in LRRK1 is much less prone to form inclusion bodies in transfected cells, thereby suggesting that LRRK2 is inherently more pathologically toxic than LRRK1(Greggio et al. 2007). This major difference has invoked various other studies to understand the functional roles of LRRK2 and LRRK1 and the link between the two (Taylor et al. 2007). Importantly, LRRK1 might have a modulatory role in the signaling network of LRRK2 and, therefore, affect the risk of developing PD (Dachsel et al. 2010; Klein et al. 2009; Reyniers et al. 2014). Unfortunately, the limited amount of structural information available for LRRK1 and LRRK2 does not allow definite conclusions to be drawn.

2.3.1 Biochemistry

The biochemical properties of LRRK1 have not been explored well and there are only a few reports published in literature that describe its function as a GTPase or a kinase. Among the first biochemical study carried on LRRK1 was published by Korr and

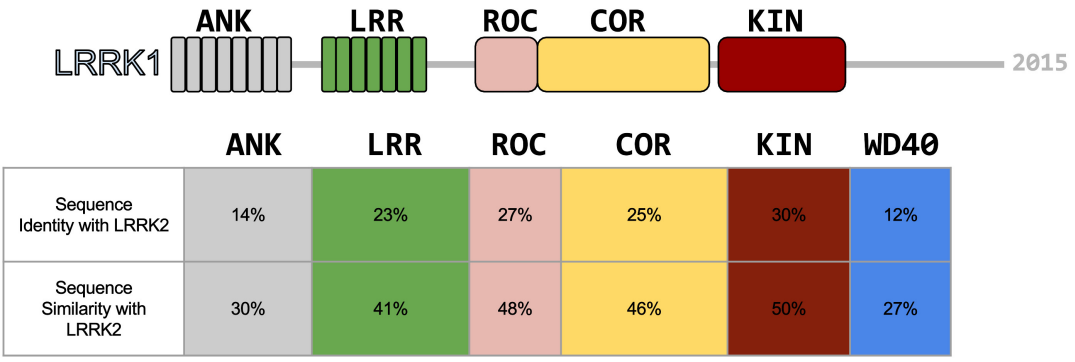

	ANK	LRR	ROC	COR	KIN	WD40
Sequence Identity with LRRK2	14%	23%	27%	25%	30%	12%
Sequence Similarity with LRRK2	30%	41%	48%	46%	50%	27%

FIGURE 2.13: Domain organisation of LRRK1. Predicted domains (Mills et al. 2014) are depicted with different colors and their relative location is drawn to scale within the full-length protein : ANK, ankyrin repeats; LRR, leucine-rich repeats; ROC, Ras Of Complex proteins GTPase; COR, C-terminal Of ROC; KIN, a kinase. Below each domain, the sequence identity and sequence similarity with domains of LRRK2 is reported in the column with same color. (Bioinformatics values adapted from Civiero et al., 2012)

colleagues, a decade ago where they proposed that like LRRK2, LRRK1 also function as a GDP/GTP binding protein via the ROC domain and undergoes autophosphorylation(Korr et al. 2006). In the same study, the kinase activity of LRRK1 was measured by saturating the GTP-binding site, which resulted in loss of kinase activity, suggesting the dependence of kinase activity in LRRK1 on the GTPase domain. The efficiency of the catalytic activity of LRRK1 was found to be lower than that of LRRK2(Deng et al. 2011; Bosgraaf and Van Haastert 2003). One key difficulty in studying the biochemistry of LRRK1 and LRRK2 is the lack to known substrate for the kinase and GTPase activity. To make things difficult, the commonly used kinase substrate that are routinely used to study other kinases in cells such as MBP (myelin basic protein), casein and histone H1 are not phosphorylated by LRRK1(Korr et al. 2006). Furthermore, till date the published reports on the studies to investigate the biological functions of LRRK1 have been on truncated recombinant form of LRRK2 or attached with affinity tags. There has been lack of efficient purification methodology that can yield good quality full-length functional LRRK1 protein, which can be used to unravel the molecular mechanism of LRRK1 functional activity.

2.3.2 Functions

Although both LRRK2 and LRRK1 display similar function and display partial intracellular co-localization, when the well-known PD associated LRRK2 mutations were introduced into LRRK1, it resulted into different phenotype. It was found that the autophosphorylation activity as well as the propensity of LRRK1 to induce cell death was

not affected by the LRRK2 PD associated mutation, as observed for mutated LRRK2 protein(Korr et al. 2006; Greggio et al. 2007). It has been reported that LRRK2 is predominantly a functional dimer in the cell and the kinase activity is modulated by the dimeric nature of LRRK2(Deng et al. 2008; Greggio et al. 2008; Berger et al. 2010; Sen et al. 2009). However, there are also report of LRRK2 to be present in cell in monomeric form which is probably inactive(Ito and Iwatsubo 2012). Based on these findings and the fact that there is high level of homology and similarity in domain organization between the LRRK2 and LRRK1, it is conceivable to deduce that LRRK1 too has very similar quaternary-structural properties as that of LRRK2. A study confirmed the hypothesis that dimerization is a general attribute of the ROCO family of proteins including LRRK1, LRRK2 and DAPK1(Klein et al. 2009). Another interesting study also revealed the occurrence of formation of heterodimers between LRRK1 and LRRK2(Dachsel et al. 2010). This phenomenon is also seen in other class of proteins called GAD, which stands for G-proteins activated, by nucleotide-dependent dimerization. GAD undergo pseudo trans homodimerization whereby two different G-protein that share similar family and near identical active side residues can form dimers(Gasper et al. 2009). Similarly, LRRK1-LRRK2 heterodimerization could have an affect on the kinase activity and maintaining the equilibrium between the dimer and other oligomeric states. But there is further need to establish the role of LRRK1 as modulator of LRRK2 3D structure and also the affect of pathogenic PD mutations on heterodimerization.

There have been few studies that demonstrated the role of LRRK1 in endocytosis of EGFR (epidermal growth factor receptor). It was shown that LRRK1 forms a stable complex with activated EGFR by forming and interacting with another protein Grb2 (growth-factor-receptor-bound protein 2)(Hanafusa et al. 2011). LRRK1 is also reported to regulate endosomal trafficking in cells. EGFR regulates LRRK1 kinase activity through Try944 phosphorylation(Ishikawa et al. 2012). When Tyr944 residue of LRRK1 was mutated (Y944F), EGF stimulated tyrosine phosphorylation was halted. This resulted in gain of function for LRRK1 kinase activity and increased mobility of endosomes towards particular region. The same group of researchers also found that LRRK1 interact with NudC and CLIP-170 (cytoplasmic linker protein 170), linking the role of LRRK1 to endocytosis(Hanafusa et al. 2011). Recently, CLIP-170, a microtubule plus-end protein, has been identified as downstream targets of LRRK1. This further promotes the association of CLIP-170 with dynein-dynactin complexes, hence providing a new biological function of LRRK1 in the dynein-driven transport of EGFR(Kedashiro et al. 2015). These observations when compared with the known functions of LRRK2, implies that LRRK1 and LRRK2 may share cellular functions. The association of LRRK2 with PD and no clear involvement of LRRK1 in PD has lead to a far wider research into exploring the cellular function of LRRK2, while for LRRK1, a lots of inspection is still needed.

2.3.3 Localization of LRRK1

To localize LRRK1 in cells, the common strategy used in the studies is to measure the LRRK1 mRNA and protein level in different tissues and organs, together with LRRK2, the data are suggestive that the expression of the LRRK1 and LRRK2 usually overlaps and in few organs such as the kidneys and the brain, level of LRRK2 mRNA expression is much higher than that of LRRK1(Dachsel et al. 2010; Biskup et al. 2007). In tissues like these where the expression of LRRK1 is lower, the functional overlap of LRRK1 and LRRK2 is nullified because of the low quantity of one protein but in other organs where the expression of both LRRK1 and LRRK2 is similar, the functional overlap can compensate for the deficiency of one protein. In a recent study, detailed analysis of LRRK1 and LRRK2 was carried out using radioactive in situ hybridization to explore the localization, expression level and distribution of the proteins. The expression profiles of both genes at low level from embryonic stage E9.5 onward, which progressively increased up until birth, showed that there are no prominent LRRK2 mRNA signals at these time-points. Although, after the birth, the level of LRRK2 in the brain especially in the striatum and the cortex of adult mice is very strong, while LRRK1 levels were comparatively very low and only detectable in mitral cell layer of the olfactory bulb(Giesert et al. 2013). Therefore a redundant function of LRRK1 and LRRK2 in the pathogenesis of PD seems unlikely as observed in the non-overlapping expression patterns in the mouse brain.

2.3.4 LRRK1 and LRRK2

Although, LRRK1 and LRRK2 both share a common evolutionary ancestry, they are both specialized for different functions. The catalytic core of the LRRKs i.e. the ROC-Cor-Kinase domain imparts similar molecular mechanism to perform these different task but the higher degree of variation in the repeating domains (ARM, ANK, LRR, WD40) which are crucial for the protein-protein interactions may play an important role in regulating the binding partner and target their cellular functions. Therefore, for a better understanding of the functions and dysfunctions of LRRKs, there is a need to study the actions of LRRK2 and LRRK1 in parallel in different animal models(Civiero and Bubacco 2012). There has been a study to understand LRRK1 and LRRK2 specific cellular processes by identifying their interacting partner. Using protein microarray-based interaction screen, coimmunoprecipitation and followed by mass spectrometry, specific as well as common interacting proteins were identified for both LRRK1 and LRRK2 in parallel (Reyniers et al. 2014). The study confirms both the protein can carry out distinct functions by interacting with different cellular partners, suggesting

that the LRRK1 signalling does not intersect with LRRK2 signalling, thereby reflecting a different role of both LRRKs in pathogenicity of PD.

2.4 Electron microscopy

2.4.1 Introduction and History

The invention of microscopes has been from long one of the most fascinating events in understanding the secrets of living forms. The resolution of human eye is in the order of 100 um which makes anything smaller than the thickness of human hair unseenable to the human eyes. In the past centuries, light microscopy has pushed this resolution limitation and has been instrumental in many of the important discoveries in biology and medicine. However, at the end of nineteenth century the resolution limit of a conventional light microscope reached its limit, which is approximately 250 nanometers equal to the wavelength of the incoming light used to illuminate the sample. In 1930s, Ernst Ruska and Max Knoll came up with a prototype of a new kind of microscope that uses an illumination source with a smaller wavelength need and this source was high voltage electrons and gave birth to the Electron Microscope (EM) (Borries and Ruska, 1938). This enabled scientist to view the structures inside the cells well below the reach of light microscope and opened an entire new field in biology.

There are two common types of electron microscopes: scanning electron microscope (SEM) and transmission electron microscope (TEM). In a typical SEM, biological sample of interest is first coated with a electron reflecting metal. This metal layer also acts as a conducting surface and protects the sample from charging, when the electron beam from the microscope scans over the biological sample. The resulting image formed by the bouncing electrons off the surface reveals a 3D picture of the specimen without any internal information. In contrast, a TEM produces an image that is a 2D projection of the biological object, including not only the surface but also the internal structure. When the beam of electrons from the microscope, interacts with the sample, it passes through the entire thickness of the sample, hence enabling to differentiate the internal structures based on the different projections obtained. These different projects of the same biological entity from different directions or views can then be computationally combined to deduce a 3D reconstruction. But before the technique could be used as a general structural biology method, three key challenges needed to be overcome. First, the biological sample has to sustain the ultra high vacuum that is required for the functioning of the TEM. Secondly, a workaround to decrease the radiation damage to the sample caused by the high-energy electron beam. And lastly, the contrast generated

from the biological sample is very low. It was David DeRosier and Aaron Klug who for the first time in late 1960s tackled these problems by using the heavy-atoms salts as staining chemicals. They used computational Fourier-Bessel approaches to mathematically combine the multiple projections of T4 bacteriophage tail, which compose of molecules arranged in a helical order (De Rosier & Klug, 1968). This gave birth to the field of 3DEM. Though the use of heavy-metal staining in EM called negative staining is still a popular method, which generates high-contrast image and protects the sample from the radiation damage, there are some major limitations to this method, the staining and drying of the sample can cause the sample to collapse and most importantly limit the resolution to get a detailed biological insight of the sample. The major breakthrough for high resolution EM came from the work of Ken Taylor and Robert Glaeser (Taylor & Glaeser, 1974). They demonstrated that high-resolution features of a protein can be protected by keeping the sample frozen hydrated at cryogenic temperatures. Their work shifted the field of EM into cryo-EM. Later Dubochet and colleagues developed the method of vitrification of samples for cryo-EM which is still routinely used (Dubochet et al., 1988). During the year of development of the cryo-EM field, several pioneering work bought high-resolution atomic models of biological samples. These include the structure of bacteriorhodopsin (Henderson et al., 1990), acetylcholine receptor (Unwin, 1995) and Icosahedral viruses (Bttcher, Wynne, & Crowther, 1997; Conway et al., 1997). All these samples either formed naturally occurring 2D crystals or have had some form of symmetry that limited the use of 3DEM to a group of biological specific following in those categories. Methodology to deal individual macromolecular complexes in cell that doesnt form helical or crystalline arrays and adopt random multiple orientation when vitrified in a EM grid, came from the study of ribosomes by Frank and colleagues (M. J. Frank, 2005). Their work broaden the horizon of cryo-EM field and enable many more biological complexes to be structurally determined by the so called single particle reconstruction.

2.4.2 The Electron Microscope

The basic layout and working of a transmission electron microscope is in a way very similar to that of a conventional compound optical microscope (Figure 2.14). At the top of the TEM, a high voltage electron source is placed, which generates very high voltage electron beam, which travels down the column passing through the sample and a series of magnifying magnetic lenses. The column chamber is protected and maintained at a very high vacuum to avoid any interaction of the electron beam and the air particles. The electron beam is finally focused on a viewing screen or a detector to collect images. The following are the components of a TEM:

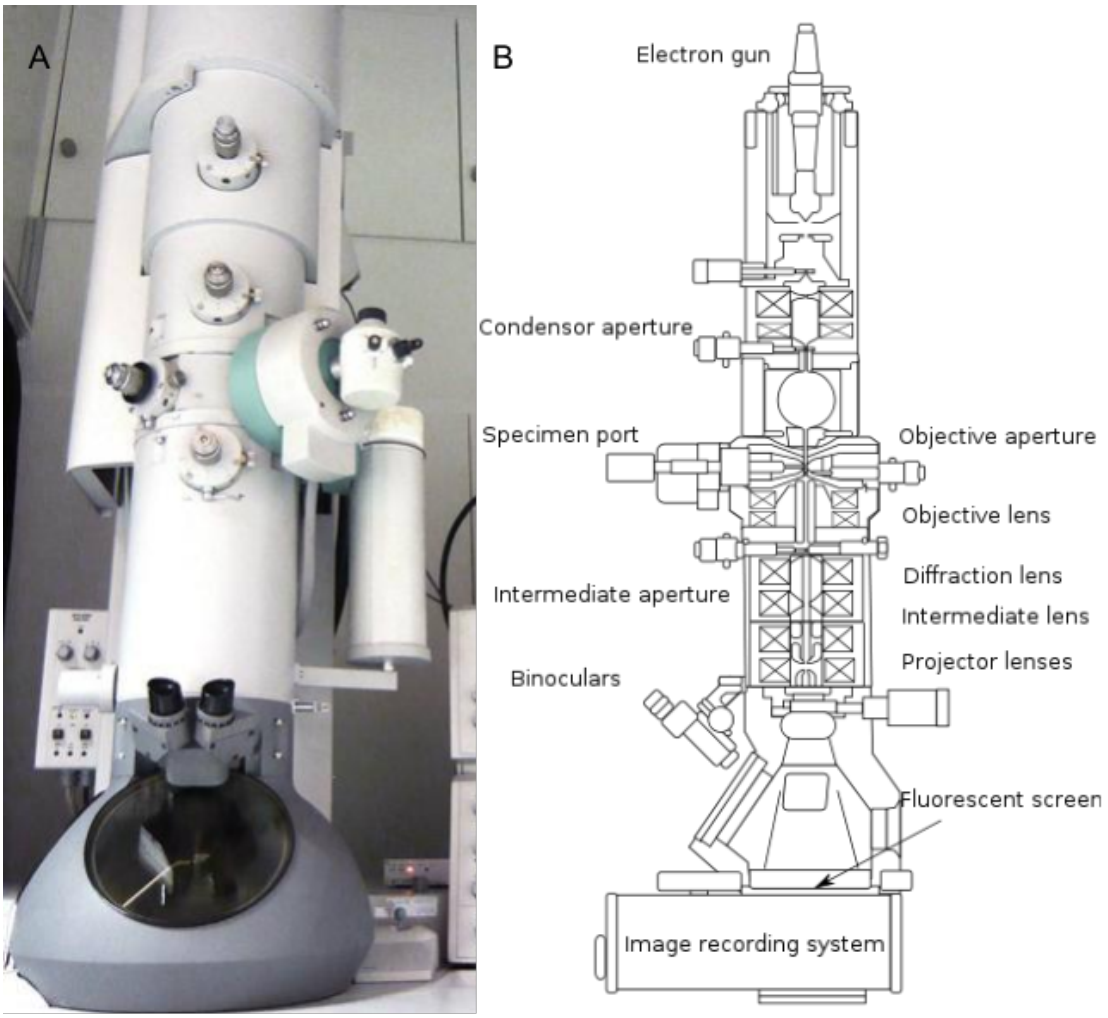

FIGURE 2.14: Outline of a Transmission Electron Microscope. (A) CM200, an inhouse 200kV FEG instrument with Gatan-626 side-entry cryo holder (LN2 temperature) and TVIPS F416 CMOS camera. Used to collect data in this dissertation. (Image Courtesy : Philippe Ringler) (B) General outline of a TEM and its various components are highlighted.

2.4.2.1 The gun

This is the source of the high voltage electron beam, which is the essence of a TEM. Traditionally, the most common electron source used was tungsten or lanthanum hexaboride (LaB6). The electron source is superheated (3000°C) by using an electric current, until the energy of the electron is large enough to leave the metal. These escaped electrons are accelerated with several hundred kilovolts (80-300 kV) by an electric field. These electrons need to be collated into a coherent beam before they can be sent down along the microscope column. In modern TEM, field emission guns (FEG) is now used, where the tungsten filament is reduced into a small nanometer sized tip, thus producing spatially and temporally more coherent and brighter electron beam.

2.4.2.2 The lenses

The lenses in a TEM are composed of magnetic coils that generate a circular magnetic field and helps focus the incoming electron beam. Three different set of magnetic lenses are used in a typical TEM. The top most lens is called the objective lens and does the very first step in focusing of the electron beam and image magnification. The next set of lens is the intermediate lens, which functions to adjust and manipulate the required magnification of the biological sample. The last part of lens system is a set of projector lens, they are primarily used to focus and project the image on the visualising screen or detector to collect images.

2.4.2.3 The apertures

Another important component of the TEM apart from the lenses are the apertures. These apertures act like holes along the microscope column and function to limit and control the size of the beam that can pass through them. They are present at different location on the TEM and affect the function. The very first aperture is the condenser aperture, which is located on the top of the column. The functions of the condenser aperture is to condense the electron beam coming out from the electron gun and maintain a coherence electron beam. The second aperture is located just below the sample, after the objective lens. Its function is to control the generated contrast in the image by a method called amplitude contract.

2.4.2.4 Detector

Traditionally all the high-resolution data collected in TEM were recorded on photographic films that needed further development and digitization. With the development of CCD (charge-coupled device) cameras, the need to digitalization was obliterated and faster and more automated data collection was possible but in terms of attainable resolution from the data, photographic films still leaded. This was the limitation of how a CCD works, where the electron from the TEM must be first converted to photos via interaction with a scintillator. These multiple electron scattering events in the scintillator restricts the quality of signal at high resolution and introduce extra noise to the images. Very recently, this bottleneck in TEM has been overcome by the development of direct electron-detection cameras (or direct detectors). These direct detectors are able to detect electrons directly on a silicon wafer. They have a resolution and sensitivity greater than film and have an added advantage of faster readout rate than CCD detectors.

2.4.3 Principles of EM image formation

In a transmission electron microscopy, images are formed from the very thin objects by passing very high energy electrons through them. When the electron beam interacts with the specimen in the microscope, there are three possibilities. If the electron does not hit any atom of the specimen, it will continue to travel in the same line as the incident beam of electron and hit the detector. The electron can come in contact of the matter in the specimen and bounce off from the incident path without the transfer of energy between the electron and the sample; this is called elastically scattered electrons. The last possibility is when the electron can come in contact of the matter in the specimen and bounce off from the incident path and transferring some energy to the sample, this is called inelastically scattered electrons. The electrons can also interact with the specimen and get reflected by an angle greater than 90°, in that case they never reach the detectors located at the end of the microscope. These type of electrons known as backscattered electrons are generally not used in TEM. The inelastically scattered electrons are the cause of noise in the TEM micrographs. The amount of energy that is transferred to the sample by inelastically scattered electrons is variable and random, therefore when these electrons hits the detector, the energy and the angle of incidence is unknown causing noise. The elastically scattered electrons are the one that give contrast to the TEM images and contain the high-resolution information. The amount of energy that is transferred to the sample by inelastically scattered electrons is constant and according to the law of conservation of momentum, the angle at which it will be reflected can be determined. The contrast in the TEM images results from the interference of the unscattered electrons beam with the elastically scattered electrons. This interference can be constructive or destructive. To enhance the contract in the images the objective aperture is used and functions by blocking the electrons that are deflected to a greater angle. This is termed as the amplitude contrast and the most common imaging mode in bright field EM.

2.4.4 CTF

As explained in the previous section, the images recorded in the TEM are phase contrast images and can be considered good approximation of the specimen. As the electron interacts very weakly with the light atoms of the biological specimen, it is impossible to image the specimen at focus (the distance of the object from the focal plane). Instead images are collected at slight under-focus or defocus, which imparts phase contrast to the image. The mathematical functions that describe how this information is transferred as a function of spatial frequency is called contrast transfer function (CTF). Essentially

the images recorded on a TEM can be best viewed as the convolution of a real image with a point spread function (PSF) of the microscope. CTF is an oscillation function and some information is absent when it crosses zero and therefore it is impossible to fully correct a single image taken at a specific defocus. Therefore, it is necessary to use different defocus setting that results in the images having CTF with different zero at varying spatial frequencies.

2.4.5 Negative stain

This is the most common method used in electron microscopy to generate contrast in the biological sample inserted into the TEM. Staining is usually done with the use of heavy metals such as uranium or molybdenum. The biological sample is deposited on an EM grid and covered with the negative stain (e.g 2% uranyl acetate). The stain effectively surrounds the sample. The heavy metals interact readily with the incoming electron beam and generate phase contrast. When the electron beam passes through the sample, it is deflected well by the stain and less by the volume occupied by the sample. This gives a good contrast image, which can be inverted (hence negative) to reveal the projection of the sample of interest. There are few drawbacks of this technique, firstly the structural information contained in the projections of the particle is limited to the shape of the molecule and suffer from distortion while drying of the stain or non-uniform staining of the molecule. Secondly and most importantly, the resolution of negative stain images is limited to approximately 20-25 and cannot be used to generate atomic information of the biological molecule. But the simplicity of the technique makes it a popular method still used actively.

2.4.6 Cryo-EM

To counteract the limitations of negative stain EM and preserve the native hydrated structure of the biological specimen, unstained imaging methods are used. The high vacuum of the EM can cause severe dehydration of the biological molecules and can use collapse and distortion of the structure (Bremer et al., 1992). To avoid the use of staining solution but still protect the sample, there are two widely used methods to achieve this. First method is to replace the water of hydration that surrounds the biological molecule with a less volatile medium such as sugars(glucose or trehalose), first demonstrated by Henderson and Unwin (Henderson & Unwin, 1975). The second method is the snap-freeze the sample in a very thin layer of vitreous ice, thus producing a hydrated environment around the sample. This further requires the sample grid to be kept at liquid nitrogen temperatures to maintain the vitreous ice around the particles

and also prevent the sample from some effects of beam damage. Low dose imaging conditions are also employed for data collection in cryo-EM to cause least damage to the sample. The resulting images has high-resolution information but very low signal to noise ratio.

2.4.7 Image processing

The general steps of single particle analysis (SPA) are shown in Figure 2.15 and explained in the next sections. The schematic also shows the image processing used in this dissertation to process electron microscopy data.

2.4.7.1 Particle picking

The very first step in single particle reconstruction is particle picking. In order to reconstruct a 3D structure of a protein complex, it is necessary to combine several thousands of experimental 2D projections (particles). These particles have to be picked or boxed out from the recorded EM micrographs prior to the image processing. There are manual as well as automatic particle picking softwares to perform this task. When there are only few micrographs (for example in negative stain data), often the easiest way is to visually inspect the micrographs and identify and single out all the projections which looks like your sample by hand and thus avoiding any bad particle coming from contaminations like stain or ice. But for bigger routine datasets when the number of micrographs collected is in the range of few hundreds, it can be tedious to do manual particle selection and one has to use automated particle picking softwares. There are several different algorithms for picking particles from noisy EM micrographs based on template matching, gaussian approaches and edge detection. There are several specific softwares that use these algorithms in slightly different way.

2.4.7.2 CTF correction

EM images are typically acquired using defocus contrast. This along with the aberrations inherent in the objective lens system of the TEM creates blurring of the acquired EM micrographs, visible as a point spread function (PSF). These modulations when observed in the reciprocal space by doing a Fourier transform of the image are more obvious and the areas of positive values become visible as Thon rings (Thon, 1966). The combined effect of the imaging conditions is termed as the Contrast transfer function (CTF). The effect of CTF can be corrected mathematically as a function in reciprocal space. There

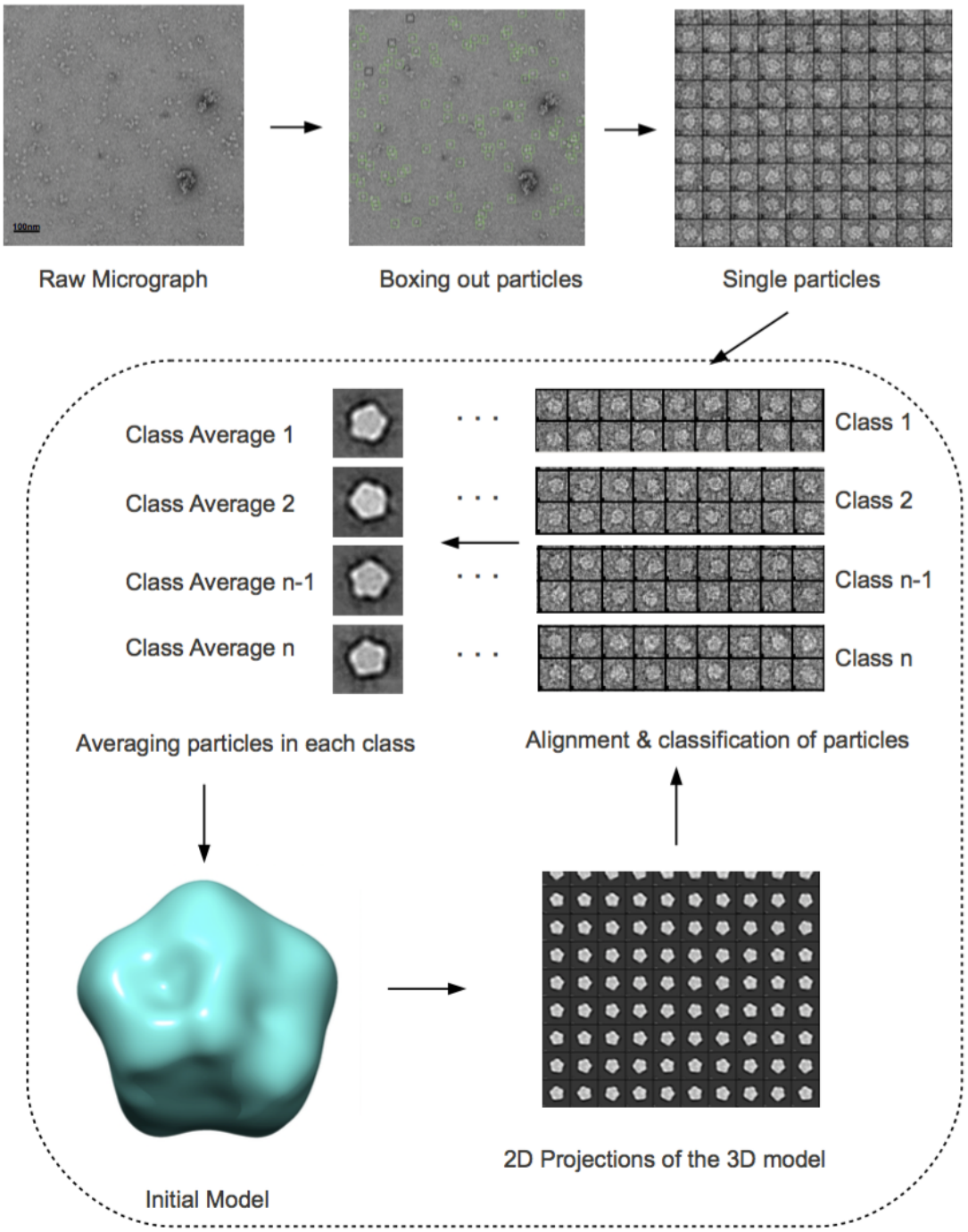

FIGURE 2.15: Main steps involved in the single particle image processing, starting from the raw micrograph to 3D model generation.

are specialised techniques that are a part of single particle image processing to correct CTF and these include phase flipping, amplitude correction and Wiener filtering.

2.4.7.3 2D Classification and Averaging

After picking the particles and correcting for the CTF, the next challenge in single particle image processing is enhance the low signal to noise ratio (SNR) of the individual particle images. The low SNR of the individual particles makes it hard to see any structural features of the protein complex, therefore, similar particles that have the same orientation are clustered and this process is called 2D classification. Once the 2D classes are generated, all the particles of the same class can be averaged to enhance the SNR. For high-resolution cryo-EM data, secondary-structure elements such as alpha helices are easily seen in such class averages. 2D classification and averaging starts by alignment of the particles. The picked particles are centered and positioned to allow locating the correct in-plane rotation and translation along the x-y direction. This step places all the particles in similar relative position that is prerequisite for clustering them into separate classes. Both reference and reference free alignments of the particles are possible. To avoid any kind of reference bias in the low SNR particles, reference free alignment is mostly used. After the particles are nicely aligned, next task is to identify similar views or orientation of the sample and group them together in separate classes. A method called Multivariate statistical analysis (MSA) is used to perform this task. MSA works by compressing the large EM data mathematically into eigen images and then common features are identified within the eigen images via cluster analysis. Another popular method to perform 2D classification is by maximum likelihood approaches where the classification begins with a random set of reference images from the set of particles. Then for each projection image, probabilities are calculated with respect to its translation, rotation and the degree of matching with each reference. Subsequently rotated and translated particles are formed and their 2D Fourier transforms, appropriately weighted by the CTFs, are combined to form the overall average images. The new generated averaged images now form the new references and the same procedure is iterated for several rounds, resulting in a set of representative class averages.

2.4.7.4 Orientation determination

Once we have class averages of different views from the 2D projection of the particles, the next challenge is to determine 3D orientation to these different class averages. There are two approaches for this, angular reconstitution and projection matching.

Angular reconstitution method is based on the central projection theorem that states that the center of the Fourier transforms of any two-dimensional projection images of the same object intersect at the center of three-dimensional Fourier space. Utilizing the central projection theorem, the goal to determine the orientation is to find the overlapping pieces (or common lines) of data. Applying central projection to single particle analysis implies that if between two images there exist some overlapping data, and then the corresponding relative orientation between those two images can be computationally calculated.

Another method used for orientation determination is projection matching which can be applied for any set of particles for which there is already previously determined structure or a 3D model generated by other methods. The starting model is used to generate simulated projections and these are then compared computationally with the experimental projection images generated in class averages to determine the orientation using cross correlation.

2.4.7.5 3D Reconstruction

Once we have the class averages and have assigned their relative orientation in 3D space, they are all combined into one 3D model, this process is termed as 3D reconstruction. The method used for 3D reconstruction is called weighted back-projection. In principle, weighted back projection method is quite similar to inverse Fourier transform. In the same way as a real space 2D Image is generated from a 2d Fourier space image by using 2D inverse Fourier transform, a weighted back-projection determines the real space 3D volume of the protein complex from a series of 2D Fourier space images using a series of transformation.

Chapter 3

Structural insights obtained for homodimeric full-length LRRK2 and LRRK1 protein complexes

Kushal Sejwal[1], Mohamed Chami[1], Rosmarie Suetterlin[1], Paul Baumgartner[1], Henning Stahlberg[1] and Jean-Marc Taymans[2 3]

[1]Center for Cellular Imaging and NanoAnalytics (C-CINA), Biozentrum, University of Basel, Basel 4056, Switzerland

[2]Jean-Pierre Aubert Research Center, UMR-S1172, Early Stages of Parkinson's disease, Place de Verdun, 59045 Lille, France

[3]KU Leuven, Laboratory for Neurobiology and Gene Therapy, Department of Neurosciences, 3000 Leuven, Belgium

*Corresponding authors: H Stalhberg; henning.stahlberg@unibas.ch

*Corresponding authors: J-M Taymans; jean-marc.taymans@inserm.fr

(Manuscript in preparation)

Author's Contribution: K.S. purified the protein, collected EM data and performed image processing; M.C. supported in EM data collection; R.S. maintained cell cultures; P.B and J-M.T. supported in protein purification; K.S., HS, J-M.T. analysed the data.

3.1 Introduction

Parkinson's disease (PD) is the second most common neurodegenerative movement disorder. It affects 1-2% of all people above the age of 65 (Lees et al. 2009) and is at present incurable, although treatments are available to alleviate the symptoms. Genetic studies have identified several genes involved in PD pathogenesis. Of these, the leucine rich repeat kinase 2 (LRRK2) gene is a key gene, with mutant forms being the most prevalent known causes of genetic PD and genomic variants at the LRRK2 locus are common risk factors of sporadic PD (Hernandez et al. 2016). In addition, LRRK2 appears to act upstream of several other PD genes and PD risk factors such as alpha-synuclein, tau, cyclin G associated kinase (GAK) and RAB7L1 (Cookson 2015; Taymans and Cookson 2010). The 144 kb long LRRK2 gene encodes for the 2527 amino acid (aa)-long, cytosolic enzyme LRRK2, which functions as a GTPase as well as a kinase. Most of the pathologically important mutations are clustered in its catalytic core of this protein, hinting that altered GTPase and kinase activities may play a crucial role in pathogenesis (Zimprich et al. 2004; Bekris et al. 2010). Targeting the LRRK2 protein pathway is currently regarded as one of the most promising approaches in drug development for PD (Lee et al. 2012).

LRRK2 is a member of the ROCO protein family (Bosgraaf and Van Haastert 2003). It has a multidomain organization containing several protein-protein interaction domains, including armadillo (ARM), ankyrin repeats (ANK), leucine-rich repeats (LRR), Ras Of Complex proteins GTPase (ROC), C-terminal Of ROC (COR), a kinase (KIN) and WD40 (Mills et al. 2014). (Figure 3.1). LRRK2 is known to be involved in several cellular functions including autophagy and neurite outgrowth regulation and related to some mitochondrial diseases ((Gmez-Suaga et al. 2012) (MacLeod et al. 2006), (Cherra et al. 2013)). Biochemical experiments suggest that LRRK2 kinase and GTPase activities may be regulated by dimerization (Greggio et al. 2008; Danils et al. 2011; Taymans 2012; Sen et al. 2009).

Three other ROCO proteins have been identified in humans: Leucine-rich repeat kinase 1 (LRRK1), death-associated kinase 1 (DAPK1) and Malignant fibrous histiocytoma amplified sequence 1 (MFASHI1). Out these, LRRK1 is the closest homologue of LRRK2. The domain organization is similar, and like LRRK2, LRRK1 is known to purify as homodimer (Civiero L et. al., 2012). LRRK1, a 2015 aa-long protein, lacks the ARM domain and while the C-terminal region of kinase is present as in LRRK2 but it does not correspond to a WD40 domain. Otherwise, the sequence identity and similarity between the domains of the two proteins varies between 14% and 50% (3.1). Despite this similarity, mutations in LRRK1 have not been linked to PD. This difference has stimulated various studies to understand the functional roles of LRRK2 and LRRK1

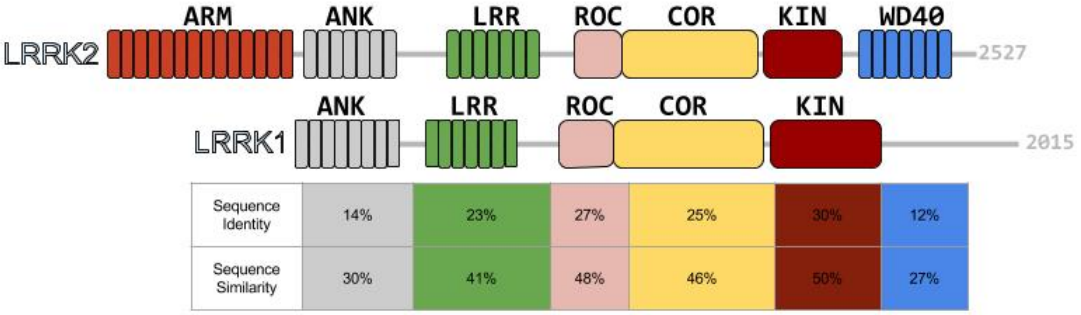

FIGURE 3.1: Predicted domains (Mills et al. 2014) are depicted with different colors and their relative location is drawn to scale within the full-length protein: ARM, armadillo repeats; ANK, ankyrin repeats; LRR, leucine-rich repeats; ROC, Ras Of Complex proteins GTPase; COR, C-terminal Of ROC; KIN, a kinase; WD40, WD40 repeats. Below each domain, the sequence identity and sequence similarity is reported in the column with same color.

and the link between the two (Taylor et al. 2007; Civiero and Bubacco 2012) (Reyniers et al. 2014), (Dachsel et al. 2010), (Klein et al. 2009). Up to now, it has been a challenge to isolate a sufficient quantity of intact, full-length LRRK2 or LRRK1 protein for structural analysis. The available structural knowledge about LRRK2 comes from the study of related ROCO proteins in lower organisms. Only crystal structures for the ROC, ROC-COR and kinase domain have been published so far (Gotthardt et al. 2008; Deng et al. 2008; Gilsbach et al. 2012). Although, these structures have advanced our understanding of LRRK2 functions, the inferred functionality of the full-length protein is indirect. Similarly, structural information about LRRK1 is minimal with no 3D structures reported, neither of full length nor of LRRK1 fragments. Thus, determination of the full-length structure of both LRRK1 and LRRK2 remains an important goal to further our understanding of LRRK proteins in general as well as the structure function relationships that contribute to pathological activity of LRRK2 in particular. In this study, we report the first 3D structures of the homodimeric complexes formed by full-length LRRK2 and LRRK1, respectively, analyzed by cryo-electron microscopy (cryo-EM) imaging and computational single particle image analysis. Both, 2D analysis of the two complexes and the 3D models ($\sim$ 25 Å resolution), reveal a striking similarity between the domain organization of LRRK2 and LRRK1.

3.2 Materials and Methods

3.2.1 Protein expression and purification

The very first step to structural biology projects is to prepare protein with adequate quality and quantity. Compared to x-ray crystallography, in cryo-EM the quantity required for data collection is much lower, i.e., in micrograms range compared to milligrams required for making protein crystals. The protein of interest can be either purified from a natural source or can be overexpressed artificially. Usually, the amount of protein naturally produced in cells is far less for experimental work. For overexpression of proteins, there are two kinds of broad choices, a prokaryotic expression system or a eukaryotic expression system such as yeast, insect or mammalian cells. In prokaryotic or bacterial expression systems, it is comparatively easier and faster to make the constructs and express proteins. But for big complex eukaryotic protein complexes, the lack of eukaryotic post-translational machinery required for the post-translational modification and proper folding of the target protein, often results in insoluble and aggregated protein. Yeasts are single cell eukaryotes, which grow fast like bacteria and are also easy to culture, but compared to bacterial system, yeast expression system contains eukaryotic post-translational setup. The problem with yeast cell is the chitinaceous cell wall, which is very difficult to lyse, and makes purification of cytoplasmic proteins troublesome. In contrast, insect and mammalian cell expression system are much more time consuming and expensive, and the resulting yield of the target protein is also lower. But the main advantages of a mammalian cell expression system is that it provides the correct folding of protein by performing the correct post-translational modifications such as carrying out complex glycosylation, multi-subunit protein assembly and so on. Therefore, overexpressed protein from mammalian cell culture is much more closer to the natural protein in the respect of the tertiary structure and biological function.

3.2.1.1 Constructs

Constructs for the mammalian expression of 3flag-LRRK1 and 3flag-LRRK2 included the pCHMWS-3flag-LRRK1 and pCHMWS-3flag-LRRK2 constructs, described previously (Danils et al. 2011; Civiero et al. 2012). The protein expression and purification of LRRK2 and LRRK1 from these constructs was carried out in Jean-Marc Taymans lab in Leuven University and were shipped to our lab in Basel on ice bags (4 °C) through FedEx. Another construct used for mammalian expression of 3flag-LRRK2 was the p3XFLAG-CMV-10-LRRK2 (a generous gift from Prof. Takeshi Iwatsubo, described in

(Ito et al. 2007)). This was send on ice through FedEx to setup LRRK2 expression and purification in our lab in Basel (Figure 3.2).

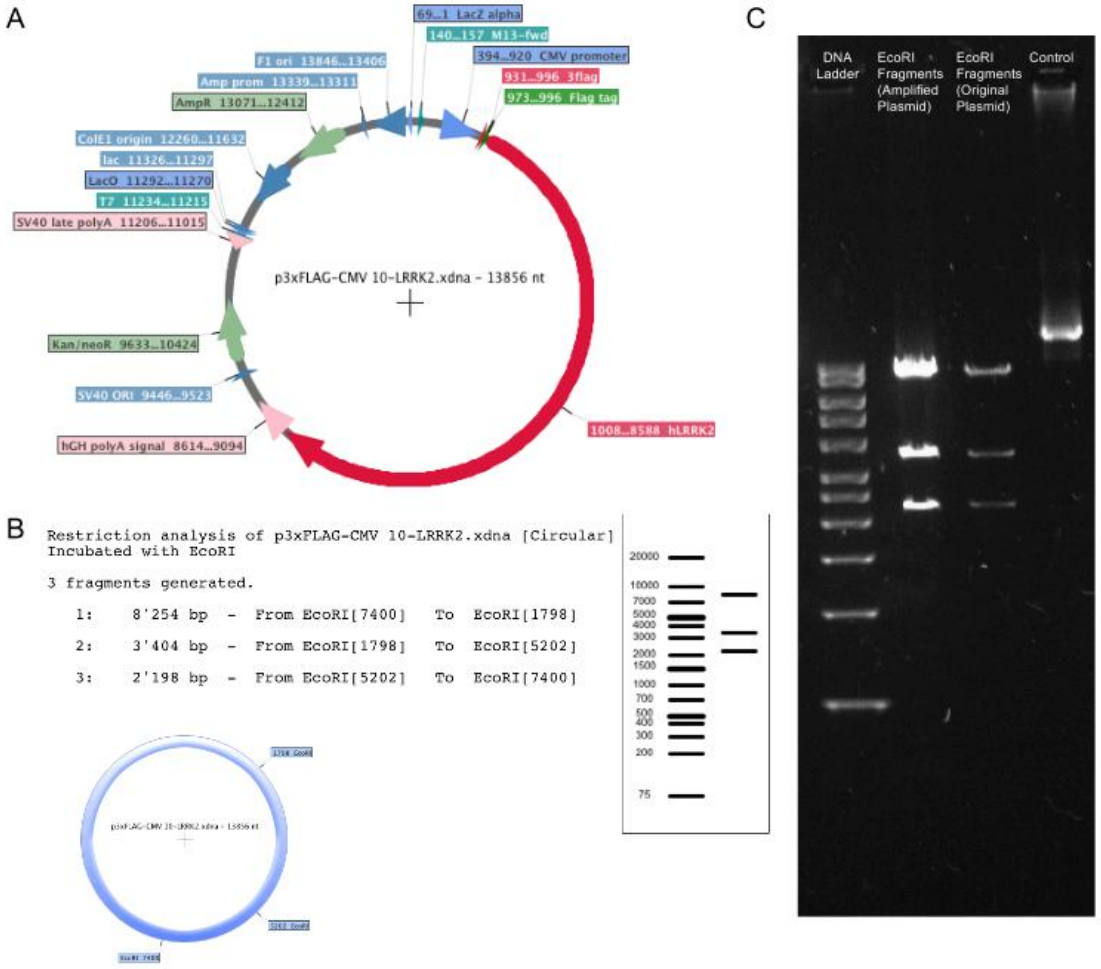

FIGURE 3.2: Plasmid of LRRK2, features and restriction digest. (A) LRRK2 plasmid used for expression and purification. (B)Rragments generated by restriction enzyme EcoRI generated using virtual cutter tool in Serial Cloner v2.6 (C) Gel electrophoresis of the restriction digest fragments.

For plasmid amplification, GenElute HP Plasmid Maxiprep Kit from Sigma were used. Before using the kits, plating was carried out. 1.5 g of Bacterial Agar was measured in a 500 mL conical flask and dissolved in 100 mL LB in microwave for a minute until it was clear. After it got hand warm, 100μlof Ampicillin (100mg/mL Stock) was added to this solution and poured into three petri dishes, evenly and left to get solidified. In the meanwhile DH5 competent cells were thawed on ice. 2μlof diluted plasmid (2 ng/uL) was added to 50μlof DH5 cells. They were further Incubated on ice for 15 min, followed by heat shock at 42 °C in water bath for 30 seconds and further incubation on ice for 2 minutes. 250μlLB medium was added to it and shaken for 60 min at 37 °C on a shaker @ 750 rpm. Around 10% of the total solution was pipetted out onto first agar plate. For rest of the volume, the solution was spinned on a table centrifuge at a maximum rpm for

12-13 seconds. The supernatant was removed and the pellet was resuspended and put onto the second agar plate. Third plate was used as a control.The E. coli was spread gently with sterile glass rod across the agar surface. The plates were incubated overnight at 37 C. Making sure there are good colonies in plate, 5 ml of LB (Take 2 mL of LB if you cant wait for the whole day) was added with 6μlAmp. antibiotic to a 100 ml conical tube. A well-formed, smooth-edged, isolated colony on the agar plate was selected with a sterile toothpick.The tip was then dipped into the LB medium, containing Ampicillin. This was placed on a shaking incubator at 37 C, 200-250 rpm for 8 hours. Check after 3-4 hours, the medium should turn cloudy. 20μlof this starter culture was added to 500 mL LB and 600μlAmp in a 2 L conical flask and placed on a shaking incubator at 37 C, 180 rpm for overnight. The overnight culture was collected on ice and followed the protocol for GenElute HP Plasmid Maxiprep Kit from Sigma to extract and purify the amplified copies of plasmid. The final concentration of the plasmid was measured on the NanoDrop 2000 spectrophotometer (Thermo Scientific).

Before using the shipped plasmid for protein expression and purification, a routine diagnostic restriction digest was performed on the plasmid to confirm its identity. Serial Cloner v2.6 was used to view features and check restriction sites on the amplified p3XFLAG-CMV-10-LRRK2 plasmid. Using the virtual cutter tool in the software, fragments generated by restriction enzyme EcoRI were calculated. EcoRI was used to carried out to digestion the plasmid and fragments were checked by electrophoresis (Figure 3.2,B,C).

3.2.1.2 Cell culture and transfection

HEK293FT cells (Life Technologies) were cultured in 15 cm Corning petri dishes (Sigma), at 37°C in an atmosphere containing 5% CO_2. The culture medium was comprised of Dulbecco's Modified Eagle's Medium (DMEM), 10% fetal bovine serum, 0.1 mM MEM nonessential amino acids (NEAA), 2 mM L-glutamax and 1 mM MEM sodium pyruvate. The medium was changed every 2-3 days and cells were split at 90-100% confluence. During sub-culturing of fresh or thawed cells, the culture medium was supplemented with 500μl/ml Geneticin (G418). One day before transfection, ∼12.105 cells were plated out on a single 15 cm petri dish. Transfection was induced by the addition of polyethylenimine (PEI) (Sigma); 30μg of plasmid (LRRK2 or LRRK1) and 60μl sterile PEI solution (1 mg/ml, pH 7.0) were dissolved in 800μlDMEM (without additives) and added to the petri dish. To check the efficacy of transfection of HEK293T cells, a petridish was transfected with GFP plasmid in parallel to the LRRK1 and LRRK2 transfections and checked in confocal microscope as a positive control.

3.2.1.3 Protein Purification

The constructs for expression of LRRK2 and LRRK1 included the 3xFlag tag and the purification of LRRK2 and LRRK1 followed the two step affinity purification (Figure 3.3). To start, 48 hours after transfection with LRRK1 and LRRK2 constructs, the cells were rinsed with phosphate-buffered saline (PBS) and lysed in 1 mL lysis buffer (20 mM Tris/HCl pH 7.5, 150 mM NaCl, 1 mM EDTA, 1% (v/v) Triton X-100, 10% glycerol and protease inhibitor cocktail (Sigma)), on ice, for 10 min. The collected lysate was centrifuged at 4°C for 10 min at 18280 g to remove cell debris. The supernatant was incubated overnight with lysis buffer equilibrated anti-Flag M2 agarose beads (Sigma-Aldrich) at 4°C on a rotator mixer (STARLAB, Germany). Beads were washed four times with wash buffer (25 mM Tris/HCl pH 7.5, 400 mM NaCl, 1% (v/v) Triton X-100). Washing was done in batch by first pelleting the agarose beads by low speed centrifugation (400g for 2 minutes at 4°C) or allowing them to sediment at 4°C (i.e., on ice). After the wash step, protein was eluted from the beads by adding 5 volumes of elution buffer (20 mM Tris/HCl pH 7.4, 200 mM NaCl, 5 mM MgCl2 1 mM DTT, 0.02% (v/v) Triton X-100) with 100μg/ml of 3xflag peptide (Sigma) and rotating this on a wheel at 4 degrees for 30 minutes (STARLAB, Germany). Afterwards, the beads were spun down at 400 g for 2 minutes and supernatant containing the eluted protein was collected. The purified protein was used straight away for EM analysis or stored in 50% glycerol in -20 °C for future use. All the buffer noted above were used before the ProteoPlex screening buffer screening (next section), for LRRK2, new buffer conditions were used for purification and data collection. For LRRK1, the above noted buffers were used for purification and cryo-EM analysis.

3.2.2 SDS-PAGE and Silver Staining

Sodium dodecyl sulfate-polyacrylamide gel electrophoresis (SDS-PAGE) is a common method used for separating protein mixtures according to their molecular mass by electrophoresis. SDS is a strong ionic detergent that is used to denature the proteins and decorate them with negative charges. A discontinuous polyacrylamide gel is used a as a support medium. For LRRK2 and LRRK1, NuPAGE Novex 3-8% Tris-Acetate precast commercial gels were used (Life Technologies). These gels are designed for optimal separation and resolution of large proteins (36 - 500 kDa) under denaturing gel electrophoresis condition. Purified protein were mixed with 2x SDS loading buffer and left at RT for at least 20 minutes before loading them into the gel. Heating the sample for denaturing was avoided as it caused migration artifacts in the gel on staining. Gels were inserted into the Bio-rad chamber gel kit and filled with NuPAGE Tris-Acetate SDS

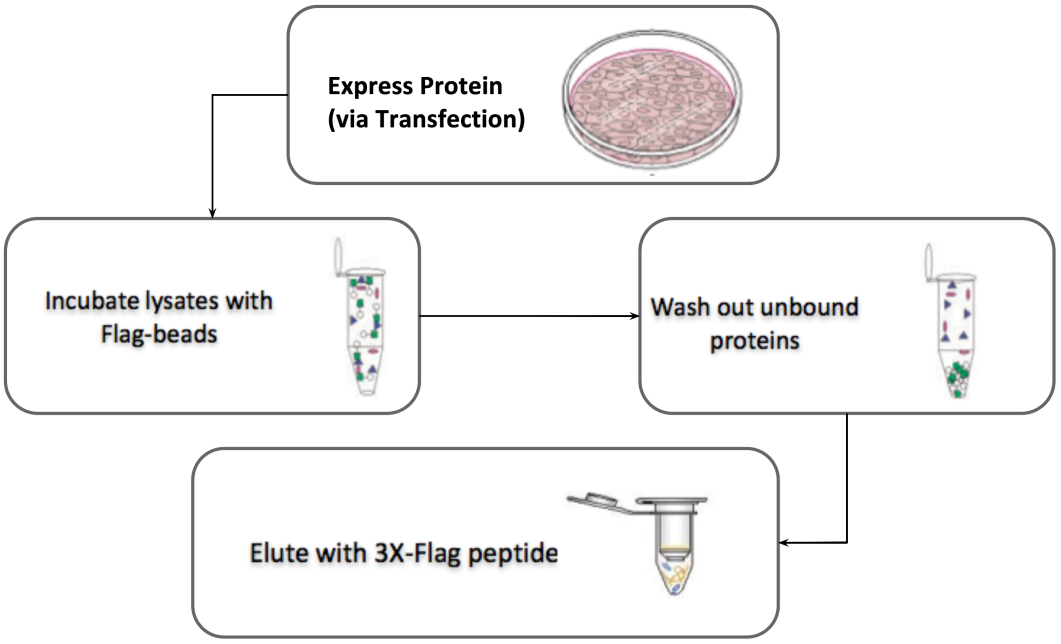

FIGURE 3.3: Workflow of the protein purification of LRRK2 and LRRK1.

Running Buffer (Invitrogen). 10 - 20 micrograms of protein per well are added, along with molecular mass markers (Precision Plus Protein Dual Color Standards, 10-250 kDa, Bio-rad) for size estimation. High voltage running condition were used for the pel at 35 mA for 1 hour. After electrophoresis the module was disassembled and the gel was carefully removed.

Protein Gels were stained with Coomassie Brilliant Blue G (Sigma). The gel was placed in solution containing 0.05% Coomassie, 50% methanol, 10% acetic acid, water and placed on a shaking plate for 30 minutes to overnight, until the gel displayed a uniform blue color. Once the staining is complete and the gel was no longer visible in the dye solution, it was rinsed in distilled water and destained for 4 - 24 hours in 50% methanol, 10% acetic acid, water. A paper or sponge was also used to absorb extra dye. Destaining was done until the background was clear. Coomassie staining works best to detect protein sample on the gel which as at least 100 ng per band. The yield of LRRK2 was usually lower than 100 ng per band, therefore it was only visible in coomassie stained gels when the yield was exceptionally good or concentration of the protein was increased prior to SDS-PAGE. Therefore the gel were further stained by silver staining method. Silver staining is a sensitive gel staining technique that utilises the protein binding properties of silver ions, which are then reduced to silver metal using a developing solution, creating a visible image. The primary benefit of silver staining is its high sensitivity, as it is able to detect less than 1 ng of protein (Weiss et al., 2009), making it extremely useful for applications involving low protein levels.

For LRRK2 and LRRK2 the routine yield from different preparation was between 10-20 ng/ml, silver staining was an appropriate staining method. For silver staining, the first step is the fixation step where the gel after SDS-PAGE was placed in a solution of Fixer 50% methanol, 12% acetic acid and water. Next is the sensitizing step, where the gel was washed thrice in 30% ethanol solution for 20 minutes each, following 1 minute incubation with solution containing sodium thiosulphate. The third step is the silver reaction, where the gel was rinsed in distilled water thrice for 20 seconds each before incubating in silver nitrate and formaldehyde solution for 20 minutes. The fourth and the final step is the development of silver stain gel for which, the gel is rinsed briefly in water for 20 seconds and placed in a sodium bicarbonate and formaldehyde solution for few seconds to minutes and carefully inspected, until the bands starts to appear on the gel. Immediately after that, the gel should be placed back into the starting fixing solution to stop the gel form being overexposed.

3.2.3 Western Blotting

To perform western blotting, polyacrylamide gels after running SDS-PAGE were blotted onto polyvinylidenedifluoride (PVDF) membrane in transfer buffer using the Fusion FX apparatus from Witec AG. PVDF membranes were prepared by dripping them in methanol solution for 1 minutes and placing in a transfer buffer comprising of Tris 50 mM, Glycine 40 mM, SDS 0,04%, Methanol 20%. A sandwich is prepared by wetting filters and sponge pads before in the transfer buffer. Care has to be taken not to trap any air bubbles between filter paper, gel and membrane, which would hinder protein transfer. The sandwich was placed in blotting apparatus with blotting membrane facing the positive pole for wet blotting for 1-2 hours at 30 Volts, 200 mA. Afterwards, the module was disassembled and the membrane was labelled for orientation of loaded samples. For subsequent immuno-probing, unspecific binding sites were blocked by placing the membrane in phosphate buffered saline (PBS) blocking buffer containing 0.1% Tween 20, 5% nonfat dry milk for 30 min to 2h at RT or overnight at 4°C. The blocking solution was removed and the membrane was then incubated for 3h at room temperature to overnight at 4°C with primary antibody, anti-LRRK2 antibody [MJFF2 (c41-2)] (Abcam) at an appropriate dilution of 1:1000, in PBS, 0.1% Tween 20, 5% nonfat dry milk. The PVDF sheets are washed in PBS and 0.1% Tween 20 (three to four times for 10 min) at room temperature. Incubation with secondary antibody, anti-rabbit IgG - peroxidase antibody produced in goat (Sigma) at 1:20.000 dilution in incubation buffer followed. The blots were washed in PBS, 0.1% Tween 20 or PBS, 0.1% Triton (three to four times for10 min) at room temperature and rinsed in PBS.

For detection enhanced chemiluminescence plus (ECL+) technique (Amersham Pharmacia Biotech, Little Chalfont, England), was used. The reagent consists of two components, enhanced luminol reagent and oxidizing reagent, that are mixed in a 1:1 ratio shortly before use. The membrane was lightly blotted against tissue paper after washing to remove excess liquid and then incubated with 1 ml detection agent for 1 min. Excess detection solution was removed with tissue paper. The membrane was transferred into a film cassette, covered with plastic foil and exposed to an X-ray film (Hyperfilm, Kodak) in a darkroom. The film was exposed for a few seconds up to 30 min or longer depending on the amount of protein to be detected. Films were developed in a Fusion FX apparatus from Witec AG.

3.2.4 Liquid chromatography-mass spectrometry (LC-MS)

Purified LRRK2 samples were prepared for LC-MS analysis by dissovling in a lysis buffer (2% sodium deoxycholate(SOC) in 100 mM ammonium bicarbonate) in the volume two times bigger than the volume of protein sample. 1μl TCEP buffer was added per 40μl protein extract. It was vortex for 10 sec and then ultrasonication of samples was done for 2x10 sec with a vial Tweeter. (Samples were put on ice between steps) The samples were then heated for 10 minutes at 95°Cat 1000 rpm. The samples were allowed to cool down and spin down at 10,000 rpm for 10 sec. This was followed by protein digestion by trypsin was added to the samples to a final protein ratio of 1:50 and digested at 37°Covernight. Trifluoroacetic acid TFA was added to a final concentration of 1%. The SOC in the sample precipitated and the samples were centrifuged at 14000 rpm for 30 min at 4 C. The supernatant was transferred to a new tube and it was centrifuged again at 14000 rpm for 15 min at 4 C. The supernatant was then used for solid phase extraction.

The C18 columns were conditioned with 150μl acetonitrile at 1600 rpm for 30 sec and this step was repeated 2 times. Then the columns were equilibrated 2X with 150μl buffer A at 2400 rpm for 30 sec. The samples were then loaded and spin into a new tube at 1800 rpm for 2 minutes. The flow through was reloaded and spin again at 1800 rpm for 2 minutes. The columns were then washed 3X with 150μl°Cat 2400 rpm for 30 sec. The bond peptides were eluted into new tubes with 2X 150μl buffer B at 1600 rpm for 30 sec. The eluted peptides mixture were concentrated under vacuum to dryness for 1-2 hours. The peptides were dissolved in LC-MS/MS LC buffer A right before use; using 1X5 sec ulltrasonication and shaking it at 1400 rpm at 25°C for 5 minutes before LC-MS/MS analysis. The final concentration of peptide was adjusted to 0.5 ug/uL using LC- buffer A. The samples were filled into LC vial (minimum 10μl, better 20μl) and the air bubbles were removed either by shaking the vials or a short centrifugation at low

rpm. The samples were then stored at -20°C before they are analysed at the LC-MS instruments at the Proteomic Core Facility at the Biozentrum, University of Basel. The data generated from the LC-MS was analysed in Scaffold Software version 4.4.

3.2.5 Grafix

Purfied LRRK2 were subjected to stabilization in a continuous glycerol/glutaraldehyde gradient by the GraFix method (Kastner et al. 2008). Using gradient master (Biocomp Instruments) a continuous 10-30% (vol/vol) glycerol gradient in 4 mL centrifuge tubes (Beckman). 120μlof the sample were applied on the top of the tube, together with 0.025-0.1% glutaraldehyde and allowed to settle for 1h at 4°C. As a control, sample was also applied into a similar glycerol gradient without the cross-linking agent, which were later used for LC-MS analysis to determine the presense of LRRK2. Centrifugation was performed at 34,000 rpm in a SW 60 Ti-Rotor rotor (Beckman) for 14 h at 4 °C. After centrifugation, 300 μl fractions were collected from the top of the tubes and 80 mM glycine pH 8.0 to quench the cross-linking.

3.2.6 Sample optimization by ProteoPlex screening

One of the major challenges in cryo-EM and other structural biology approaches in general is to obtain purified macromolecules in an intact and stable manner. Most of the macromolecular complexes amiable for cryo-EM analysis are composed of several individual biomolecules or a single protein is consists of several individual domains. These complex assemblies are often prone to dissociation and aggregation. This imparts conformational heterogeneity in the purified protein. Therefore, optimisation of the sample preparation for cryo-EM is a crucial step and can often be limiting step towards getting a 3D structure to interrogate their function within cells. ProteoPlex is a new method that is based on Differential scanning fluorimetry (DSF), which can aid in the study of stability of your interest of protein complex as a function of buffer conditions. DSF is a method that has been used successfully in x ray crystallography studies to determine stabilizing buffer conditions and measure ligand interaction of single chain proteins. Proteoplex take the methodology further and develop a new thermodynamic framework to incorporate complex unfolding curves which are characteristic of macromolecular assemblies. In ProteoPlex, small amount of protein is used to screen a range of buffer conditions at different pH in a 96-well plate together in the present of a fluorescent dye. The whole system is heated up and upon subsequent unfolding of the protein sample; the hydrophobic side chains in the residues are exposed, which results in the dye getting

hyperfluorescent. As the concentration of the unfolded protein is increased, the protein starts getting aggregated and the hydrophobic residues are hidden from generating fluorescence signal (Figure 3.4). Hence the melting temperature of the protein in that particular buffer composition can be determined and is related to the stability of the protein. The higher is the needed melting temperature, the more stable is the protein.

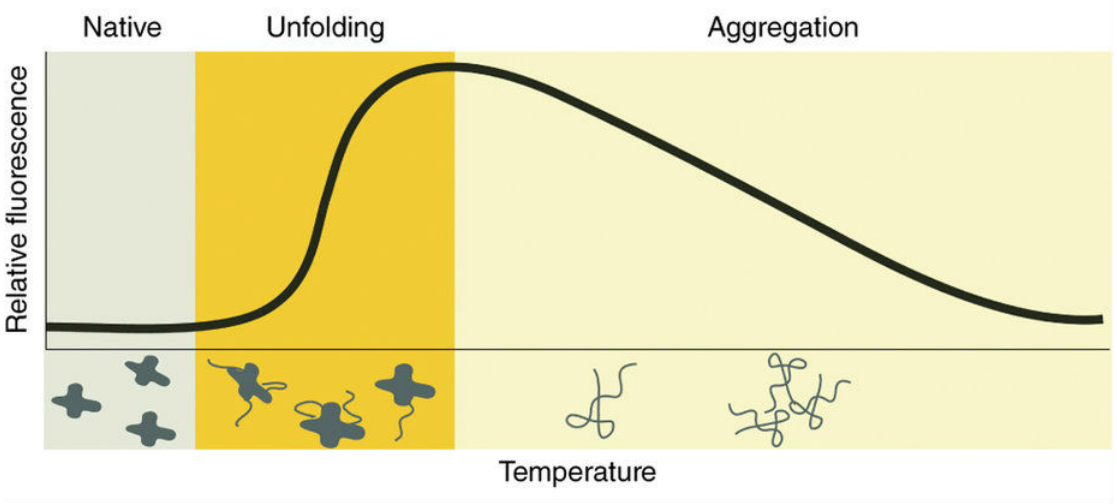

FIGURE 3.4: Basics of ProteoPlex : Representative unfolding transition as obtained by ProteoPlex or DSF. The transition consists of three phases. (i) In the native state, proteins or macromolecular complexes do not interact with the dye Sypro orange. (ii) In the unfolded state, exposed hydrophobic regions bind Sypro orange, causing the dye to become hyperfluorescent. (iii) During the aggregation phase, the proteins or macromolecular complexes interact with each other and compete for dye-binding sites, leading to a decrease in fluorescence. (Chari et al., 2015)

During the purification, a few aliquots of anti-Flag M2 agarose beads with bound LRRK2 were not treated further, but stored in storage buffer (20 mM Tris/HCl pH 7.4, 200 mM NaCl, 5 mM MgCl2 1 mM DTT, 0.02% (v/v) Triton X-100, 50% glycerol) and shipped on ice (4°C) for ProteoPlex analysis. The ProteoPlex assay was performed in a 96-well plate as explained in (Chari et al. 2015); the 20-μl reaction mixtures contained different buffers at various pHs (Table S1). Following the outcome of ProteoPlex screening, new optimum buffers were used during the purification of LRRK2 for binding and elution of pure protein. LRRK1 was purified with buffers as noted in previous section.

3.2.7 Electron microscopy

For negative stain transmission electron microscopy (TEM), 3.5 μl of purified protein sample was pipetted onto a glow-discharged, carbon-coated copper grid and left to adsorb for 1 minute. The grid was then washed on three droplets of milliQ water, and

subsequently stained on two droplets of 2% uranyl acetate for another 1 minute, blotting between each step. Grids were scanned using a Philips CM10 TEM (FEI Company, Eindhoven, The Netherlands) operated at 80 kV under low-dose conditions (20 electrons/Å2). Images were collected at a nominal magnification of 96,000x at various defocus values between -0.5 to -1.5 μm, and recorded with a 2K Veleta side-mounted TEM CCD camera (Olympus), corresponding to a pixel size of 3.8 Å at the specimen level.

For cryo-EM, 3.5 μl of the purified protein sample was pipetted onto a glow-discharged, holey carbon films (Quantifoil R2/2, Quantifoil Micro Tools, Jena, Germany) with an additional thin layer of carbon, and left to adsorb for 1 minute (Figure 3.14, B). The grids were then rapidly plunge frozen in liquid ethane, cooled by liquid nitrogen, using a MarkII Vitrobot (FEI, Eindhoven, Netherlands). The frozen grids were transferred to a Gatan-626 cryo-holder. Micrographs were recorded under low-dose conditions (25 electrons/Å2) on a CM200 TEM (FEI Company, Eindhoven, The Netherlands) operated at 200kV with 58,000x nominal magnification. Data was collected using a TVIPS F416 CMOS camera (TVIPS, Gauting, Germany). The range of defocus used for collecting micrographs was between -1 to -2.5 μm.

3.2.8 Image processing

The EMAN2 software suite (Tang et al. 2007) was primarily used. Particles, i.e., image of LRRK2 or LRRK1 complexes, were boxed out interactively from the negative stain TEM or cryo-EM micrographs using the e2boxer interactive procedure. Contrast transfer function (CTF) correction was accomplished by producing high-pass filtered phase-flipped particles, using the e2ctf program. Reference-free class averages were generated using the e2refine2d program, requesting the generation of 128 classes with a maximum of 100 particles per class. Initial models were produced with the e2initialmodel utility from the best 2D class averages (10 in all), both without imposed symmetry and with imposed C2 symmetry. The final 3D maps were refined using the standard iterative projection matching, class-averaging and Fourier reconstruction procedure of EMAN2. The resolution of each reconstruction was determined by the gold standard Fourier shell correlation criterion. UCSF Chimera (Pettersen et al. 2004) was employed to visualize and analyze the final maps. For comparison, after the CTF correction in EMAN2 the particles were fed into the Relion software (Scheres 2012) and compared. Using the newly incorporated e2refinetorelion2d functionality in EMAN2 (Bell et al. 2016), same particles as processed in EMAN2 were exported and run for 25 rounds of 2D reference-free class refinement in Relion 1.2 with 128 classes in total.

3.3 Results and discussion

3.3.1 Purified LRRK2 and LRRK1 are unstable for longer period

At the beginning of the project, purification of LRRK2 and LRRK1 was carried out in the research group of Jean-Marc Taymans at University of Leuven, Belgium and shipped in small aliquots on ice (Figure 3.5). Proteins were aliquoted and shipped at 4 °C in two different ways: Purified proteins eluted in elution buffer (20 mM Tris/HCl pH 7.4, 200 mM NaCl, 5 mM MgCl2 1 mM DTT, 0.02% (v/v) Triton X-100) and non-eluted protein bound to anti-Flag M2 agarose beads stored in storage buffer (20 mM Tris/HCl pH 7.4, 200 mM NaCl, 5 mM MgCl2 1 mM DTT, 0.02% (v/v) Triton X-100, 50% glycerol). The latter was washed in normal elution buffer several times to remove any traces of glycerol which not suitable for cryo-EM sample preparation and eluted with 3xflag peptide to get purified protein. The shipping time for the protein aliquots ranged between 2-3 days. The aliquots where the protein LRRK2 and LRRK1 was already eluted and purified, negative strain grids were made straightway to test the protein quality. The particles appeared mostly aggregated on the grids and the quality was not good. Cryo-EM grids were also made for the same sample but the similar aggregation was observed. When the silver stain of the protein preparation was compared with the particles from EM, the protein sample looked much more cleaner on the gel with good quality and no major contamination. We suspected the LRRK2 and LRRK1 to be unstable on ice for a longer period post their elution during the shipping. Next, we checked the aliquots of LRRK2 and LRRK1 which were shipped in 50% glycerol still bound to anti-Flag M2 agarose beads. After the washing and elution steps which took 1 hour, the purified proteins were used to prepare negative stain and cryo-EM grids. Less aggregates were visible in the preparation and some particles were clearly seen in the negative stain which were corresponding well the the expected size of the proteins. It was clear that the protein is much more stable during the shipment when bound to the anti-Flag M2 agarose beads and presence of 50% glycerol also protected the protein from aggregation. Therefore it was decided for all the subsequent shipments of LRRK2 and LRRK1 from Jean-Marc Taymans lab in Belgium will be non-eluted protein aliquots. One challenge that was still present with the protein samples shipped bound to the anti-Flag M2 agarose beads is the lack of correlation between the purity of the preparation as shown by the silver stain gel and the quality of particles in the negative stain grids. Even when the sample was very pure on the gel, it looked very heterogenous in the negative stain grids with some aggregates. The discrepancy between the silver stain gel and the negative stain EM images could be attributed to the shipment process as the sample used for silver staining were instantly denatured with sodium dodecyl sulfate (SDS) for silver staining while the protein could only be eluted for the EM analysis after 2-3 days of shipping

time. Although in some preps the particles looked reasonably homogenous and some data was cryo-EM collected to perform single particle image processing, the majority of the shipments looked too heterogenous to collect more EM data. For the preps where the quality was good and there was no presence of contaminants observable in the gel, reproducible negative staining grids and cryo-EM grids were not possible, and hence, to troubleshoot if the problem is arising from the quality of the sample degrading on ice during the shipment time or from other factors, it was decided to setup the expression and purification of LRRK2 in-house in the lab in Basel, to minimise the time between the elution of purified protein to sample preparation for cryo-EM and negative stain EM. For LRRK1, the sample quality was comparatively better than that of LRRK2 and the shipped aliquots were only used to collect cryo-EM data for 3D reconstruction.

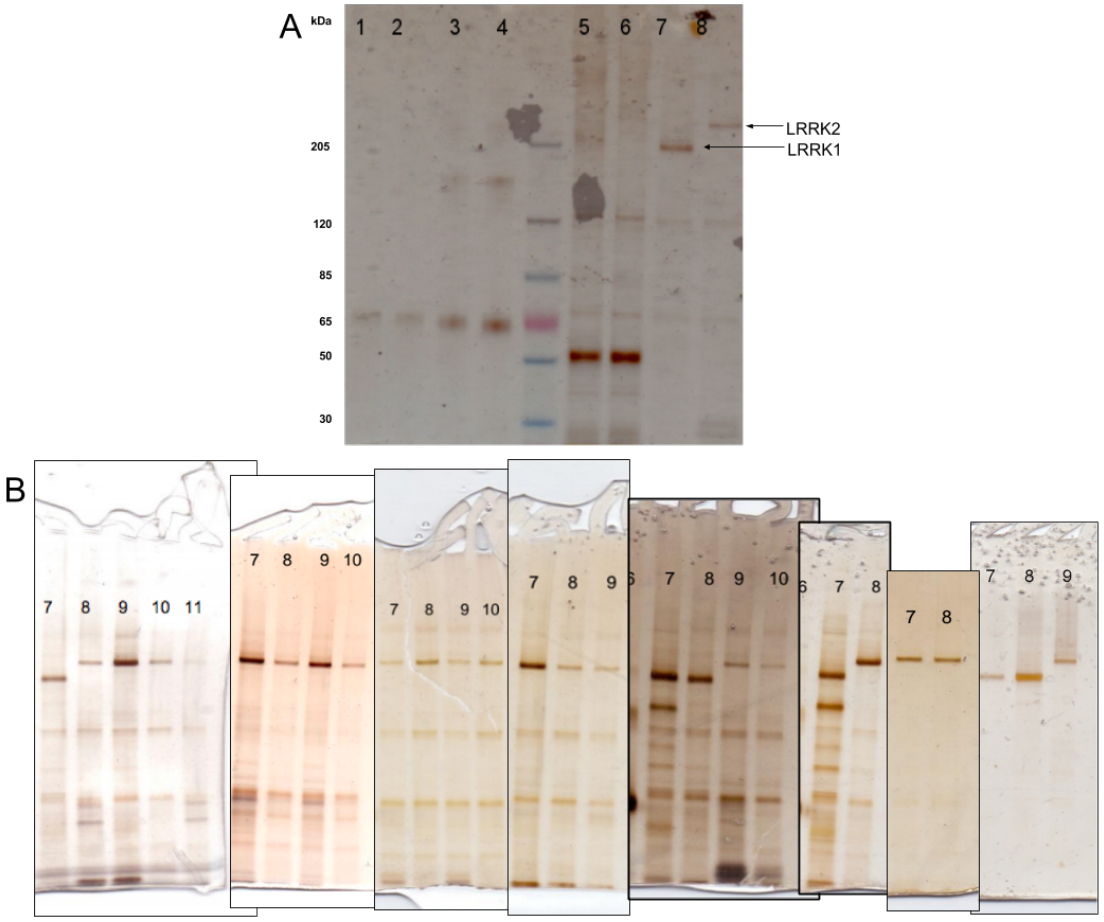

FIGURE 3.5: Purity and concentration assessment of 3flag-LRRK1 and 3flag-LRRK2, shipped form Leuven, by silver stained SDS-PAGE. (A) A representative gel form one of the purification preparation shipped on ice from Leuven. 3flag-tagged proteins adsorbed to anti-flag M2 agarose beads were eluted with 3flag peptide. Eluted samples are in lanes 7-8 and correspond to about 10 ng/μl of protein. Lanes Lanes 5-6 has anti-flag M2-agarose beads. Lanes 1-4 shows BSA at 5, 10, 20 and 40 ng/μl. (B) Montage of silver stained SDS-PAGE of all the purification preps for LRRK2 and LRRK1 send from Leuven. The quality, purity and yeild varied between different preparations.

Cell cultures for HEK293 cells was setup in our lab in Basel and transfection efficacy of the cells was tested by transfecting some cells with a green fluorescent protein (GFP) plasmid. The cells expressed the GFP well for the same transfection condition to be used for LRRK2 (Figure 3.6,A). LRRK2 expression and purification was optimised and checked with silver stained SDS-PAGE (Figure 3.6,B). Quality and yield of the purified protein was reproducible and matched well with that from Leuven (compare with Figure 3.5). Further to be sure if the purified band on SDS-PAGE, corresponding to the size of LRRK2 is inded LRRK2, western blotting was performed and LRRK2 presense was confirmed (Figure 3.6,C).

3.3.2 Buffer optimization by ProteoPlex screening

The production of protein in high yield and purity is a prerequisite for structural analysis by cryo-EM (Glaeser 2015). Each 15cm Petri dish of the cell culture yielded approximately 50μg of purified protein. This was sufficient for initial negative stain TEM imaging, and for cryo-EM if the Quantafoil grids employed were coated with an additional carbon film. Pooling the cell lysate from several Petri dishes and eluting the protein in less volume (see Materials and Methods) resulted in protein concentrations for LRRK2 and LRRK1 as high as 0.7 mg/ml (Figure 3.14, A). Ultra-centrifugal filter devices could not be used to concentrate either protein, because both tended to precipitate and bind to the membrane material. Although the concentrated purified protein sample was used immediately to minimize any degradation with time and silver stain gels showed it to be pure, negative stain TEM revealed a very heterogenous mixture of particles. The difference clearly indicated that LRRK2 is unstable in the buffer system used, Tris/HCl pH 7.4.

ProteoPlex analysis (Chari et al. 2015) was used to determine the buffer conditions that gave the highest binding of LRRK2 to the agarose beads during purification, and those that were best for the elution step and protein stability. ProteoPlex uses sparse-matrix screening of a proteins thermal unfolding behavior in under various conditions to find the optimum buffer system and pH. Similar methods using differential scanning fluorimetry are routinely used in X-ray crystallography to optimize the quality and quantity of protein sample for further crystal screening (Reinhard et al. 2013), but so far have rarely been used for cryo-EM studies. All buffers used in the LRRK2 screens contained 0.02 % of Triton X-100 (see below). Proteoplex 88 buffers screen was carried out and state transition graphs were recorded for each buffer condition. While performing the buffer screen, 3xFLAG-LRRK2 bound to M3 agarose beads. Substantial peak were detected between 20 and 45°C (Figure 3.7,A). Hepes buffer at pH 6.8 was the most favorable for protein extraction by agarose beads (Figure 3.8A). Following the findings,

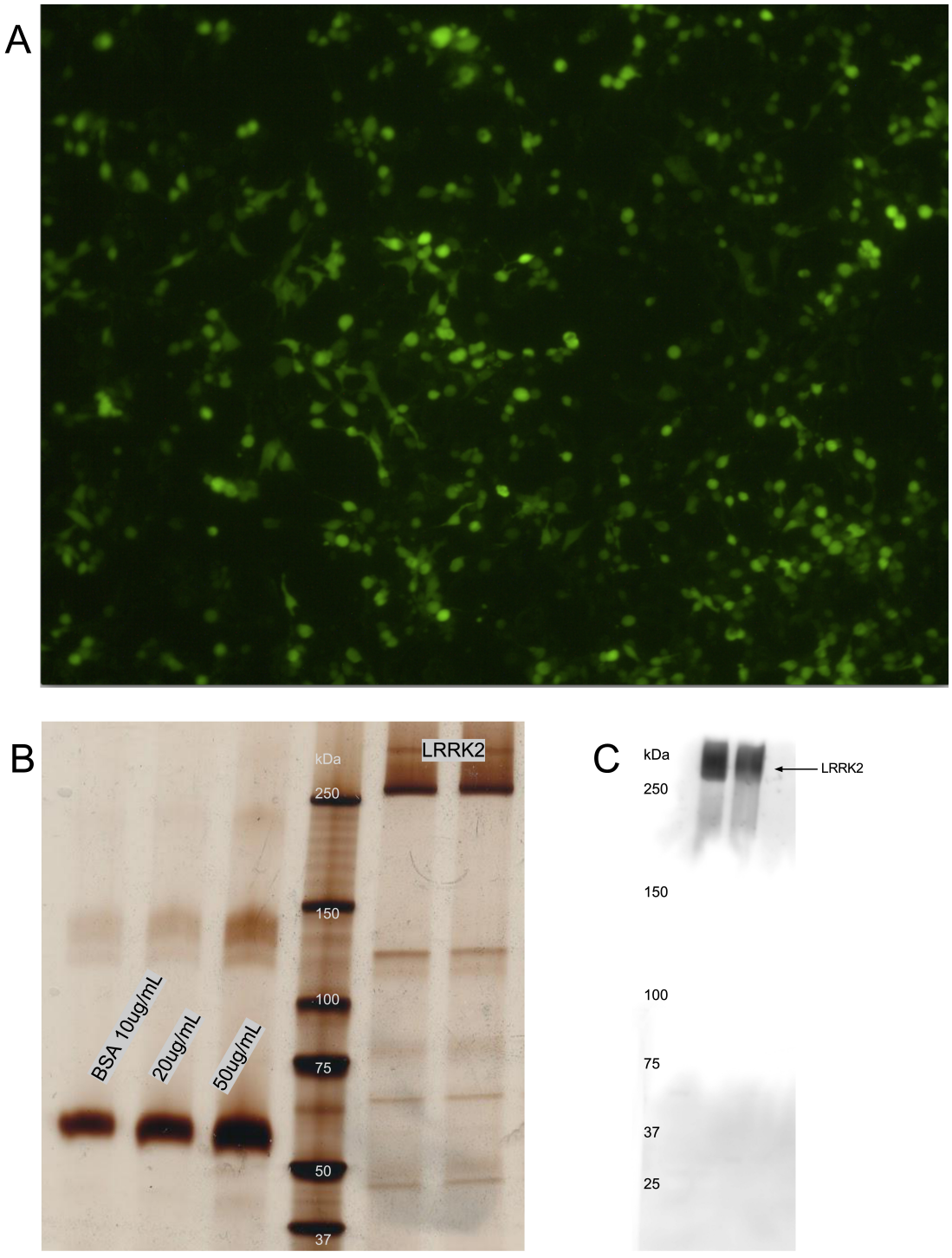

FIGURE 3.6: Expression and purification of full-length 3xFlag LRRK2.(A)Representative confocal image of HEK293T cells transfected with a GFP plasmid used as a positive control. (B)Silver stained gel of purified LRRK2. The protein concentration was roughly 10μg/ml (comparition from the BSA concentration markers in the first three lanes). There are strong bands at the molecular weights expected for LRRK2, respectively indicating highly pure protein fractions. The silver stain is slightly overexposed and the contamination visible at lower molecular weights are overrepresnted. (C) Western blot analysis of LRRK2 probed with anti-LRRK2 primary antibody followed by detection with goat anti-rabbit secondary antibody. Markers are in kilodaltons

new purification of LRRK2 was carried on using Hepes pH 6.8. We tested the new buffer conditions, together with control with binding buffer pH 7.5 by doing negative stain EM of the new purified LRRK2 at binding buffer pH 6.8. A drastic change in sample quality was observed (Figure 3.10A and B). There was a slight increase in the purity of the purified protein as seen in the silver stained SDS-PAGE, few impurities which were present in the purified LRRK2 with binding buffer at pH 7.5 were absent in the purified LRRK2 with binding buffer at pH 6.8 (Figure 3.10E). Next, the purified LRRK2 carried out with binding buffer of Hepes pH 6.8 was again used to perform ProteoPlex buffer screening for the elution buffer. When the same buffer as that of the binding buffer was used to elute the protein, state transition calculated by ProteoPlex were very weak but visible. I could not be excluded that the weak observable state transition might be due to the agarose beads that are left after the elution. Also there were protein aggregates visible in the graphs during the elution(Figure 3.8,B). Therefore, the elution conditions were also optimized as they are different from binding conditions. Proteoplex 88 buffers screen was carried out and state transition graphs were recorded for each buffer condition (Figure 3.7,B). Hepes buffer at pH 8.2 was found to provide the best conditions for elution of LRRK2 (Figure 3.9). A fresh purification of LRRK2 was started based on the new elution buffer conditions as well as the binding buffer condition form the first ProteoPlex experiment. In parallel, a control LRRK2 purification using old binding buffer and elution buffer conditions at pH 7.5 and pH 7.4 respectively, was also carried out. Negative stain grids were prepared to assess the quality and improvement in the particles were remarkably visible. A few aggregates were still visible on the negative stain TEM micrographs, but most of the complexes were intact and the background was much cleaner (Figure 3.10C and D). Based on the silver stained SDS-PAGE, a mild improvement in the purity was observed as well (Figure 3.10F).

3.3.3 Detergent is required for LRRK2 to remain correctly folded.

To maximize SNR, any unnecessary buffer components should be avoided. For membrane proteins, the detergent takes a significant toll on contrast (see Figure 2D, right panel). In addition by reducing surface tension the detergent changes the way in which the sample spreads on the support.

It is a well known fact in Cryo-EM, that any unncessary buffer components should be avoided in during the sample prepartion to maximize the SNR in the micrographs (Cabra et al. 2015). One such susbtance that was present in LRRK2 final elution buffer, which impacted the contract in the collected images was detergent. For a soluble protein, its unlikely to have detergent in the protein buffer, they are required mainly for membrane protein. In addition by reducing the surface tension of the buffer they

FIGURE 3.7: Proteoplex 88 buffers screen for binding buffer optimsation(A) and elution buffer optimisation(B)

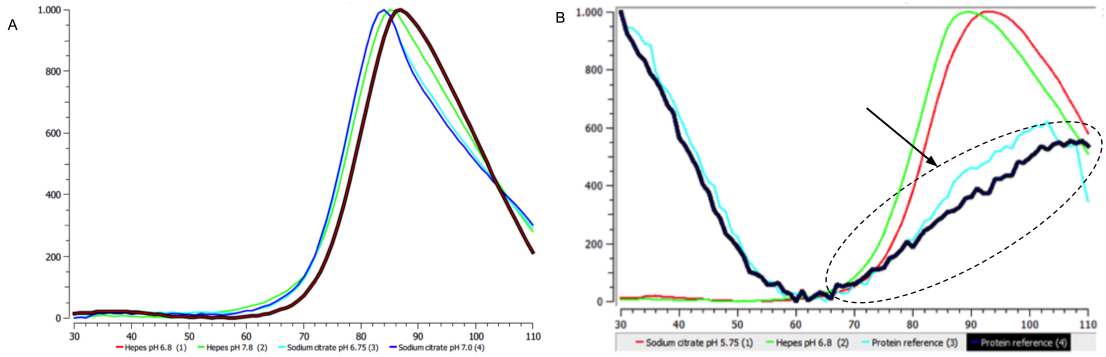

FIGURE 3.8: Binding buffer optimization by ProteoPlex screening: (A) Melting curve profiles obtained for LRRK2 in the presence of top four buffer systems. (B) Melting curve profiles when the same buffer system is used for elution of LRRK2. The arrows marks the aggregation of protein observed. Y axis is relative fluorescence and x axis is temperature.

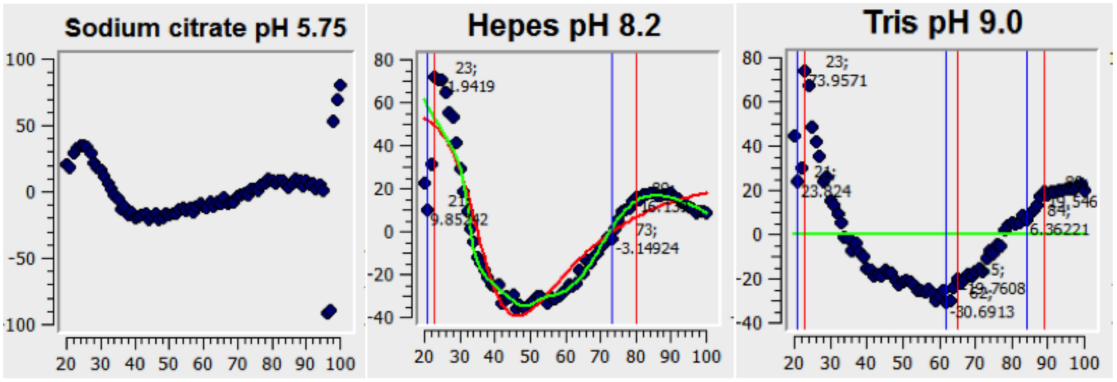

FIGURE 3.9: Elution buffer optimization by ProteoPlex screening: Melting curve profiles obtained for LRRK2 in the presence of top three elution buffer systems. Y axis is relative fluorescence and x axis is temperature

change the way in which protein sample spreads on cryo-EM grids during the blotting steps of vitrification, they also change the way. We tested removal of detegent form the elution buffer of LRRK2 and tested by negative stain. If detergent was not present in the final buffer used to elute the protein on purification, the shape of the protein changed drastically. Negative stain TEM of this preparation revealed mostly globular particles, rather than elongated particles with features (Figure 3.11). This indicates that detergent is essential for LRRK2 to remain correctly folded, and that the detergent might be stabilizing hydrophobic amino acid residues on the surface of the protein. The observation is consistent with reports that LRRK2 associates with membranes (Alegre-Abarrategui et al. 2009; Saha et al. 2009; Schapansky et al. 2014; Biskup et al. 2006). It suggests that LRRK2 has an affinity for lipids. The effect of detergent on LRRK1 was not tested but owing to the similar domain organization to LRRK2 and overlap of cellular functions, similar effect is likely to be expected.

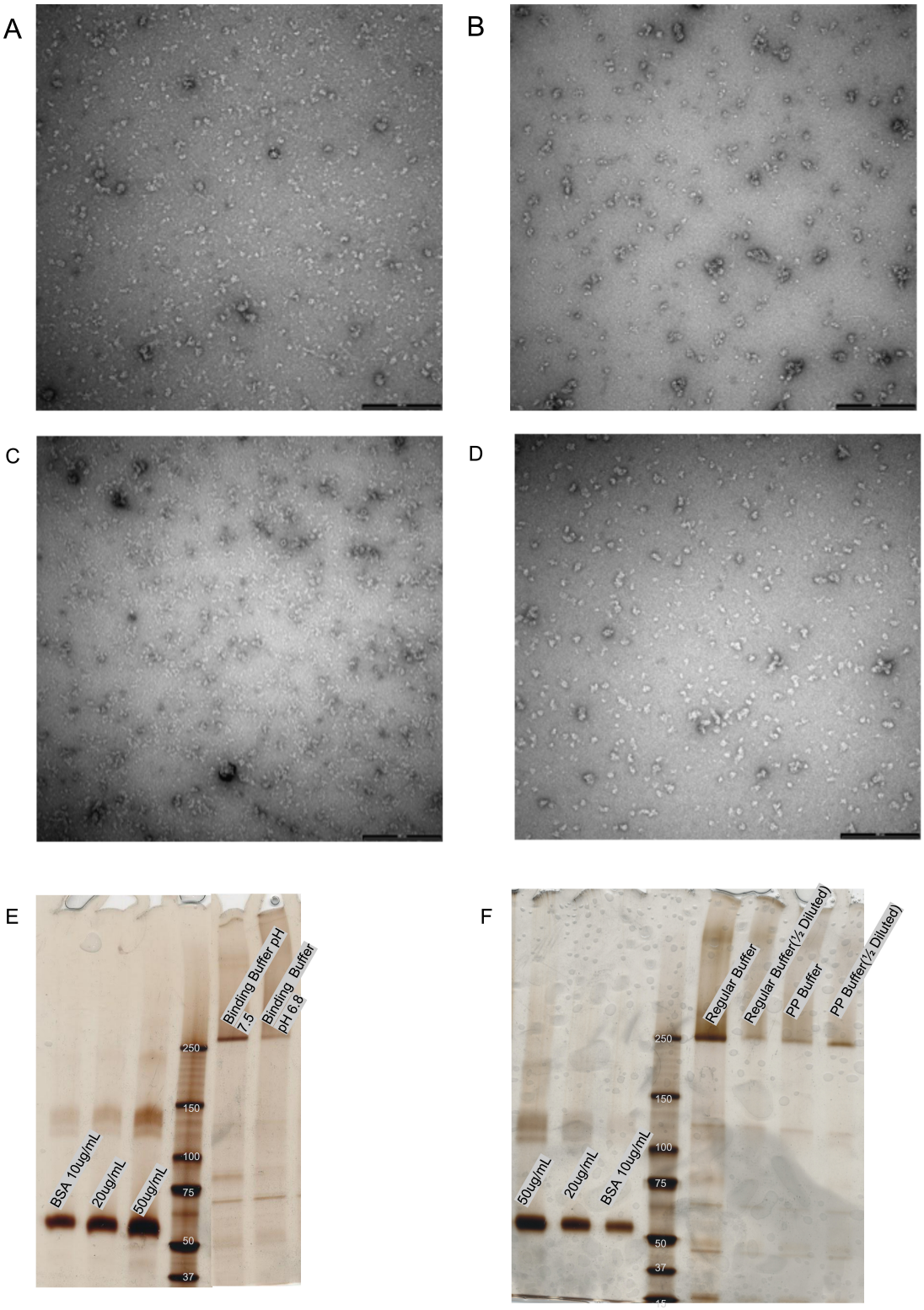

FIGURE 3.10: Buffer optimisation by ProteoPlex: (A)-(B) Comparison of particles in negative stain TEM micrograph of LRRK2 purified in the regular binding buffer (Tris/HCl pH 7.5) vs LRRK2 purified in the ProteoPlex suggested binding buffer (Hepes pH 6.8) (C)-(D) Comparison of particles in negative stain TEM micrograph of LRRK2 eluted in the regular binding buffer (Tris/HCl pH 7.4) vs LRRK2 eluted in the ProteoPlex suggested elution buffer (Hepes pH 8.2) (E)-(F) Silver stained SDS-PAGE of purification of LRRK2 in different buffers used in (A)-(D) Scale bars: 100 nm.

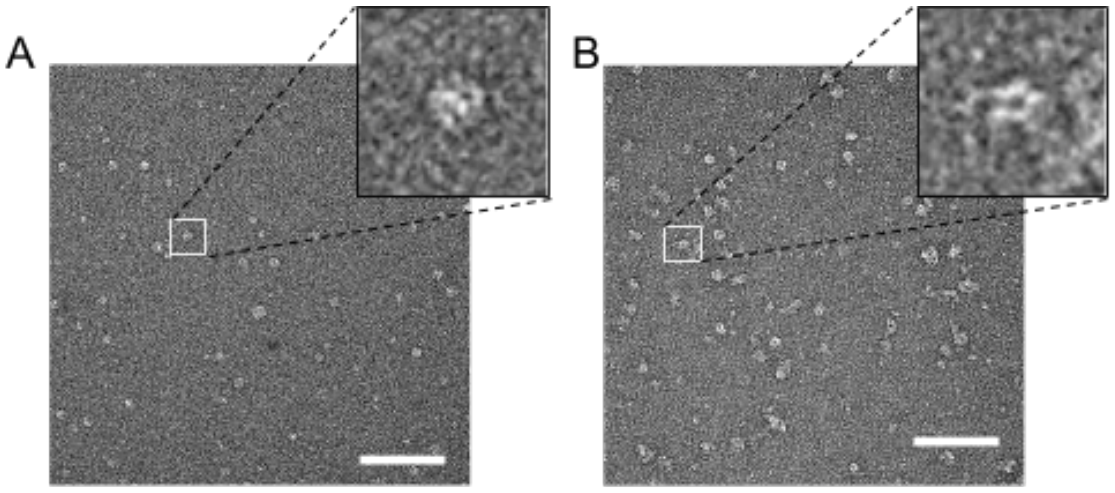

FIGURE 3.11: Effect of detergent on LRRK2 structure.: Negative stain TEM images of LRRK2 eluted using in 20 mM Tris/HCl pH 7.4, 200 mM NaCl, 5 mM MgCl2, 1 mM DTT A. Without the addition of detergent; almost all of the particles have a globular appearance and structural details are not visible. B. With 0.02% of Triton X-100; many of the particles have an elongated shape and some structural detail is evident. Dimeric sides-views are clearly visible (inset). However, there are also some globular particles demonstrating that even in the presence of detergent the protein is not completely stable in the Tris buffer employed. Scale bars: 100nm.

Different types of detergent were also tested in place of the Triton X detergent which was originally used in the all the buffers during the process of protein purification. The detergents that we tested were n-decyl--D-maltopyranoside (DM), NP-30, Lauryl Maltose Neopentyl Glycol (LMNG) and Tween 20. The concentration of these detergents in the elution buffer were kept same as that of Triton, 0.02%. The silver stained SDS-PAGE of the purified LRRK2 in different detergents revealed that the quality of the purified protein doesnt change with the change in detergent (Figure 3.12). Some difference in the quantity of the purified protein as observed with NP-40 and Tween 20, where a slightly higher yield of the purified protein was seen as compared with control preparation with Triton X detergent. The change in the yield was marginal and comes from the slight different surface tension of these detergents which can promote the elution of protein from the M3 agarose beads with 3xflag peptide during the rotation on the wheel before the final elution. If the surface tension of the detergent is higher, the mixing of the 3xflag peptide with the the M3 agarose beads is not fully efficient and leads to lower yield of the purified protein. As far as the shape and structure of the LRRK2 particles, a clear difference was not seen between using different detergents (Figure 3.13). Therefore, 0.02 % of Triton X detergent was continued to be used during the purification steps of LRRK2.

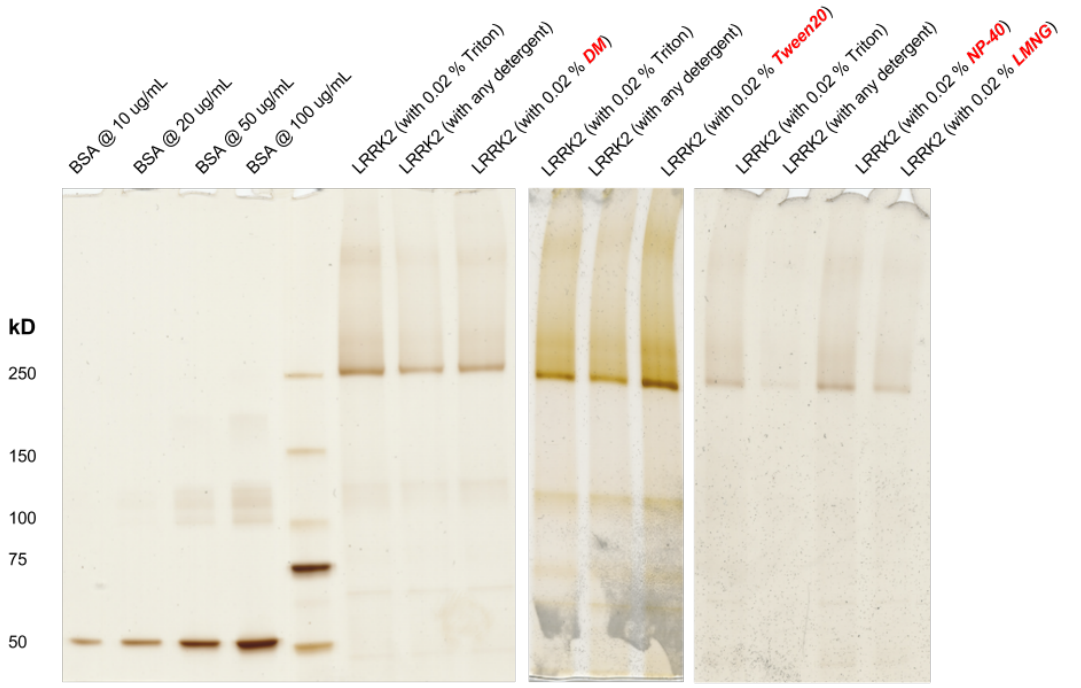

FIGURE 3.12: Silved stained SDS-PAGE of LRRK2 purified with different detergents. (A) n-decyl–D-maltopyranoside (DM) (B) NP-30 (C) LaurylMaltose Neopentyl Glycol (LMNG) (D) Tween 20. The concentration of these detergents in the elution buffer were kept same as that of Triton, 0.02%.

3.3.4 Cryo-EM of LRRK2

The time between elution of purified LRRK2 and cryo-EM grid preparation was kept minimal (60 minutes). The presence of 0.02 % of detergent in the final elution buffer (20 mM Tris/HCl pH 7.4, 200 mM NaCl, 5 mM MgCl2 1 mM DTT, 0.02 % Triton X-100) complicated sample preparation for cryo-EM because of the reduced surface tension of the liquid. After application of the sample to holey carbon grids, blotting and plunge freezing, protein particles were only present on the thick carbon mesh, and none in the vitreous ice regions spanning the holes (Figure 3.14,B). Neither increasing the protein concentration ten fold, nor using Lacey grids, which have mesh-like openings of different sizes and shapes, helped. However, coating the grids with a thin carbon film and adsorbing the protein to this, resulted in a suitable distribution of the protein on vitrification (Figure 3.14, A). These grids were imaged by cryo-EM and processed by single particle analysis. The required use of an additional continuous carbon film on one hand improves particle distribution but can cause particles to display preferred orientations, leads to CTF determination based on the carbon film and not on the particles, and is adding additional image noise from the carbon film to the micrographs. We minimized at least the last problem by using a very thin layer of carbon (5nm).

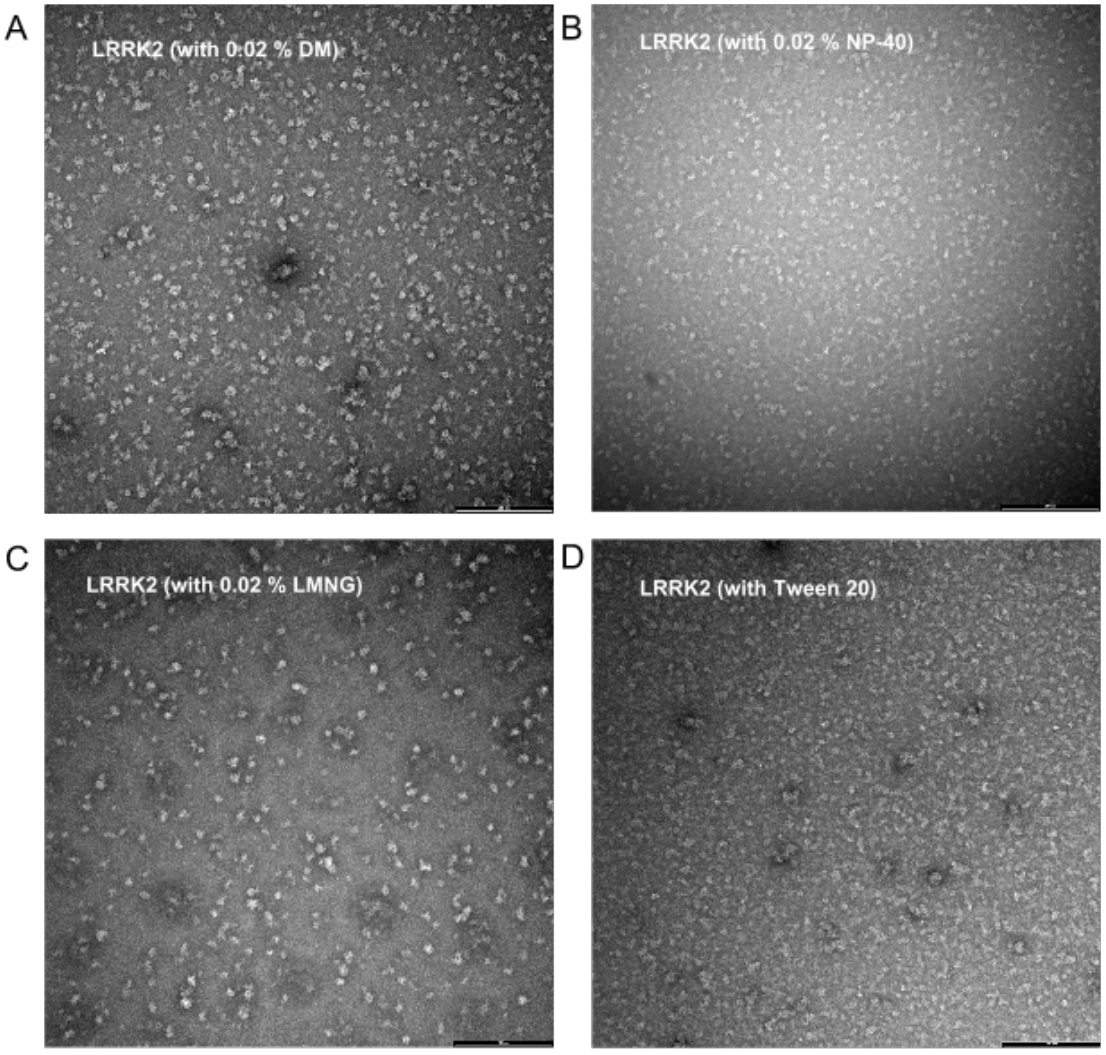

FIGURE 3.13: Negative stain microgrpahs of LRRK2 purified with different detergents. (A) n-decyl–D-maltopyranoside (DM) (B) NP-30 (C) LaurylMaltose Neopentyl Glycol (LMNG) (D) Tween 20. The concentration of these detergentsin the elution buffer were kept same as that of Triton, 0.02%.

Elongated particles with two-fold symmetry could be easily seen in the raw micrographs of negatively stained preparations (Figure 3.15, A). To obtain a 3D model, about 18280 particles were selected from the 265 micrographs and subjected to reference free alignment and classification as detailed in the Materials and Methods. The 128 class averages generated (Figure 3.15 and Figure 3.16,A) show that the LRRK2 dimeric complex has high degree of conformational flexiblity and lies in an ensemble of different conformations each giving a different projection in the cryo-EM images. This makes 2d averaging very difficult.Nevertheless, few class averages showing the side-views of the particles were very characteristic, being ∼17nm long, ∼10nm-wide with a clear 2-fold symmetry, indicating that the LRRK2 complex is a dimer (Figure 3.15). The dimensions are consistent with previous estimates (Civiero et al. 2012). The two monomers interact at both ends of

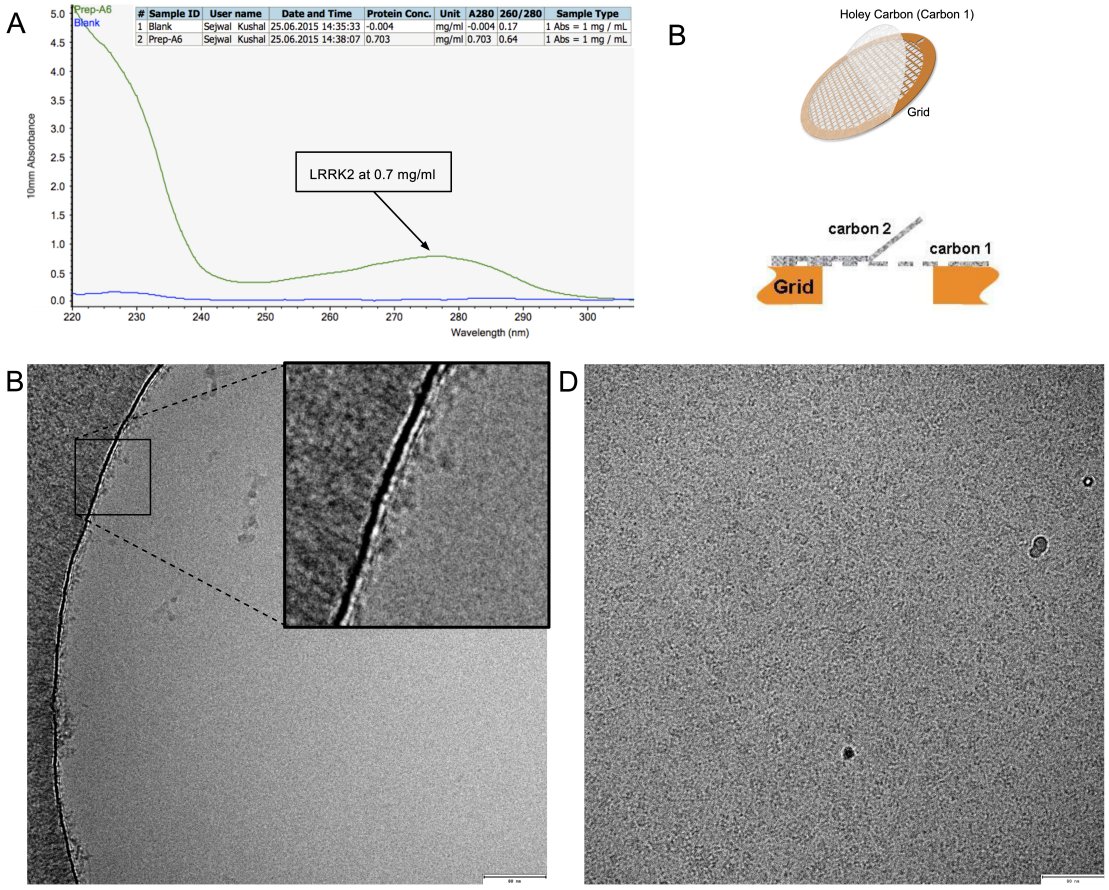

FIGURE 3.14: Effect of detergent in the buffer on vitrification of sample in cryo-EM (A) LRRK2 purified at a relatively higher yield of 0.7 mg/ml The usual yield per protein purification was 0.01 mg/ml. (B) Typical holey carbon copper grids used for Cryo-EM sample preparation(Above) and addition of an extra thin layer of carbon on top of the holey carbon layer (C) LRRK2 sample as imaged in a holey grid. The zoomed inset shows that all the LRRK2 particles are stuck to the carbon on the edges of the holes and none in the vitrified ice. (D) LRRK2 sample as imaged on a holey grid with an additional layer of carbon. Particles are spread evenly throughout the hole with carbon giving a darker contrast to the backround. Scale bars: 100nm for the micrographs

their protein cores, which together seem to form a small cavity. The ends of the complex are less distinct, which is a sign that these domains have intrinsic flexibility. To validate the analysis, the same dataset was also processed with Relion software package (Scheres 2012), which uses a Bayesian approach to infer the parameters of a statistical model from the data. The resulting class averages are very similar to those obtained by EMAN2 processing (Figure3.16).

To improve the structural flexibility of LRRK2 in order to get more defined class averages, we used the GraFix method (Kastner et al. 2008). GraFix is a robust technique that combines glycerol gradient centrifugation and limited glutaraldehyde crosslinking that is used to improve the stability of globular protein complexes. It a popular method that has been used successfully and has more than 160 citations. It aims to rigidify

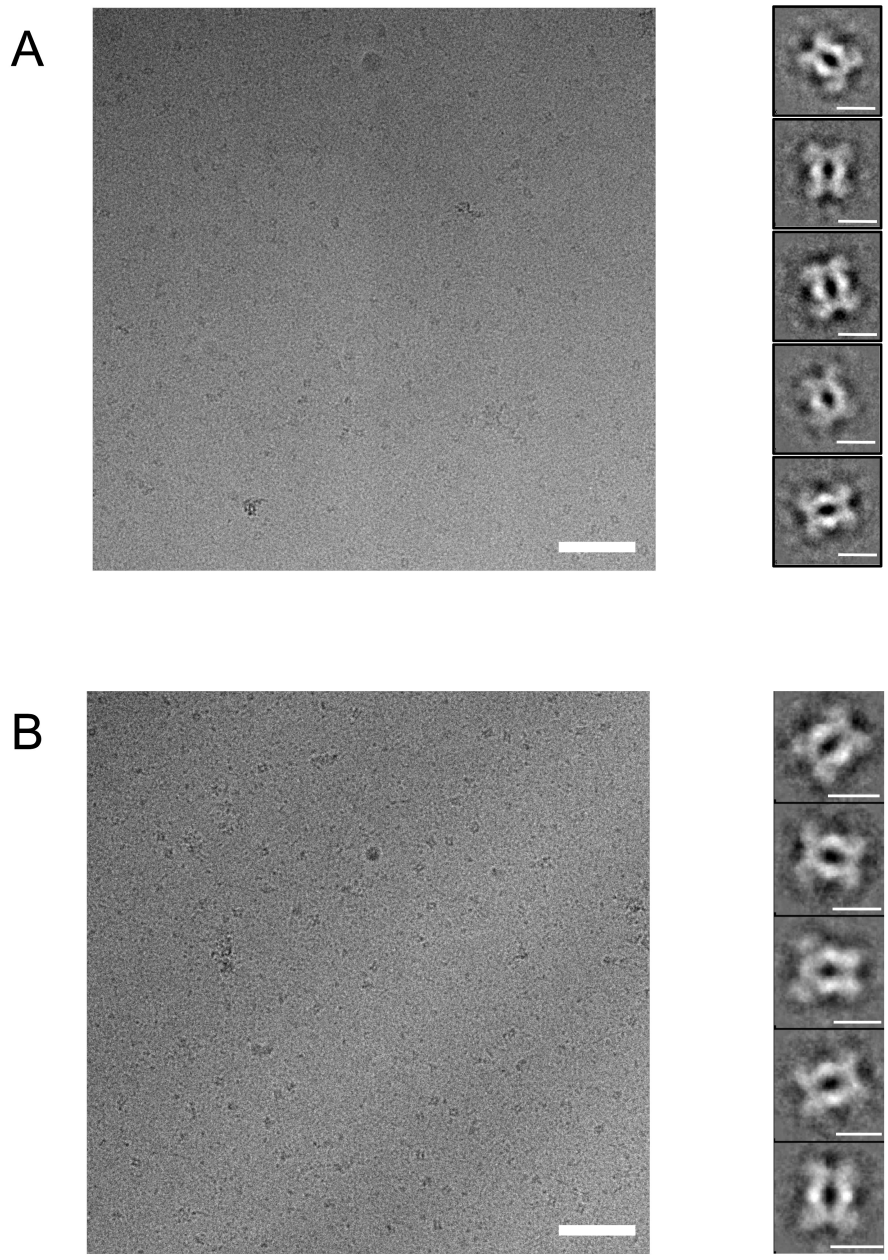

FIGURE 3.15: Cryo-EM and single particle processing of LRRK2 and LRRK1. (A) LRRK2 complexes in Hepes buffer at pH 8.2, imaged by cryo-EM. Right: EMAN2 class averages showing characteristic side-views of the complex. These views are ∼17nm long and ∼12nm wide. Their two-fold symmetry indicates that the complex is a dimer. (B) LRRK1 complexes in Tris buffer at pH 7.4, imaged by cryo-EM. Right: EMAN2 class averages showing characteristic side-views of the LRRK1 complex. These are very similar to corresponding side-views of LRRK2 but slightly smaller, being ∼16nm long and ∼10nm wide. Again they indicate that the complex is a dimer. Scale bars: 100nm for the micrographs, 10nm for the averages.

the macromolecules by mild crosslinking without inducing major structural rearrangements. The benefit of running the sample on a gradient centrifugation is also to fractionate different oligomerization states and remove smaller impurities. We use purified LRRK2 and subjected to 14 hours of gradient ultracentrifucation using glutaraldehyde as a crosslinker. In parallel LRRK2 was also subjected to same gradient ultracentrifucation but without adding any crosslinkers. Fractions were collected corresponding to different sizes manually. The LRRK2 fractions without the crosslinker were used for LC-MS detection. In all the four fractions corresponding to the size of LRRK2 dimer, mass spectrometry values detected the presence of LRRK2. The cross-linked LRRK2 fractions were imaged in negative stain and the micrographs looked much better with more homogenous particles, clear background and monodisperse population without any aggregates (Figure 3.17, A). Similar quality of the particles were seen in the unfix fractions as well (Figure 3.17, B). As the the gradient used for GraFix has glycerol, the final protein had more than 10% glycerol, this made cryo-EM of the GraFix sample impossible, without buffer exchange. We used spin desalting columns for buffer exchange but as with our earlier experience with using ultra-centrifugal filter devices, LRRK2 tend to stick to the pores and it formed more aggregates in the final buffer exchanged fractions. As cryo-EM was not possible, negative stain data was collected form the GraFixed fraction which showed the maximum mass-spectrometry value form LC-MS. A total of 40 microgrpahs were collected and a total of 1864 particles were picked form the micrographs and subjected to single particle 2D classification. The class averages displayed similar size of the particles we expected but the shape of the particles were very different(Figure 3.17, C). A probable cause of this is the vast conformational flexibility of the complex and the crossliking is unable to lock one particular conformation but rather cross-links random residues which are in closer proximity. A recent study has reported large experimentally observed distance distribution widths of $\sim$3 nm for all positions in the catalytic core of the RocCor tandem in LRRK2 bacterial homolog. Infact, the same group published the crystal structure of Roc-COR tandem for the first time and in the crystal structure of the dimer, electron density for the second Roc domain in the RocCOR dimer was missing (Gotthardt et al., 2008). They now attribute this missing density to the large conformational flexibility inherent in ROCO protein catalytic domain, which sample multiple conformations, one of which seems to be represented by their published RocCOR crystal structure. A very similar conformational flexibility can be expected with the LRRK2's catalytic domain which is highly conserved in all Roco proteins.

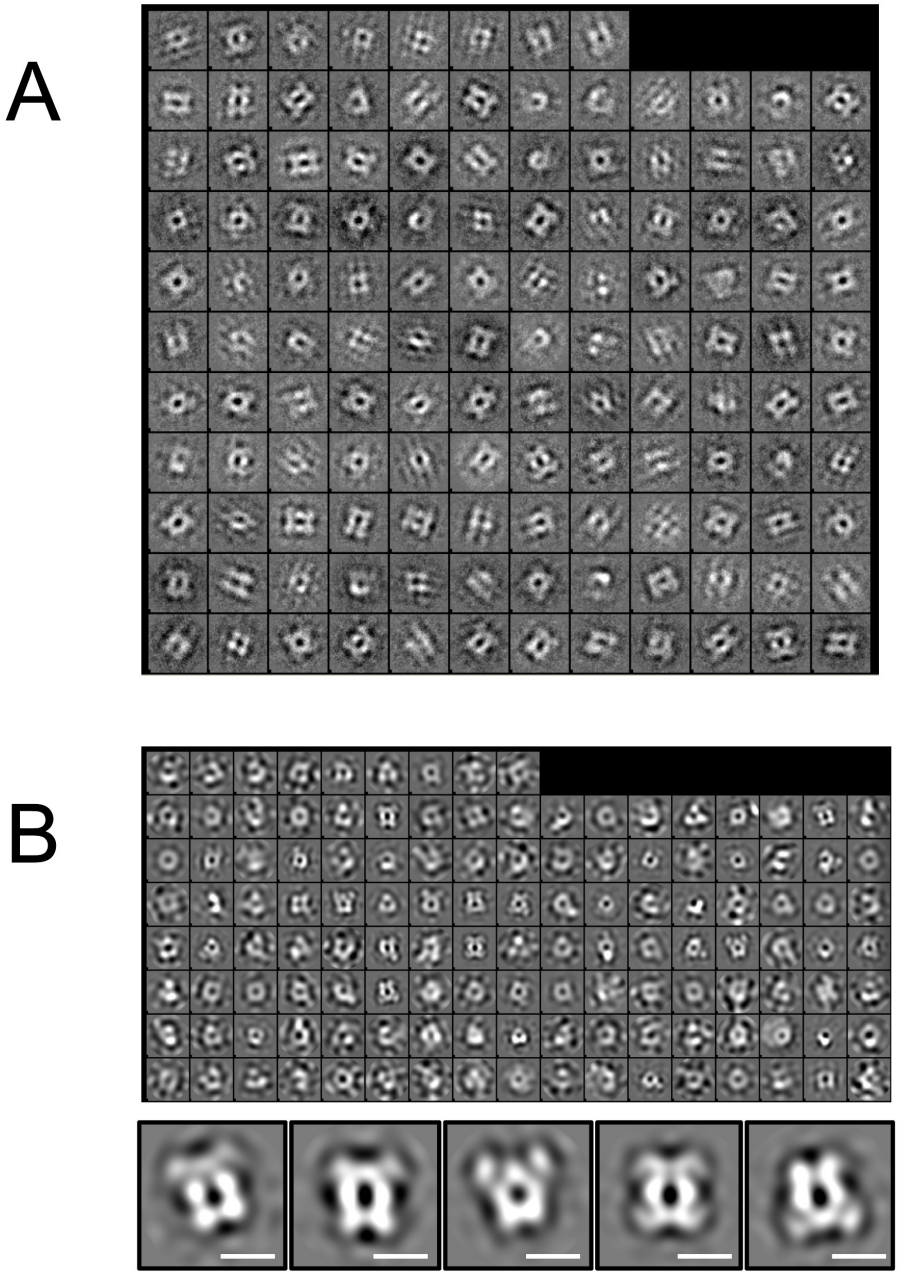

FIGURE 3.16: The total data set contained 18280 LRRK2 particles. (A) The 128 reference free class averages obtained after 5 iterations in EMAN2 using e2refine2d program. The best classes from these are shown in Figure 3.15,A and subsequently used to generate and refine the initial 3D model for LRRK2. (B) The 128 reference free class averages obtained after 25 iterations in Relion. The class averages shows structural heterogeneity among particles. Below: Selected examples. The shape and dimensions of the particles are very similar to that obtained with EMAN2. Scale bar, 10nm

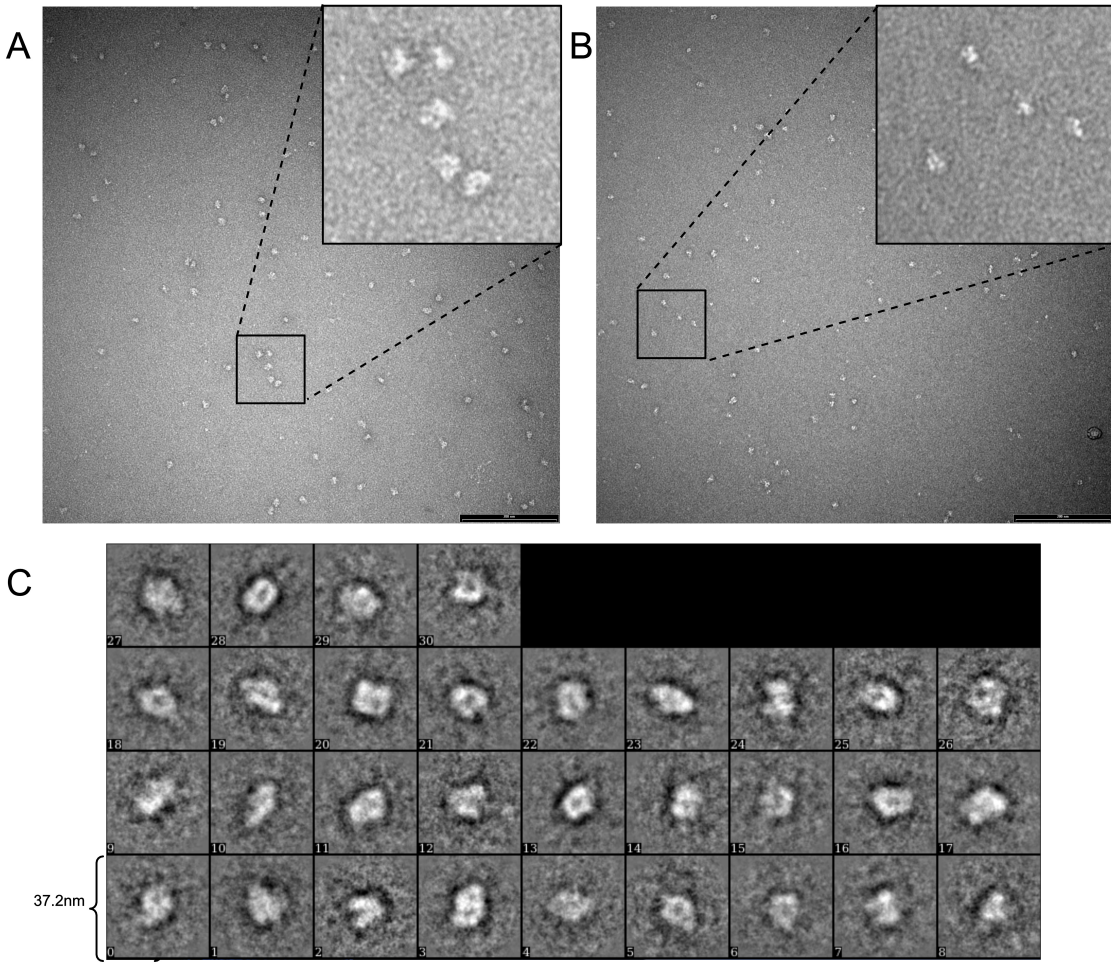

FIGURE 3.17: GraFix treatment of LRRK2. (A) Best fraction from GraFix performed on LRRK2 (B) Same fraction complimentary to (A) but without crosslinking agent. Inset shows a zoomed view of the particles in both the images. (C) 31 classes of LRRK2 GraFix particles from fraction in (A) generated by reference free 2D classification in EMAN2. Scale bar, 100nm

3.3.5 Cryo-EM of LRRK1

For LRRK1, all the EM analysis was done from the purified protein samples send from Leuven. Relative to LRRK2, the total concentration was usually always greater than that of LRRK2, which meant for the same number of micrographs collected for LRRK1, total number of particles for single particle analysis was always be greater than that of LRRK2. Also just by visual inspection of negative stain images from very new prep, it appeared that LRRK1 is more slightly more stable than LRRK2. This was a great motivation for this project and for the future structural studies of LRRK2 as well because the high homology between LRRK2 and LRRK1, makes studying LRRK1 equally important to gain structural and mechanistic information for LRRK2, which is more difficult to work with.The same procedure as that for LRRK2 was used to prepare and analyze LRRK1 for cryo-EM. For initial EM analysis and build a starting 3D model, around

684 particles were selected from 50 micrographs, aligned without the use of a reference and classified into 64 classes containing a minimum of 100 particles using EMAN2 (Figure 3.15,B). As the dataset used for class averages for LRRK1 was much smaller than that of LRRK2,the number of particles per class was lower which resulted in LRRK1 class averages that did not look quite as crisp as their LRRK2 counterparts, but the characteristic dimeric side-views as seen for LRRK2 were clearly visible (Figure 3.15,B). These side views show that LRRK1 too forms a dimer with very similar overall shape to the LRRK2 dimer, but slightly smaller in dimensions. As might be expected from the identical domain organizatoin of the two sequences (Figure 3.1). Another difference observable form the class averages are the protrusions at the ends of the LRRK1 complex, which have slightly less prominent arms. From the 2D class averages, a not of information that differentiates the LRRK2 and LRRK1 structures cannot revealed, rather more and more similarities are seen. The fuzzy appearance of the class averages also hints towards a similar conformational flexibility inherente in LRRK1 dimer.

3.3.6 Low resolution 3D model

The initial 3D model for both LRRK2 and LRRK1 using C1 (no symmetry) and C2 (two-fold symmetry) were in good agreement, which was evident from the dimeric shape of the complexes. Using the initial model as reference, iterative projection-matching reconstruction was applied with C2 symmetry. After three rounds of refinement the final reconstruction was produced at a resolution of 24.2Å and 24.3Å for LRRK2 and LRRK1 respectively (Figure 3.19A,B). Both LRRK2 and LRRK1 complexes have similar overall shape (Figure 3.18). They form elliptical homodimers with each monomer having a concave shape. Compared to LRRK1, LRRK2 displays slightly more curvature. Two dimerization contacts are visible in the low-resolution map. These two dimerization points are at roughly equal distance from the center of the plane between the monomers. The structural similarity of the two complexes observed in this low-resolution reconstruction does not contradict the idea that heterodimers might form in vitro, as postulated by Dachsel et al. (Dachsel, 2010).

3.3.7 Conformational heterogeneity in LRRK2

So far the efforts for single particle cryo-EM analysis of full length LRRK2 and LRRK1 was performed without the addition of any ligand or substrate. But as both proteins functions as active GTPase and Kinases with the Roc-COR and Kinase domain respectively, effect of substrate binding on the conformational heterogeneity was tested. The Roc-COR domain is the characteristic of the Roco family of proteins, which has

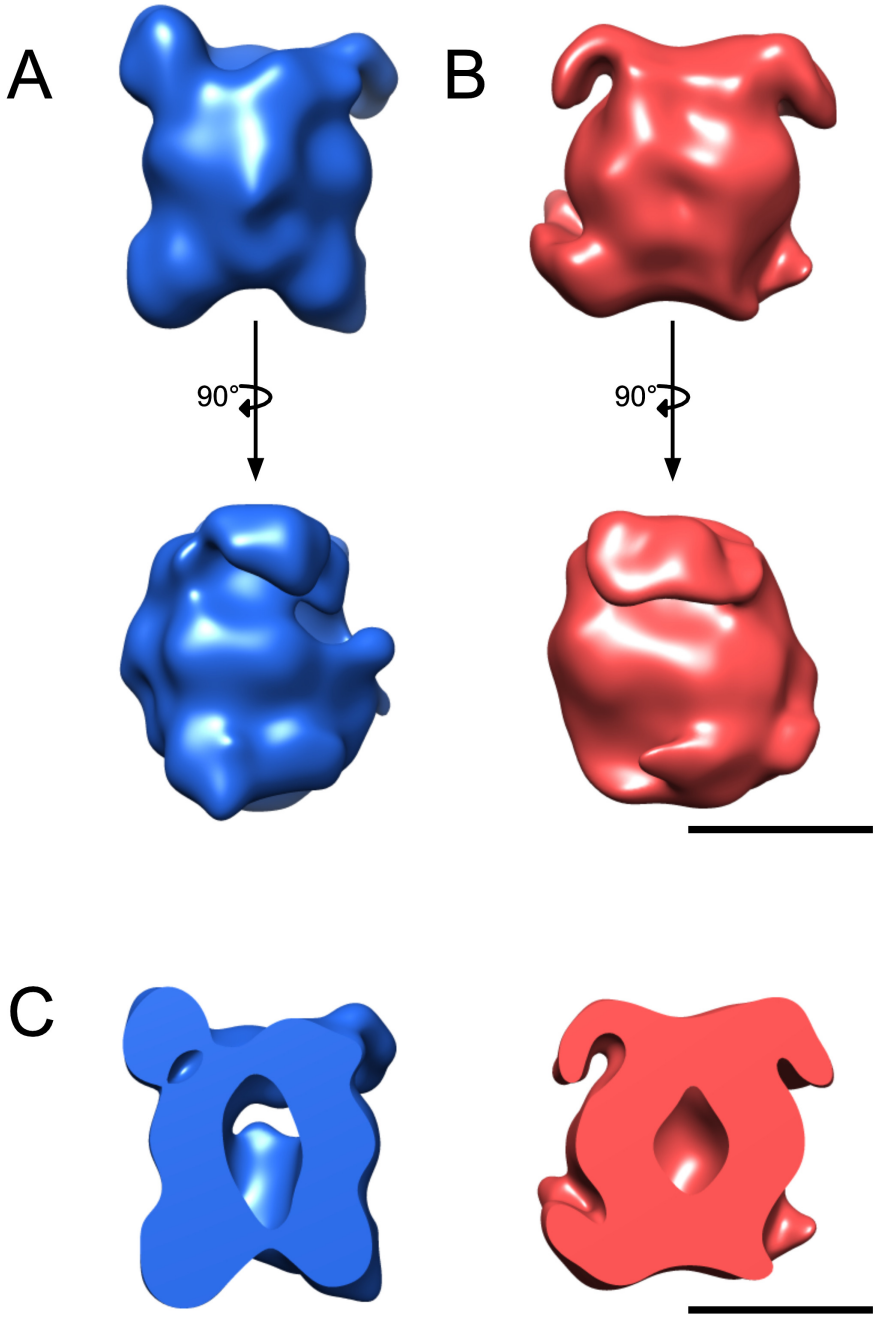

FIGURE 3.18: 3D reconstructions of the homodimeric LRRK1 and LRRK2 complexes: (A) 3D model of LRRK1 (blue) at 25 Å resolution showing two side-view orientations, the lower one being 90 degrees rotated relative to the upper one. (B) 3D model of LRRK2 (red) at 25 Å resolution showing the side-view orientations, the lower one being 90 degrees rotated relative to the upper one. (C) Cut-away of LRRK1 (blue) and LRRK2 (red). The plane of the slice is perpendicular to the dimeric plane, to show how the dimer forms. Scale bar: 10nm

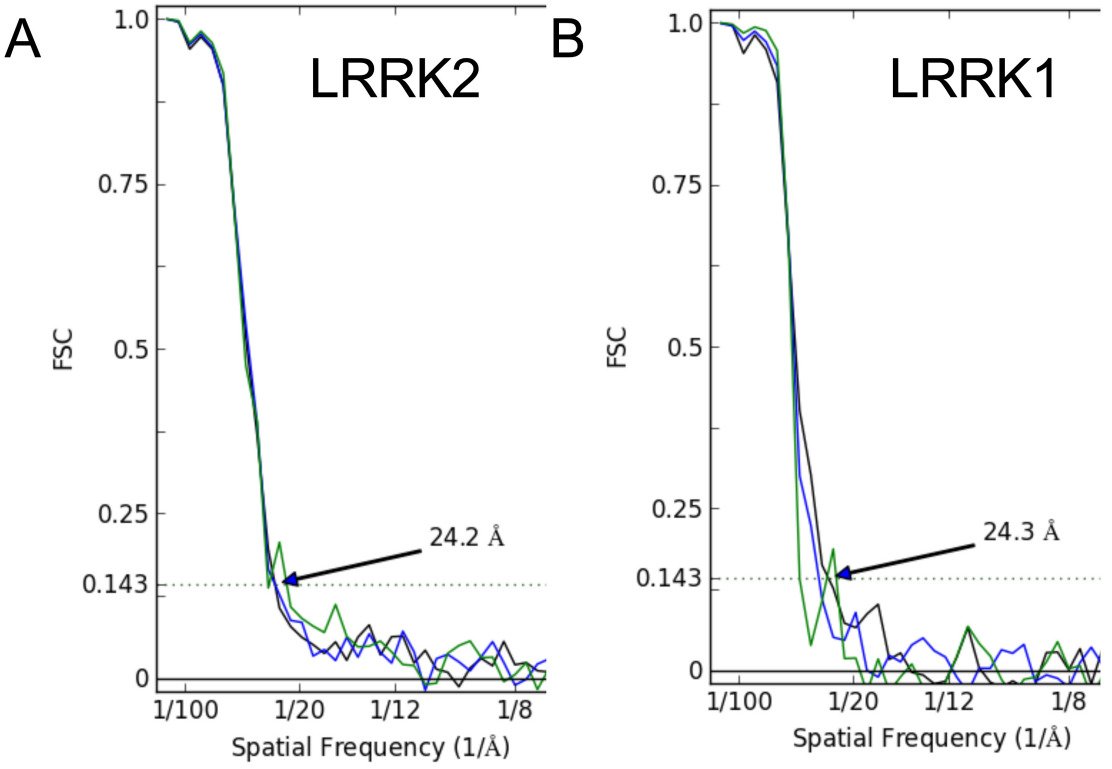

FIGURE 3.19: Resolution curves for the LRRK2 and LRRK1 3D models.: (A) The resolution of the LRRK2 is 24 Å using the gold standard 0.143 FSC cutoff criteria .(B) The resolutios of the LRRK1 is 24 Å using the gold standard 0.143 FSC cutoff criteria.

been characterised to belong to the class of G-proteins activated by nucleotide-dependent dimerization (GADs) (Gasper et al., 2009; Terheyden et al., 2015). Conventional guanine nt-binding proteins (G proteins) cycle between a guanosine triphosphate (GTP) -bound and guanosine diphosphate (GDP) -bound state with the help of regulatory proteins. The GDP-bound state is the off state while GTP-bound state is considered the active on state. There are two other important class of proteins that play a crucial functional role, these are GTPase-activating proteins (GAPs) and the guanine nucleotide-exchange factors (GEFs). GAPs functions by complementing and stabilizing the active site to increase the rate of GTP hydrolysis while GEFs speeds up the nucleotide exchange and accelerate the release of GDP or GTP. In contrast of these, GADs like LRRK2 and LRRK1 show show reciprocal complementation of their active sites and seem not to require GAPs and GEFs. The nucleotide-regulated switching cycle is therefore is carried out by the elements within the protein complex (Gasper et al., 2009). Further, the need for GEFs for nucleotide exchange is not necessary as these proteins exhibit low nucleotide affinity and dimerize upon GTP binding to supplement each other with elements needed for efficent GTP hydrolysis, hence not requiring the accessory roles of GAPs. For LRRK2, it has been a challenge to study its G-protein cycle (Gilsbach and Kortholt, 2014). A few GAPs and GEFs has been reported for LRRK2 but none of these putative regulators directly bind to the Roc domain. Therefore purified LRRK2

were incubated with GTP and GDP and analysed by negative stain EM to see the effect on the structural stability of the protein complex in the various state GTPase cycle.

LRRK2 was purified as usual, GTP and GDP were added to the solution at the final elution step together with 3xFlag peptides for 30 minutes. Purified LRRK2 without the addition of GTP or GDP was also prepared as a control for comparison. The purity of the preparation and yield of the protein was not changed much with the addition of the GTP and GDP as observed in the silver stained SDS-PAGE (Figure 3.20,F). In the negative stain images, LRRK2 particles without GTP/GDP look heterogenous with several different population of particles (Figure 3.20,E). In comparison, the particles with bound GTP and GDP looked less heterogeneous with particles resembling less conformational flexibility as judged by the similar shape of the particles. The GTP and GDP bound LRRK2 samples were kept on ice for 1 hour and negative stain grids were prepared again to compare the degradation of the sample with time. It was noticed while the sample without the bound GTP and GDP started degrading, for GTP and GDP bound LRRK2 still looked more homogenous after 1 hour. At the level of negative stain particle images, it is not possible to confirm if there are different conformation in the LRRK2 GTP and GDP bound forms but visual comparison of the particle quality between non bound LRRK2 clearly shows much more heterogeneity. Similar test was done with addition of ATP (Figure 3.21).

These findings are consistent with a recent study done with the Roc-COR tandem in bacteria Chlorobium tepidum using site-directed spin labelling and pulse EPR distance measurements to measure conformational changes during the Roco G-protein cycle (Rudi et al., 2015). The RocCor domain is highly conserved between all the ROCO protein family members. The study revealed that the Roc G-domains are highly mobile entities, sampling multiple conformations. Unlike other G-proteins, Roc-COR dimer was identified to exist in open and closed conformations but instead, sample multiple conformations and the binding of different nucleotides lead to complex alteration of the occupancies of the conformational states. It can be postulated that a similar structural and activation mechanism should occur for the Roc-COR domain for LRRK2 as well. The negative stain images shows improvement in heterogeneity in the GDP and GTP bound LRRK2. Although a great deal of small functional conformational flexibility still exist within the particles but the large scale conformational flexibility is reduced by the availability of the nucleotide.

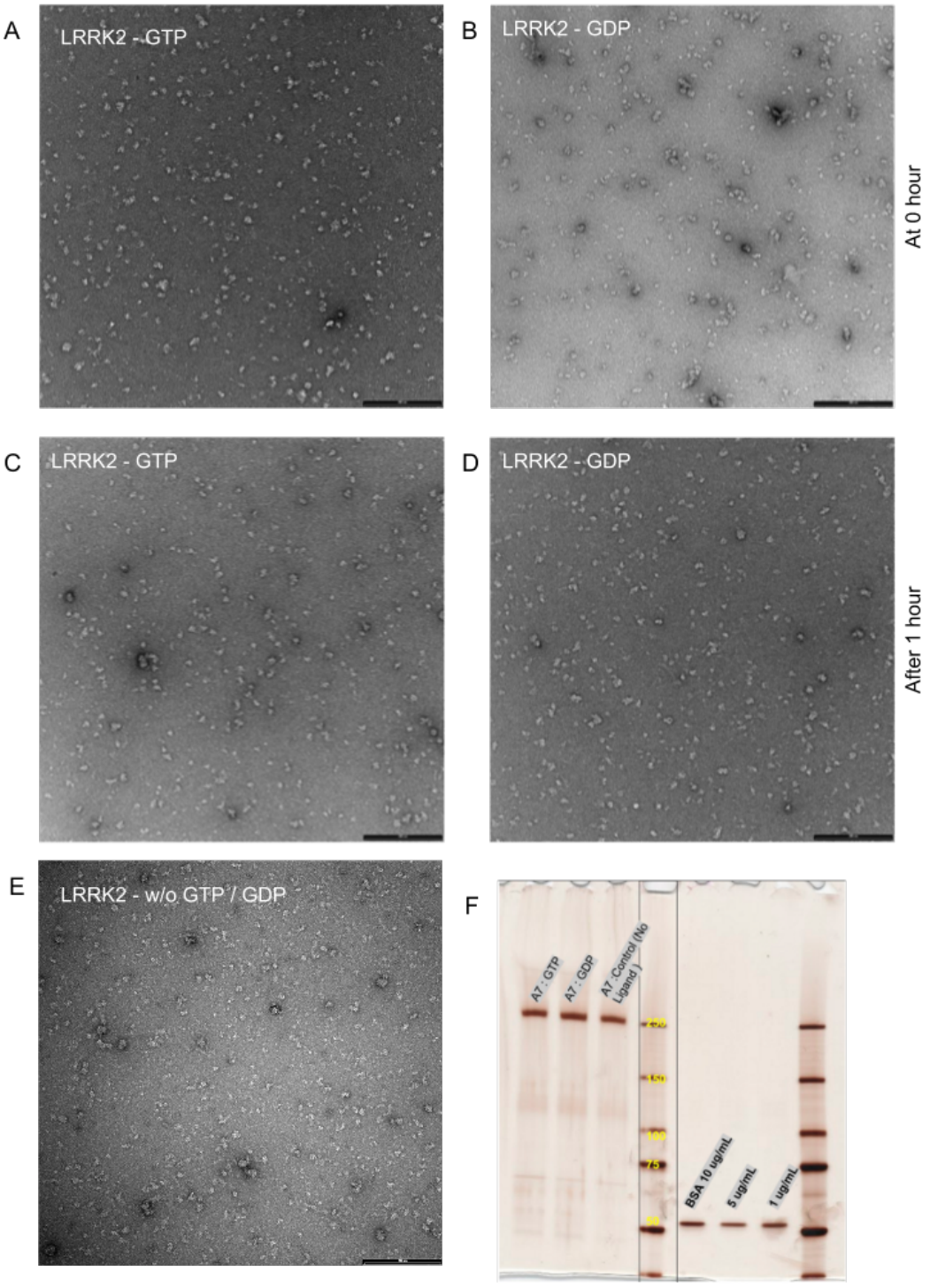

FIGURE 3.20: Negative stain micrographs of LRRK2 bound with GTP and GDP: (A) LRRK2-GTP at 0 hour of incubation (B)LRRK2-GDP at 0 hour of incubation (C) LRRK2-GTP at 1 hour of incubation (D)LRRK2-GDP at 1 hour of incubation. (E) LRRK2 without any bound GTP or GDP. (F) Silver stained SDS-PAGE of purified LRRK2 with GTP, GDP and withtout any ligand.

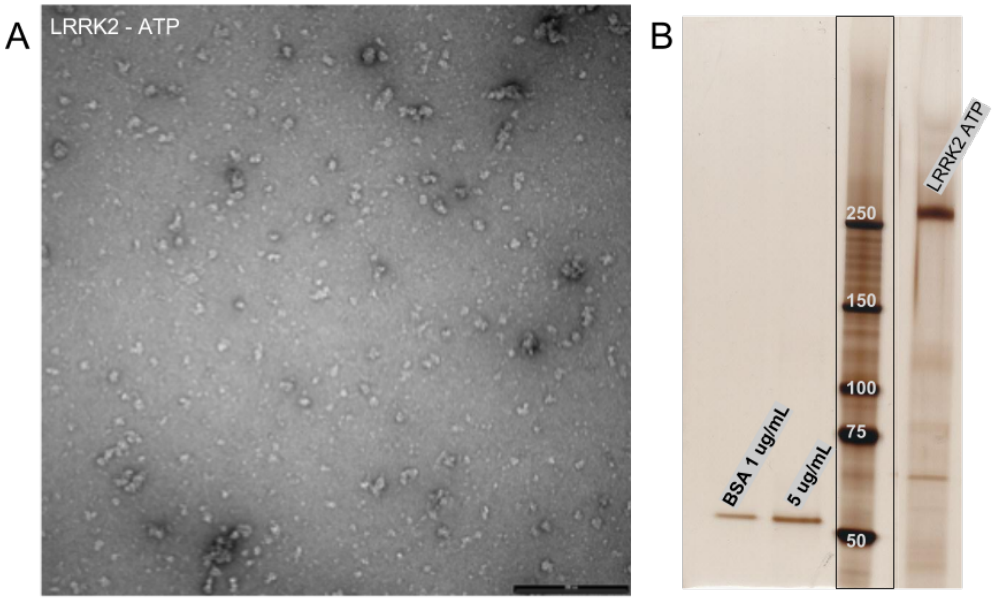

FIGURE 3.21: Negative stain micrographs of LRRK2 bound with ATP: (A) LRRK2-ATP at 0 hour of incubation (B) Silver stained SDS-PAGE of purified LRRK2 with ATP.

3.4 Conclusions

An efficient culture of HEK293 cells transfected with LRRK2 and LRRK1 3xflag tagged protein was established to express the full length proteins followed by affinity based purification to yield good quality and quantity of protein. The quality of purified particles was further optimised for cryo-EM sample preparation by doing ProteoPlex buffer screening to identify the best buffer condition for binding and elution of the protein. The effect of detergent was also tested on the sample quality and integrity of LRRK2 structurally by preparing negative stain EM grids. It was found that detergent is essential for LRRK2 to remain correctly folded, and that the detergent might be stabilizing hydrophobic amino acid residues on the surface of the protein. This supports the claim in other studies which found LRRK2 association with membranes. Cryo-EM data collection was carried out for both full length LRRK2 and LRRK1. The quality of particles on the cryo-EM grids were optimised and it was possible to easily see elongated particles with two-fold symmetry. Several cryo-EM micrographs were collected to carry out computational single particle analysis on the data. 2D class averaging on the individual LRRK2 and LRRK1 particles confirmed the homo dimeric form of both the complexes. The heterogeneity in the class averages and the blurry appearance in the periphery suggested the inherent flexibility of the dimeric complexes. The two monomers appeared to be interacting at both ends of their central protein core, which together seem to form a small cavity. The ends of the complex are less distinct, which is a sign that these domains have intrinsic flexibility. The 2D class averages of both LRRK2 and LRRK1 appeared

very similar in shape, size and overall organisation, with notable difference of LRRK1 being slightly shorter and the protrusions at the ends of the LRRK1 complex have less prominent arms. Based on the 2D class averages, an initial low resolution model was generated to seed the iterative 3D reconstruction process. After few rounds of refinement the final 3D reconstruction was produced at a resolution of 24.2Å and 24.3Å for LRRK2 and LRRK1 respectively. Both the complexes, have very similar overall shape. They form elliptical homodimers with each monomer having a concave shape. Compared to LRRK1, LRRK2 displays slightly more curvature. Two dimerization contacts are visible in the low-resolution map. These two dimerization points are at roughly equal distance from the center of the plane between the monomers. The apparent convergence of the 3D refinement to low resolution final maps for LRRK2 and LRRK1 prevented further structural analysis of the full length density map by fitting atomic models of the individual domains. This also highlights the high degree of flexibility within the protein complex and controlling the conformational diversity of the complex by binding with a substrate will be imperative for further high resolution cryo-EM steps. In conclusion, we present the first structural insight into full length LRRK2 as well as LRRK1, which will further assist follow-up work towards a high-resolution structure of these important molecules.

Chapter 4

Liposomal preparation as a tool to study membrane proteins under buffer gradients by cryo-EM

Kushal Sejwal, Mohamed Chami, Paul Baumgartner, Julia Kowal and Henning Stahlberg

Center for Cellular Imaging and NanoAnalytics (C-CINA), Biozentrum, University of Basel, Basel 4056, Switzerland

*Corresponding authors: H Stalhberg; henning.stahlberg@unibas.ch

(Manuscript in preparation)

Author's Contribution: K.S. prepared the liposomes, performed encapsulation experiments, protein reconstitution and collected EM data; M.C. supported in liposome experiments and EM data collection; P.B. and J.K. provided protein for reconstitution; H.S. supervised the project.

4.1 Introduction

Genome-wide sequence studies estimate that 20-30% of all expressed gene products are membrane proteins (Fagerberg et al. 2010). Biological membranes act as barriers between cells and their environment as well as in between intracellular organelles. The basic unit of most membranes is phospholipids, but in addition they also contain a large portion of proteins. These membrane proteins embedded within the lipid bilayer can make up 50% the mass of a biological membrane. Thereby, membrane proteins are involved in various vital processes such as energy transport during photosynthesis or respiration, transport of molecules across the membranes via channels or transporters, transmission of chemical signals, anchoring of the cytoskeleton and catalyze chemical reactions. Considering the pivotal role of membrane proteins in various cellular functions makes them of great medical importance. It has been estimated that of all the available drugs, more than 50% of them act on membrane proteins (Arinaminpathy et al. 2009). Despite their importance, however, their structural studies remain challenging, which is evident from the fact that only less than 2% of all the known proteins structures published in protein data bank (PDB) constitute the membrane proteins. Studying the dynamics and the structure of the membrane proteins not only provides important insight to the molecular mechanism of their function but also aids in rational design of novel drugs (Lounnas et al. 2013).

In contrast to cytoplasmic proteins structure determination, the robust technique of X-ray crystallography is challenging in case of membrane protein as they are difficult to purify in large amounts and hard to obtain well-diffracting three-dimensional crystals. Electron crystallography of membrane proteins has from the start proved to be an alternative approach to obtain structures of membrane protein. Electron crystallography requires much less material than X-ray crystallography methods and has the added advantage of providing a native environment to the membrane proteins. To obtain highly ordered 2d crystals for electron crystallography data collections, detergent solubilized purified proteins are reconstituted into artificial phospholipid bilayer membrane by carefully adjusting the favourable buffer conditions during controlled detergent dialysis (Figure 4.1,A). Once well ordered 2d crystals of membrane proteins in lipid bilayer are obtained, they can be vitrified or embedded in sugar to be imaged in TEM (Figure 4.1,B). Computational image processing of the micrographs and electron diffraction data is utilized to further reconstruct the 3d structure of the protein at high resolution.

Although, electron crystallography aims to provide a more native lipidic environment to the membrane protein, mimicking the conditions in cellular membranes, a major caveat in electron crystallography is that the membrane proteins are imagined as flat crystal sheets surrounded by same buffer (Buffer A in Figure 4.1), unlike in between a typical

gradient which occurs across the membrane in cells. There is always a different ion concentrations on either side of the membrane which cause a potential difference across it, known as the membrane potential (typically -40 to -80 mV). This gradient can also arise due to the difference in salts, pH and ligands. Many membrane proteins undergoes conformational changes to perform their biological function like transport and signalling owing to the change in this gradient across the membrane. Therefore to truly mimic the true native functional state of the membrane protein, it is necessary to maintain a gradient across the lipid membrane while imaging membrane protein 2d crystals by Cryo-EM.

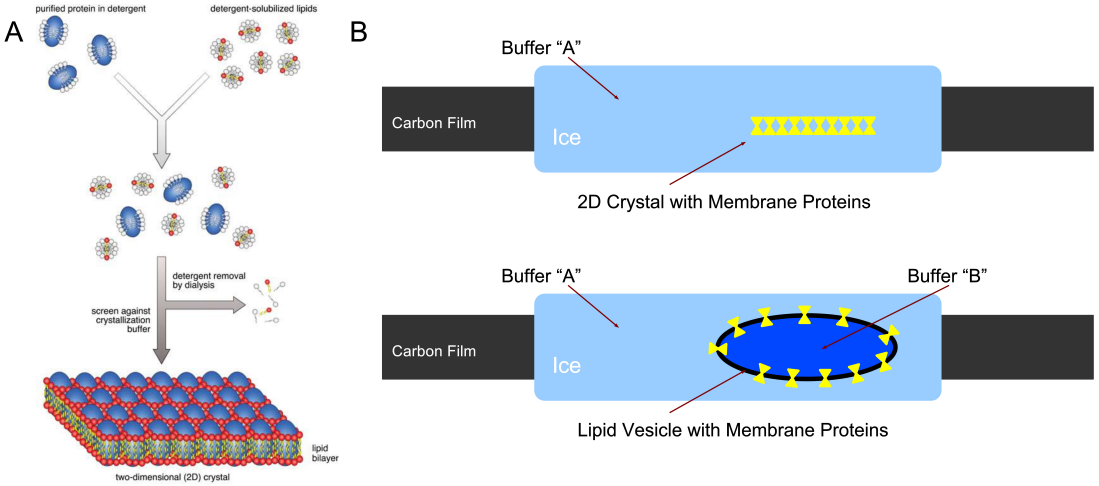

FIGURE 4.1: Schematic for electron crystallography of membrane proteins and vesicular 2D crystals: (A) The basic principle of 2D crystallization of membrane proteins. (B) Vitrification for cryo-EM data collection of 2D crystals (Above) and vesicular 2D crystals (Below). Vesicular 2D crystals have the advantage of using two different buffer system, inside and outside.

To achieve this goal, we extended the methodology of electron crystallography and used liposomes to reconstitute the membrane proteins. The advantage of using liposomes is that we can control the environment of inside and the outside of the liposomes by altering the buffers to provide a more native gradient to the reconstituted membrane proteins. Membrane proteins embedded in such liposomes can therefore be captured in action and more closer to their native functional forms (Figure 4.1,B). The general idea is to put forward a method to study the structure of 2D crystalline membrane proteins while they are embedded in specific buffer solutions. The membrane protein will first be purified and crystallized in buffer "A", and the buffer on the outside of the vesicular crystals will be changed to buffer "B" via column filtration prior to vitrifying the grids for cryo-EM data collection.

There are four major challenges to establish and optimise this method for any membrane protein : preparation of liposomes with different buffer solution inside and outside ;

reconstitution of membrane proteins in such liposomes ; Cryo-EM of 2D crystals as round vesicles ; and 3D reconstruction of the vesicular 2D crystals. The membrane protein that we used as a test is MloK1, a bacterial transmembrane protein which works as a voltage gated potassium channel, modulated by cyclic nucleotides. Our lab already determined three-dimensional (3D) maps of MloK1 at 7Å resolution in the presence and absence of its ligand, cAMP (Kowal et al. 2014). A mechanism of channel gating upon cyclic nucleotide binding was formulated from the observed conformational change between the two models in the presence and absence of cAMP. Reconstituting MloK1 into liposomes and adding ligand to the buffer outside of the vesicles will in effect introduce the same conformation change. In addition compared to classical electron crystallography, this method will have two additional advantages. Firstly to generate a 3D model, there is no tilting of the specimen required as the spherical geometry captures the protein projection in all possible orientation. Secondly, as MloK1 forms 2D crystals in 180-degree screw-axis symmetry (p4212), it will place adjacent membrane proteins in alternating up/down orientations in the membranes, allowing us to determine the 3D structures of oppositely regulated states in one experiment.

4.2 Methods

4.2.1 Liposomal Preparation

Two types of of lipids were used for preparing the liposomes : Polar extract phospholipids from E. coli and 1,2-Dimyristoyl-sn-glycero-3-phosphocholine (DMPC). Both the lipids were purchased from Avanti Polar Lipids, Inc. There were different methods used for preparation of liposomes, buffer encapsulation and exchange. (Figure 4.2).

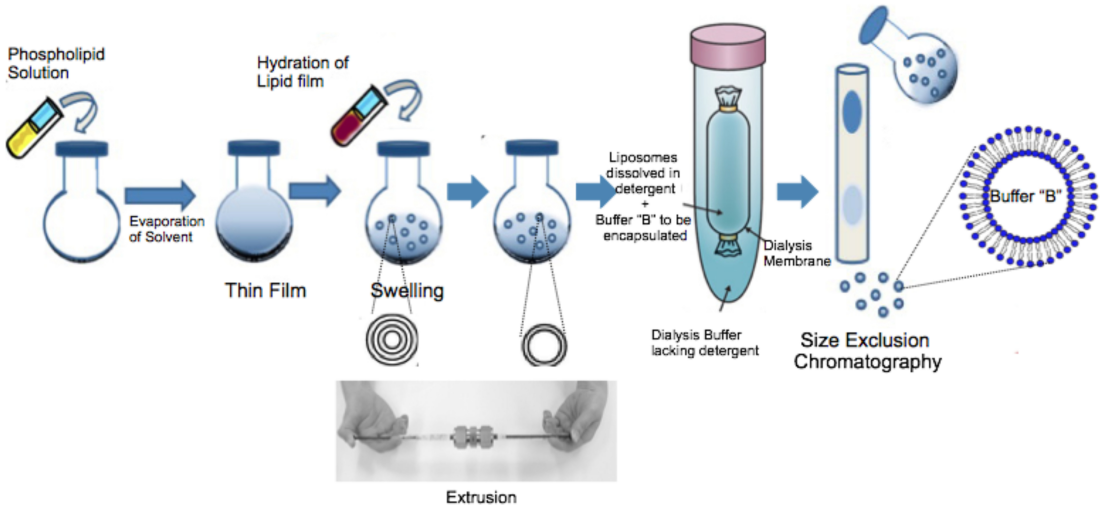

FIGURE 4.2: General scheme of lipsosome formation, encapsulation and buffer gradient formation.

4.2.1.1 Film dispersion method

Liposomes were prepared by using the film dispersion method. The preparation starts by transferring lipids in chloroform into a glass tube. Lipids were always stored in -20 by sealing tightly by a teflon tape. The lipids were kept at room temperature for 15 minutes and thereafter, the solvent was evaporated by a stream of argon gas. A film of lipid was formed inside the glass surface at the bottom. The lipids were then kept under vacuum for 30 min while it is still pumping. Afterwards, the vacuum vent was closed, motor pump stopped and the lipids were kept overnight to remove any trace of the solvent. Based on the experiment the concentration of lipid take ranged from 5 to 10 mg/ml. Next day, the lipid film were rehydrated using an aqueous desired buffer that resulted in spontaneous swelling to form multilamellar vesicles (MLV) and large unilamellar vesicles (LUV).

4.2.1.2 Dialysis

For making liposomes by dialysis, 1 ml of the lipid - detergent mixture was loaded into dialysis buttons and dialysed against detergent-free buffer (20mM Tris-HCl pH 7.6, 20mM KCl, 1mM BaCl2, 1mM EDTA) for at least 24 hours. Following dialysis the liposome mixture was extruded 11 times through a polycarbonate filter of pore size of 100 or 200 nm, in a mini extruder (Avanti). The extrusion helps to maintain a uniform distribution of size and attain unilamellar vesicles.

4.2.2 Liposomal Encapsulation

Fluorescent dyes and other material at 100mM concentration were used for liposomes encapsulation experiment. 1 mL of the encapsulating buffer or dye was added to the glass tube with lipid film. The tube was vortexed until no lipid film is seen sticking to the glass tube walls.

4.2.2.1 Column Gel Filtration

To prepare a column for gel filtration, sephadex G-25 resin were hydrated in 20mM Tris-HCl pH 7.6, 20mM KCl, 1mM BaCl2 and 1mM EDTA to form a slurry. The buffer was mixed well with the slurry and allowed to settle. After the slurry settles, the extra buffer was decanted and the process was repeated 2-3 times. The column was then packed with the slurry and equilibrated with the same buffer 2-3 time again. The liposomes were passed through the column, eluted with the same buffer and different fractions were collected. Another method that was used to to exchange the buffer and remove non encapsulated material from the liposomes was ultracentrifugation. Liposomes encapsulated with a desired buffer were centrifuged at 70,000 rpm in TL100 ultracentrifuge (Beckman) for 1 hr at 4°C. A thick pellet of the liposomes at the bottom of the ultracentrifuge tube was observed and the supernatant containing the unencapsulated buffer was removed. The pellet was resuspended with the new desired buffer to be present in the outside of the liposomes.

4.2.3 Protein Purification - MloK1

Intact, full-length, cyclic nucleotide-modulated potassium channel MloK1 was expressed and purified as described in a recent publication (Kowal et al. 2014). The C-terminal hexahistidine-tagged MloK1 construct was transfected into E. coli cells (BL21(DE3)). These transformed cells were grown in L-broth at 37 °C, and the expression was induced

with 0.2 mg/ml anhydrotetracycline for 2h, as the OD600 reached 0.7. Sonication was used to pellete and lysed the cells. 50 mM n-decyl--D-maltopyranoside (DM, Anatrace) was used to solubilize the membrane proteins. Purification of MloK1 was done in two steps, first over a Co^{2+}-affinity chromatography and then with gel-filtration chromatography (Superdex 200, GE).

4.2.4 Protein Reconstitution in Liposomes

For reconstitution of purified detergent-solubilized MloK1, two methods were used: Dialysis and Bio-beads. For dialysis, detergent-solubilized MloK1 in purification buffer was mixed with E. coli polar lipid extract at different lipid-to-protein ratio ranging from 1 to 10. It was further dialysed against detergent-free buffer (20 mM Tris–HCl pH 7.6, 20 mM KCl, 1 mM BaCl2, 1 mM EDTA) in small dialysis buttons for 1-2 days at room temperature. Another method used for membrane protein reconstitution in liposomes was using biobeads. Biobeads are insoluble hydrophobic polymer beads that interacts with the hydrophobic tail of detergent molecules. The rate of binding is rapid and the detergent coated beads can be removed easily by sedimentation or centrifugation. We started by mixing detergent-solubilized MloK1 and desired amount of E. coli polar lipid extract according to different different lipid-to-protein ratio that was needed to be tested in small vials. To these few microlitres of biobeads were added using a blunt cut pipette tip were added and left for 3-4 hours at room temperature. The protein reconstituted vesicles are tested in EM and the sample was carefully transferred and stored in fresh vials, leaving the biobeads.

4.2.5 Cryo-EM

For cryo-EM, 4 μL of the liposomes was pipetted onto a glow-discharged, holey carbon films (Quantifoil R2/1, Quantifoil Micro Tools, Jena, Germany). Using a fast blotting time of 1 second and a bolting force of 1, the grids were then rapidly plunge frozen in liquid ethane, cooled by liquid nitrogen, using a MarkIV Vitrobot (FEI, Eindhoven, Netherlands). The frozen grids were transferred to a Gatan-626 cryo-holder. Micrographs were recorded under low-dose conditions (25 electrons/Å2) on a CM200 TEM (FEI Company, Eindhoven, The Netherlands) operated at 200kV with 58,000x nominal magnification. Data was collected using a TVIPS F416 CMOS camera (TVIPS, Gauting, Germany). The range of defocus used for collecting micrographs was setup enough to see the lipid bilayer of the liposomes in the projections.

4.3 Results and Discussion

4.3.1 Liposome Encapsulation

The very first goal of the project was to make liposomes with a gradient across the lipid bilayer. To achieve this liposomes were prepared and encapsulated with a desired buffer while on the outside a different buffer is present. For the ultimate goal of cryo-EM data collection of such liposomes, visualizing the buffer gradient across liposome in TEM images was also critical. The liposome preparation and encapsulation method should therefore sustain three important properties - Liposomes should not leak the encapsulated content. Liposomes should not burst or contract due to osmotic pressure. Liposomes should be able to undergo vitrification for Cryo-EM. To visualize the buffer gradient across the liposomes we added a marker in the inside buffer that was used during liposome formation and encapsulation, while the outside buffer that was used in the subsequent washing step was absent of the marker. These liposomes having a buffer gradient were imaged by Cryo-EM. We tested several different markers.

4.3.1.1 Carboxyfluorescein

Carboxyfluorescein is a well known fluorescent dye commonly used as a tracer agents. The dyes being membrane-impermeant can be incorporated into liposomes, and has been used routinely in pharmaceutical studies where it allow for the tracking of liposomes as they pass through the body using fluorescence microscopy. We tested if a small amount of carboxyfluorescein added to the buffer inside the liposomes can be visualised using cryo-EM. In cryo-EM images, it was not possible to observe any change in grayscale value between the inside dye-rich buffer and outside buffer. Similar results were achieved with caesium chloride (CsCl) and ferric chloride($FeCl_3$) (Figure 4.3)

4.3.1.2 Gold Nanoparticles (GNPs)

GNPs are the colloidal suspension of gold particles of nanometer sizes and are routinely used in cryo-electron tomography as fiducial markers for tomograph alignements. We used GNPs of 10nm size with the encapsulating buffer and washed the liposomes using size exclusion chromatography to remove unencapsulated GNPS. The cryo-EM images shows a possible leakage in the liposomes with free GNPs visible outside the liposomes.

A possible cause of the leakage of GNPs is the detergent coating which commercially available GNPs comes with. To test this, GNPS were incubated with Antibody to

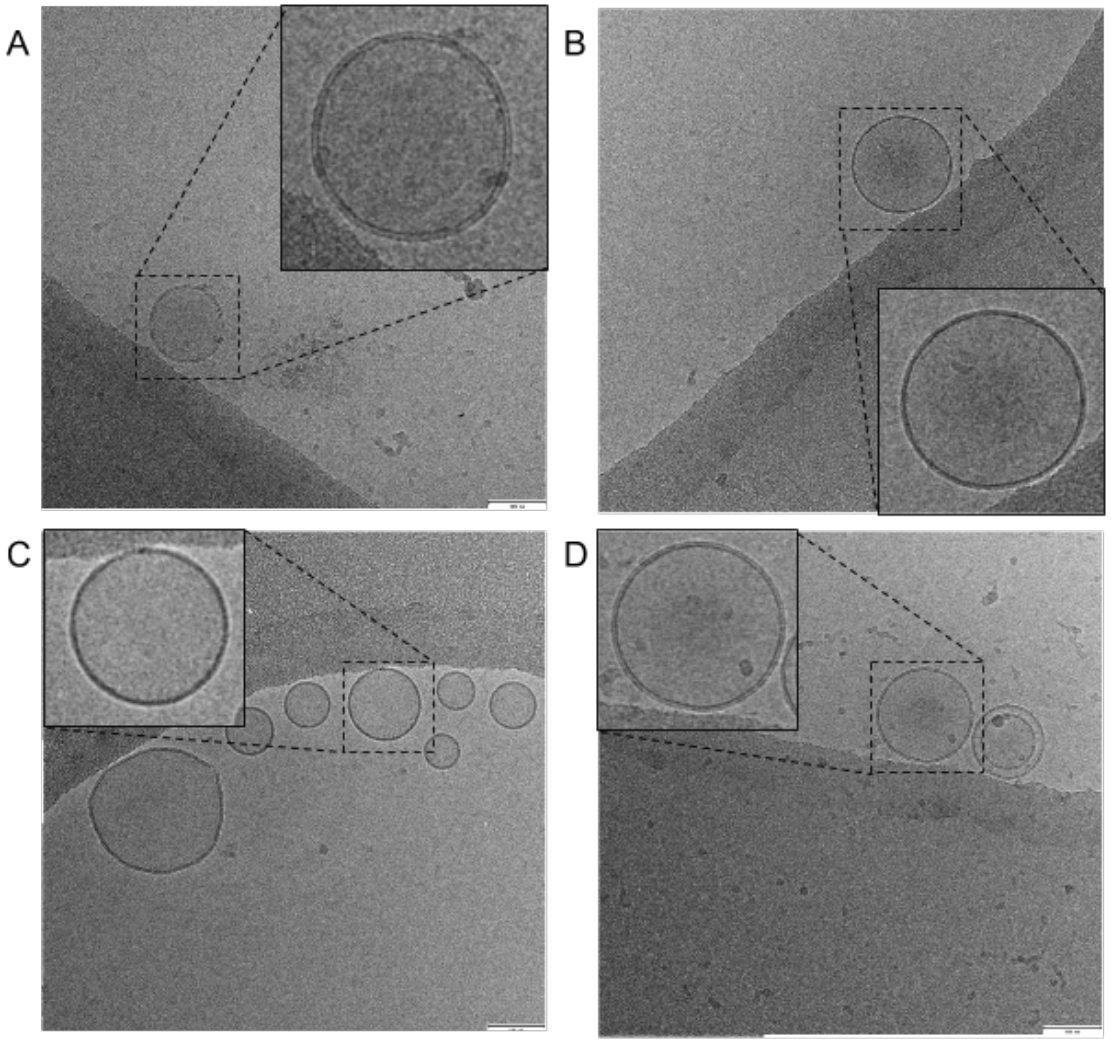

FIGURE 4.3: Cryo-EM image of encapsulated fluorescent dye and heavy metal chemicals: (A)Control liposome with no encapsulating material. (B) Liposome encapsulated with Carboxyfluorescein (CF) (C) Liposome encapsulated with caesium chloride (CsCl) (D) Liposome encapsulated with ferric chloride($FeCl_3$. Inset displays a zoomed view of the liposomes. Scale bars:100nm.

form GNP-Antibody conjugates. This lead to aggregation of GNP-Antibody conjugates. (Figure 4.4)

4.3.1.3 Bovine serum albumin (BSA)

BSA is a serum albumin protein derived from cows. It is available commercially and used as a protein concentration standard in biochemical experiments. We used different concentration of BSA to encapsulate in the liposome. Size exclusion chromatography was used to exchange outside buffer and remove free BSA. The liposomes sustained vitrification and fully BSA encapsulated liposomes were observed. At protein concentration

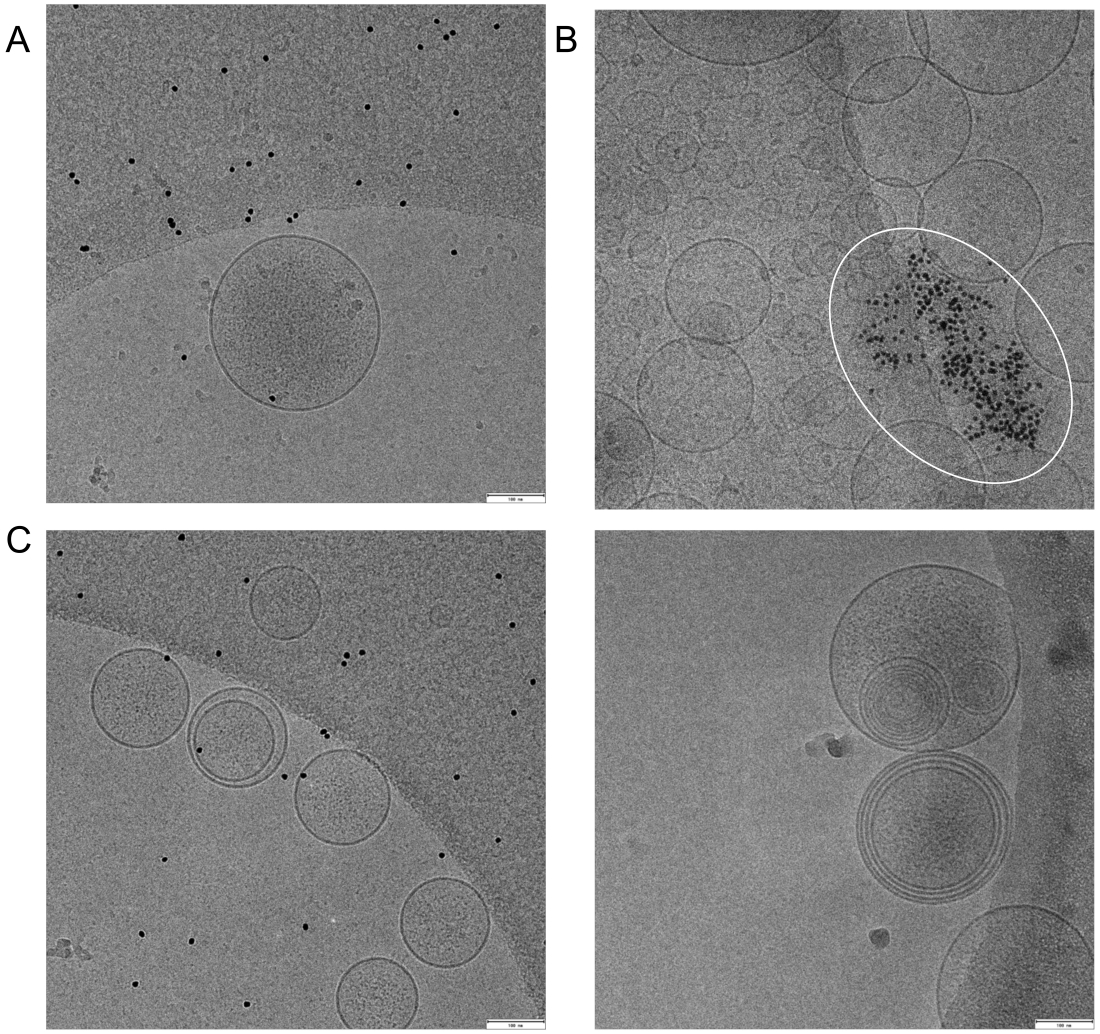

FIGURE 4.4: Cryo-EM image of encapsulated gold-nanoparticles (GNPs). (A) GNPs does not get encapsulated fully and a most of them stick to the carbon on the EM grids (B) GNP-Antibody conjugates aggregated (C) Affect of size exclustion chromatography (SEC) on the liposomes encasulated with GNPs and BSA. One left are the liposomes before SEC and on right are the liposomes after SEC. Scale bars:100nm.

less than 10mg/ml, the content in the liposomes is more difficult to visualise. There was no leakage of the liposomes. (Figure 4.5)

When BSA and GNPs were used together to encapsulate into the liposomes. After size exclusion chromatography, there were no GNPs inside the liposomes while the BSA was still present, which further supports the fact that the GNPs are permeable through lipid membranes.

4.3.1.4 Other proteins : Apoferritin and Urease

Using another protein apoferritin at higher concentration of around 10 mg/ml better encapsulation is achieved. Urease at slight lower concentration (2.5 mg/ml) was also used

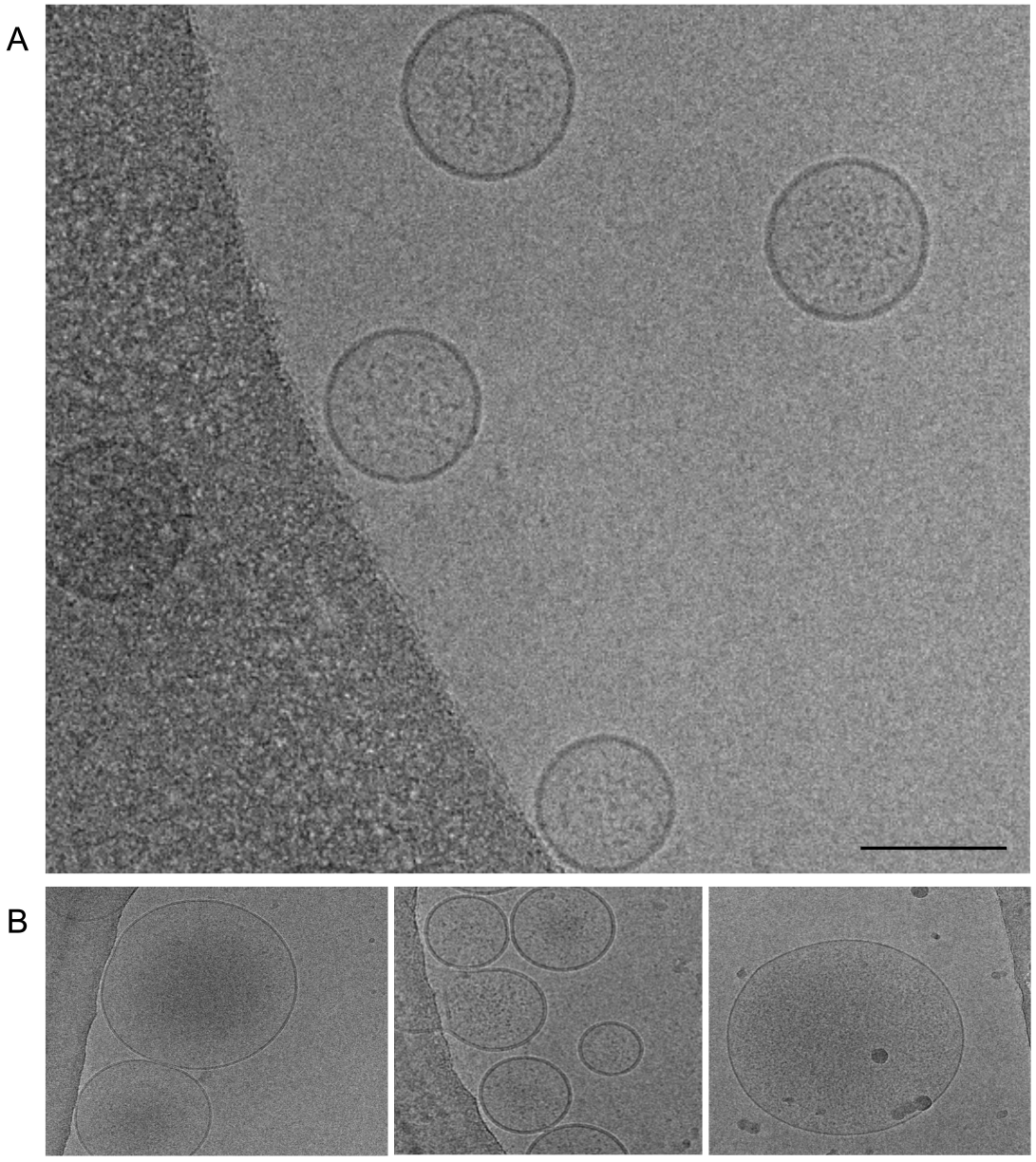

FIGURE 4.5: Cryo-EM images of encapsulated BSA. (A) BSA at 33 mg/ml (B) BSA encapsulated in liposomes at three different concentration 5 mg/ml (left), 10 mg/ml (middle) and 50 mg/ml (right). Scale bars:100nm.

and partial encapsulation was achieved as indicated by yellow arrows used to show encapsulated urease and black arrows for the non-encapsualted urease outside the lipsomes (Figure 4.6).

4.3.2 Reconstituting protein in buffer gradient liposomes.

After establishing methods to make liposomes and establish a buffer gradient between the inside and outside of the liposomes, the next task was to reconstitute membrane protein into the liposomes and make proteoliposomes. We used purified detergent solubilized

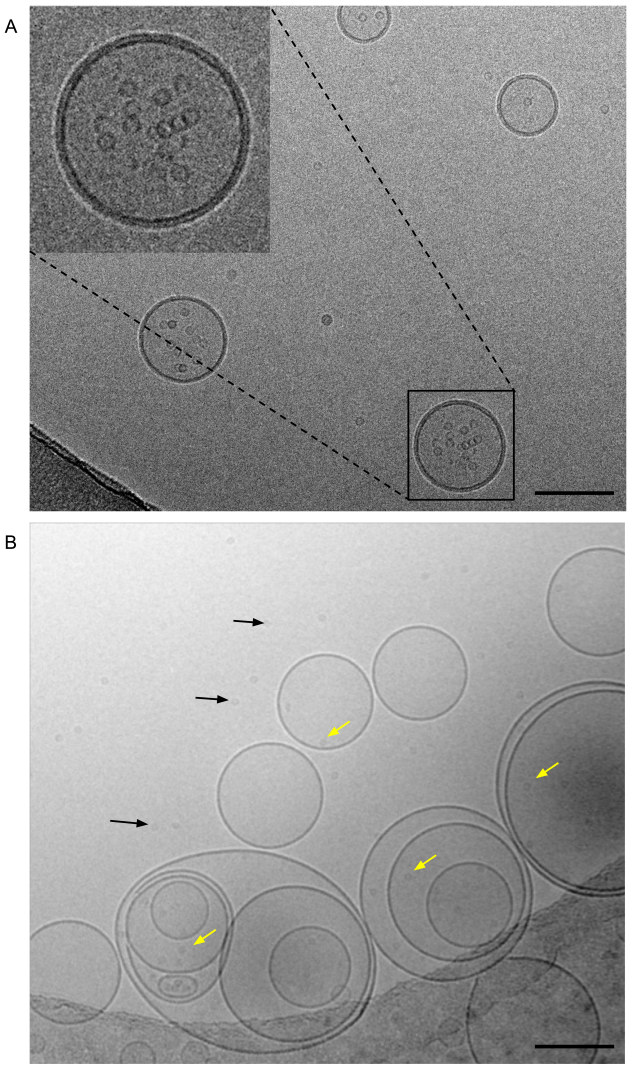

FIGURE 4.6: Cryo-EM images of encapsulated apoferritin (A) and urease(B). Scale bars:100nm

MloK1 to be reconstituted into the liposomes. We tested different lipid to protein ratios (LPRs) which affects the growth of 2D crystals. We noticed at lower LPR (1 or less) very large crystals are formed. We increased LPR to 5 and 10 to generate small crystalline vesicles. The liposome preparation, protein reconstitution and vitrification, all can affect the quality of proteoliposomes and therefore a lot of conditions has to be tested and optimised. There are often proteoliposomes aggregates visible in the sample and the shape of few proteoliposomes is distorted and not perfectly spherical. Another problem at higher LPR is the presence of semi-crystalline vesicles where the reconstitution of MloK1 was partial (Figure 4.7,A), this was evident with the lack of diffraction spots emerging from these liposomes when their fourier transform is calculated. Only perfectly crystalline vesicles displays the diffraction spots that are characteristic of MloK1 crystal packing. The intensity of the diffraction spots was very low due to the curvature of the liposomes (Figure 4.7,B).

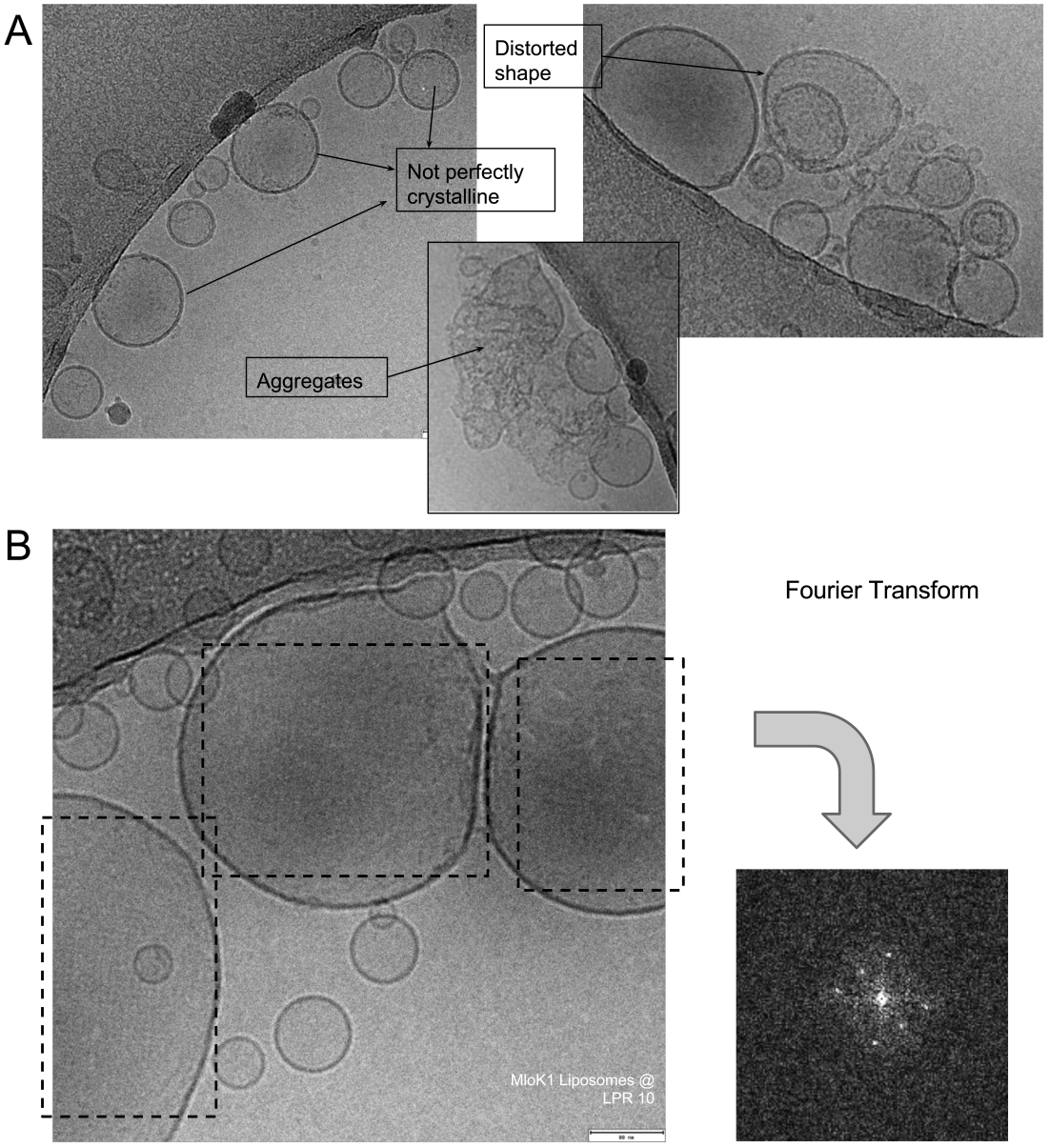

FIGURE 4.7: Cryo-EM images of liposomes reconstituted with MloK1 (A) Optimisation of MloK1 reconstitution in lipsomes with changing lipid to protein ratios (LPR), some examaples of non perfect proteoliposomes are shown (B) Perfectly crystalline vesicular MloK1 liposomes at LPR of 10, on right a Fourier transform of the crystalline patches from the proteoliposomes with weak diffraction spots. Scale bars:100nm.

4.4 Conclusions

With the technological advancement in the field of cryo-em in the last few years with the additional of powerful direct electron detectors and the software enhancements, there is a need for novel sample preparation method to take advantage of this technological advancement. Here we demonstrated a proof of principle for the use of liposomes as a tool to study membrane proteins under buffer gradients by cryo-EM. Liposomes not only provides an ideal near native lipidic environment to the membrane protein but can easily be exploited to establish a buffer gradient across the lipid bilayer thereby mimicking the true physiological conditions present in the cell. We showed it is possible to make unilamellar vesicles by hydration and dialysis methods of smaller sized diameter (<200um) which can be vitrified for cryo-EM. Using column gel filtration, we exchanged the outside buffer of the liposomes to establish a buffer gradient. We showed that the use of fluorescent dyes and heavy metal chemicals does not provide contrast in the cryo-EM images and therefore fails to serve as a marker to visualise buffer gradient. There is a possibility of leakage and bursting of the liposomes during the blotting step of vitrification, therefore we used proteins like BSA, apoferritin and urease as a marker. The encapsulated liposomes with buffer containing these marker proteins but absent in the outside sustained vitrification. Next, we used the bacterial potassium channel MloK1 as a test membrane protein to reconstitute into the liposomes in order to make crystalline proteoliposomes. We tested various different LPRs to find the best conditions for making perfectly crystalline MloK1 vesicles.

Chapter 5

General Discussion and Outlook

This dissertation was mainly committed to gain structural insight into the full length protein complex by using cryo-EM and single particle image processing. The project initially started as a collaborative project with the lab of Dr. Jean-Marc Taymans in Leuven, Belgium. In the initial phase of the project, purification of LRRK2 and LRRK1 was carried out in Leuven and shipped on ice to Basel. With several testing, it was concluded that both the protein LRRK2 and LRRK1 were not stable over time. To minimise the time between protein purification and preparation of cryo-EM grids, HEK293 cell culture and protein expression was setup in Basel starting with the LRRK2 plasmid. Within a relative short period of four months, purification of LRRK2 was fully optimised with similar quality as that was purified in the Taymans Lab in Leuven. Another advantage of the in house protein purification was the increase in yield that could be easily achieved by upscaling the purification. The time between the elution of purified protein and grid preparation for negative stain EM and cryo-EM could be reduced to less than one hour, which avoided protein from aggregating but the problem of heterogeneity was still present. To address the heterogeneity in the sample, ProteoPlex buffer screening was employed. ProteoPlex uses sparse-matrix screening of a protein's thermal unfolding behavior in under various conditions to find the optimum buffer system and pH, similar to differential scanning fluorimetry used in X-ray crystallography. The binding and the elution buffer for LRRK2 were kept at around pH 7.5, which was not optimal for the protein stability from ProteoPlex assays. Different binding and elution conditions at pH6.8 and pH 8.2 were suggested for greater stability. New binding and elution buffers were incorporated in the purification and better homogeneity of the particles were seen in the negative stain as well as cryo-EM image. The particles looked intact with similar size and a clear background was seen. This enabled cryo-EM data data to be collected and single particle analysis to be performed for LRRK2 and LRRK1, which resulted in final 3D reconstruction produced at a resolution of 24.2Å and 24.3Å for LRRK2 and LRRK1

respectively. Although, at low resolution, this is the first reported full-length structure for LRRK2 and LRRK1. The dimeric arrangement of both the proteins is confirmed. Both the complexes, have very similar overall shape forming elliptical homodimers with each monomer having a concave shape. The convergence of the 3D refinement to low resolution final maps for LRRK2 even with a bigger cryo-EM data, highlights the high degree of flexibility within the protein complex and controlling the conformational diversity of the complex by binding with a substrate will be imperative for further high resolution cryo-EM steps. This was further confirmed by the GTP-GDP bound LRRK2 negative stain analysis. In conclusion, we present the first structural insight into full length LRRK2 as well as LRRK1, which will further assist follow-up work towards a high-resolution structure of these important molecules.

Mutations in the LRRK2 gene are the greatest known genetic contributor to Parkinson's disease. Today, LRRK2 is seen as promising target to treat Parkinson's disease by several research groups around the world. Pharmaceutical companies are developing LRRK2 kinase inhibitors to correct the effects of most common PD related mutations. The field has made enormous progress since the discovery of LRRK2 mutations in 2004. The understanding of the genetic basis of this disease has increased exponentially since this time but the elucidation of the precise atomic structure of this complex, and the dynamics of this interaction in a functional context, remain a huge challenge. We believe this study will foster the structural elucidation of LRRK2 dimeric complex at high resolution by Cryo-EM. With the technological improvements in Cryo-EM field, its is now possible to routinely achieve resolutions that are sufficient to visualize side-chain densities and to determine de novo atomic structure. But the major bottleneck for attaining high resolution cryo-EM maps still remains the biochemical sample preparation for flexible and dynamic protein complexes. Therefore the next challenge towards high resolution cryo-EM data collection for LRRK2 and LRRK1 would be address the inherent conformational flexibility. LRRKs are special protein having two catalytic domains a GTPase and a Kinase. Without a known substrate, it is necessary to use GTP/GDP to stable the different conformational states of the protein. Our results with GTP and GDP bound LRRK2 reveals improvement in the particles shape in negative stain EM. The next step, should be to collect cryo-EM data and perform single particle on these stabled GTP/GDP bound LRRK2 and compare the 2D class averages. If the conformations are stabilized, it is possible to infer high resolution informations which are not blurred out in averaging. Another possibility is to use GTPgammaS, which is a non-hydrolyzable (or slowly hydrolyzable) G-protein-activating analog of GTP. This can further improve conformational heterogeneity in LRRK2 particles by locking a particular functional conformation for a longer period of time. Another approach that can be used to address the conformational flexibility in LRRK2 is to target the kinase domain. There are several

kinase inhibitors now known for LRRK2 and binding of these kinase inhibitors can be tested to improve the stability of the protein for cryo-EM sample preparation and data collection. A high resolution structure of LRRK2 and LRRK1 will answer a lot of open questions related to pathobiology of LRRK2 linked mutation in PD.

The novel method of liposomal preparation used as a tool to study membrane protein under buffer gradient extends the technique of electron crystallography. 2D crystallisation can be intrinsically difficult to achieve for some membrane proteins. It requires the screening of hundreds of different crystallization conditions and various membrane protein do not form large crystals at all, which hinders the subsequent image processing. On the other hand, reconstituting membrane proteins in small unilamellar liposomes is a relatively feasible task. Different LPRs can be tested in parallel, which controls the crystalline behaviour of membrane proteins embedded in liposomes, eg. liposomes at higher LPR (10:1) tends to make membrane proteins semi-crystalline in densely packed membranes. Our proposed method can be broadly applied to other membrane proteins and the gradient across the membrane can be precisely controlled to suit the native environment of the purified membrane protein.

The next challenge that still needs to be tackled to prove this technique as a viable alternative to classical electron crystallography is the computational image processing of the crystalline vesicles of membrane proteins. The crystal unbending and Fourier filtering methods routinely used for electron crystallography are well established and works well in cases where flat well-ordered 2D crystals are available and high resolution structure determination is possible. However, these methods are limiting when applied to 2D crystals that are badly ordered or non-flat. One approach to deal with these badly ordered non-flat 2D crystals of membrane protein is to treat them as single particles while still exploiting neighbourhood correlation between adjacent proteins in the 2D crystal to address the low signal to noise ration of the 2d crystal images. This method was successfully applied to improve resolution and higher structural details for MloK1 dataset and incorporated as a part of inhouse 2dx software (Scherer et al. 2014). The single particle approach can be applied to the proteoliposomes as well but there the algorithm has to take into consideration two additional aspects, the spherical geometry of the liposomes and the presence of overlapping lattice in the collected cryo-EM images of proteoliposomes. The position of a membrane protein on the spherical vesicles can be directly used to determine two of the three Euler angles of orientation. As the sphericity of the vesicles can be maintained during vitrification, this method simplifies orientation determination which is usually difficult for small membrane proteins in projection matching routines used in single particle reconstructions.The presence of two layer of lattice coming from the upper and lower hemisphere of the vesicles respectively in the projection images of the proteoliposomes has to be dealt by the software by deconvolution of signal coming

from both lattices. Another possibility is to combine the single particle approach with electron tomography and and sub-volume averaging. The goal here would be record the same proteoliposomes such that the crystal unit cell from the image recorded by single particle can be localized in the tomogram subsequently recorded by electron tomography. A similar approach was demonstrated to work for COPI coated vesicles (Faini et al. 2012). With the improvements in direct electron detectors and softwares, electron tomography and sub-volume averaging have been drastically improved and used to reconstruct sub-nanometer resolution structures (Schur et al. 2013; Bharat et al. 2015). The in house developed Dynamo software system provides the necessary tools to pick up individual 3D sub-volumes by exploiting the the regular arrangement of membrane proteins in the crystalline proteoliposomes and perform sub-tomogram averaging (Castao-Dez et al. 2012). Although, the resolution limit of this method will be lower than that of X-ray crystallography but the advantage of providing a more native environment to the membrane proteins, structure/function relationships can be probed by the effect of buffer gradient. These low resolution dynamic snapshots of the membrane protein can be combined to higher resolution X-ray diffraction (XRD) data, to model the protein function efficiently.

References

Aarsland, D., Brnnick, K., Ehrt, U., De Deyn, P. P., Tekin, S., Emre, M., and Cummings, J. L. (2007). Neuropsychiatric symptoms in patients with parkinson's disease and dementia: frequency, profile and associated care giver stress. *J Neurol Neurosurg Psychiatr*, 78(1):36–42.

Abou-Sleiman, P. M., Healy, D. G., Quinn, N., Lees, A. J., and Wood, N. W. (2003). The role of pathogenic dj-1 mutations in parkinson's disease. *Ann Neurol*, 54(3):283–286.

Alegre-Abarrategui, J., Christian, H., Lufino, M. M. P., Mutihac, R., Venda, L. L., Ansorge, O., and Wade-Martins, R. (2009). Lrrk2 regulates autophagic activity and localizes to specific membrane microdomains in a novel human genomic reporter cellular model. *Hum Mol Genet*, 18(21):4022–4034.

Andres-Mateos, E., Mejias, R., Sasaki, M., Li, X., Lin, B. M., Biskup, S., Zhang, L., Banerjee, R., Thomas, B., Yang, L., Liu, G., Beal, M. F., Huso, D. L., Dawson, T. M., and Dawson, V. L. (2009). Unexpected lack of hypersensitivity in lrrk2 knock-out mice to mptp (1-methyl-4-phenyl-1,2,3,6-tetrahydropyridine). *J Neurosci*, 29(50):15846–15850.

Arinaminpathy, Y., Khurana, E., Engelman, D. M., and Gerstein, M. B. (2009). Computational analysis of membrane proteins: the largest class of drug targets. *Drug Discov Today*, 14(23-24):1130–1135.

Au, W. L. and Calne, D. B. (2005). A reassessment of the lewy body. *Acta Neurol Taiwan*, 14(2):40–47.

Baker, M. R., Fan, G., and Serysheva, I. I. (2015). Single-particle cryo-em of the ryanodine receptor channel in an aqueous environment. *Eur J Transl Myol*, 25(1):35–48.

Bandopadhyay, R., Kingsbury, A. E., Cookson, M. R., Reid, A. R., Evans, I. M., Hope, A. D., Pittman, A. M., Lashley, T., Canet-Aviles, R., Miller, D. W., McLendon, C., Strand, C., Leonard, A. J., Abou-Sleiman, P. M., Healy, D. G., Ariga, H., Wood, N. W., de Silva, R., Revesz, T., Hardy, J. A., and Lees, A. J. (2004). The expression of dj-1 (park7) in normal human cns and idiopathic parkinson's disease. *Brain*, 127(Pt 2):420–430.

Beilina, A., Van Der Brug, M., Ahmad, R., Kesavapany, S., Miller, D. W., Petsko, G. A., and Cookson, M. R. (2005). Mutations in pten-induced putative kinase 1 associated with recessive parkinsonism have differential effects on protein stability. *Proc Natl Acad Sci U S A*, 102(16):5703–5708.

Bekris, L. M., Mata, I. F., and Zabetian, C. P. (2010). The genetics of parkinson disease. *J Geriatr Psychiatry Neurol*, 23(4):228–242.

Bell, J. M., Chen, M., Baldwin, P. R., and Ludtke, S. J. (2016). High resolution single particle refinement in eman2.1. *Methods*, 100:25–34.

Benabid, A. L., Chabardes, S., Mitrofanis, J., and Pollak, P. (2009). Deep brain stimulation of the subthalamic nucleus for the treatment of parkinson's disease. *Lancet Neurol*, 8(1):67–81.

Berger, Z., Smith, K. A., and Lavoie, M. J. (2010). Membrane localization of lrrk2 is associated with increased formation of the highly active lrrk2 dimer and changes in its phosphorylation. *Biochemistry*, 49(26):5511–5523.

Berman, S. B., Pineda, F. J., and Hardwick, J. M. (2008). Mitochondrial fission and fusion dynamics: the long and short of it. *Cell Death Differ*, 15(7):1147–1152.

Betarbet, R., Sherer, T. B., MacKenzie, G., Garcia-Osuna, M., Panov, A. V., and Greenamyre, J. T. (2000). Chronic systemic pesticide exposure reproduces features of parkinson's disease. *Nat Neurosci*, 3(12):1301–1306.

Bharat, T. A. M., Russo, C. J., Lwe, J., Passmore, L. A., and Scheres, S. H. W. (2015). Advances in single-particle electron cryomicroscopy structure determination applied to sub-tomogram averaging. *Structure*, 23(9):1743–1753.

Biousse, V., Skibell, B. C., Watts, R. L., Loupe, D. N., Drews-Botsch, C., and Newman, N. J. (2004). Ophthalmologic features of parkinson's disease. *Neurology*, 62(2):177–180.

Biskup, S., Moore, D. J., Celsi, F., Higashi, S., West, A. B., Andrabi, S. A., Kurkinen, K., Yu, S.-W., Savitt, J. M., Waldvogel, H. J., Faull, R. L. M., Emson, P. C., Torp, R., Ottersen, O. P., Dawson, T. M., and Dawson, V. L. (2006). Localization of lrrk2 to membranous and vesicular structures in mammalian brain. *Ann Neurol*, 60(5):557–569.

Biskup, S., Moore, D. J., Rea, A., Lorenz-Deperieux, B., Coombes, C. E., Dawson, V. L., Dawson, T. M., and West, A. B. (2007). Dynamic and redundant regulation of lrrk2 and lrrk1 expression. *BMC Neurosci*, 8:102.

Biskup, S. and West, A. B. (2009). Zeroing in on lrrk2-linked pathogenic mechanisms in parkinson's disease. *Biochim Biophys Acta*, 1792(7):625–633.

Boelen, M. (2007). The role of rehabilitative modalities and exercise in parkinson's disease. *Dis Mon*, 53(5):259–264.

Bonifati, V. (2006). Parkinson's disease: the lrrk2-g2019s mutation: opening a novel era in parkinson's disease genetics. *Eur J Hum Genet*, 14(10):1061–1062.

Bonifati, V., Rizzu, P., van Baren, M. J., Schaap, O., Breedveld, G. J., Krieger, E., Dekker, M. C. J., Squitieri, F., Ibanez, P., Joosse, M., van Dongen, J. W., Vanacore, N.,

van Swieten, J. C., Brice, A., Meco, G., van Duijn, C. M., Oostra, B. A., and Heutink, P. (2003). Mutations in the dj-1 gene associated with autosomal recessive early-onset parkinsonism. *Science*, 299(5604):256–259.

Bosgraaf, L. and Van Haastert, P. J. M. (2003). Roc, a ras/gtpase domain in complex proteins. *Biochim Biophys Acta*, 1643(1-3):5–10.

Braak, H., Bohl, J. R., Mller, C. M., Rb, U., de Vos, R. A. I., and Del Tredici, K. (2006). Stanley fahn lecture 2005: The staging procedure for the inclusion body pathology associated with sporadic parkinson's disease reconsidered. *Mov Disord*, 21(12):2042–2051.

Braak, H., Del Tredici, K., Rb, U., de Vos, R. A. I., Jansen Steur, E. N. H., and Braak, E. (2003). Staging of brain pathology related to sporadic parkinson's disease. *Neurobiol Aging*, 24(2):197–211.

Brooks, D. J. (2010). Imaging approaches to parkinson disease. *J Nucl Med*, 51(4):596–609.

Bttcher, B., Wynne, S. A., and Crowther, R. A. (1997). Determination of the fold of the core protein of hepatitis b virus by electron cryomicroscopy. *Nature*, 386(6620):88–91.

Cardona, F., Tormos-Prez, M., and Prez-Tur, J. (2014). Structural and functional in silico analysis of lrrk2 missense substitutions. *Mol Biol Rep*, 41(4):2529–2542.

Castao-Dez, D., Kudryashev, M., Arheit, M., and Stahlberg, H. (2012). Dynamo: a flexible, user-friendly development tool for subtomogram averaging of cryo-em data in high-performance computing environments. *J Struct Biol*, 178(2):139–151.

Chari, A., Haselbach, D., Kirves, J.-M., Ohmer, J., Paknia, E., Fischer, N., Ganichkin, O., Mller, V., Frye, J. J., Petzold, G., Jarvis, M., Tietzel, M., Grimm, C., Peters, J.-M., Schulman, B. A., Tittmann, K., Markl, J., Fischer, U., and Stark, H. (2015). Proteoplex: stability optimization of macromolecular complexes by sparse-matrix screening of chemical space. *Nat Methods*, 12(9):859–865.

Chavrier, P., Gorvel, J. P., Stelzer, E., Simons, K., Gruenberg, J., and Zerial, M. (1991). Hypervariable c-terminal domain of rab proteins acts as a targeting signal. *Nature*, 353(6346):769–772.

Cherra, S. J., Steer, E., Gusdon, A. M., Kiselyov, K., and Chu, C. T. (2013). Mutant lrrk2 elicits calcium imbalance and depletion of dendritic mitochondria in neurons. *Am J Pathol*, 182(2):474–484.

Chung, K. K., Zhang, Y., Lim, K. L., Tanaka, Y., Huang, H., Gao, J., Ross, C. A., Dawson, V. L., and Dawson, T. M. (2001). Parkin ubiquitinates the alpha-synuclein-interacting protein, synphilin-1: implications for lewy-body formation in parkinson disease. *Nat Med*, 7(10):1144–1150.

Civiero, L. and Bubacco, L. (2012). Human leucine-rich repeat kinase 1 and 2: intersecting or unrelated functions? *Biochem Soc Trans*, 40(5):1095–1101.

Civiero, L., Vancraenenbroeck, R., Belluzzi, E., Beilina, A., Lobbestael, E., Reyniers, L., Gao, F., Micetic, I., De Maeyer, M., Bubacco, L., Baekelandt, V., Cookson, M. R., Greggio, E., and Taymans, J.-M. (2012). Biochemical characterization of highly purified leucine-rich repeat kinases 1 and 2 demonstrates formation of homodimers. *PLoS ONE*, 7(8):e43472.

Clark, L. N., Wang, Y., Karlins, E., Saito, L., Mejia-Santana, H., Harris, J., Louis, E. D., Cote, L. J., Andrews, H., Fahn, S., Waters, C., Ford, B., Frucht, S., Ottman, R., and Marder, K. (2006). Frequency of lrrk2 mutations in early- and late-onset parkinson disease. *Neurology*, 67(10):1786–1791.

Conway, J. F., Cheng, N., Zlotnick, A., Wingfield, P. T., Stahl, S. J., and Steven, A. C. (1997). Visualization of a 4-helix bundle in the hepatitis b virus capsid by cryo-electron microscopy. *Nature*, 386(6620):91–94.

Cookson, M. R. (2015). Lrrk2 pathways leading to neurodegeneration. *Curr Neurol Neurosci Rep*, 15(7):42.

Cookson, M. R., Lockhart, P. J., McLendon, C., O'Farrell, C., Schlossmacher, M., and Farrer, M. J. (2003). Ring finger 1 mutations in parkin produce altered localization of the protein. *Hum Mol Genet*, 12(22):2957–2965.

Corti, O., Hampe, C., Darios, F., Ibanez, P., Ruberg, M., and Brice, A. (2005). Parkinson's disease: from causes to mechanisms. *C R Biol*, 328(2):131–142.

Critchley, E. M. (1981). Speech disorders of parkinsonism: a review. *J Neurol Neurosurg Psychiatr*, 44(9):751–758.

Cunningham, E. L., McGuinness, B., Herron, B., and Passmore, A. P. (2015). Dementia. *Ulster Med J*, 84(2):79–87.

Dachsel, J. C., Nishioka, K., Vilario-Gell, C., Lincoln, S. J., Soto-Ortolaza, A. I., Kachergus, J., Hinkle, K. M., Heckman, M. G., Jasinska-Myga, B., Taylor, J. P., Dickson, D. W., Gibson, R. A., Hentati, F., Ross, O. A., and Farrer, M. J. (2010). Heterodimerization of lrrk1-lrrk2: Implications for lrrk2-associated parkinson disease. *Mech Ageing Dev*, 131(3):210–214.

Danils, V., Vancraenenbroeck, R., Law, B. M. H., Greggio, E., Lobbestael, E., Gao, F., De Maeyer, M., Cookson, M. R., Harvey, K., Baekelandt, V., and Taymans, J.-M. (2011). Insight into the mode of action of the lrrk2 y1699c pathogenic mutant. *J Neurochem*, 116(2):304–315.

Dauer, W. and Przedborski, S. (2003). Parkinson's disease: mechanisms and models. *Neuron*, 39(6):889–909.

Davie, C. A. (2008). A review of parkinson's disease. *Br Med Bull*, 86:109–127.

De Rosier, D. J. and Klug, A. (1968). Reconstruction of three dimensional structures from electron micrographs. *Nature*, 217(5124):130–134.

Deng, J., Lewis, P. A., Greggio, E., Sluch, E., Beilina, A., and Cookson, M. R. (2008). Structure of the roc domain from the parkinson's disease-associated leucine-rich repeat kinase 2 reveals a dimeric gtpase. *Proc Natl Acad Sci U S A*, 105(5):1499–1504.

Deng, X., Dzamko, N., Prescott, A., Davies, P., Liu, Q., Yang, Q., Lee, J.-D., Patricelli, M. P., Nomanbhoy, T. K., Alessi, D. R., and Gray, N. S. (2011). Characterization of a selective inhibitor of the parkinson's disease kinase lrrk2. *Nat Chem Biol*, 7(4):203–205.

Di Fonzo, A., Tassorelli, C., De Mari, M., Chien, H. F., Ferreira, J., Roh, C. F., Riboldazzi, G., Antonini, A., Albani, G., Mauro, A., Marconi, R., Abbruzzese, G., Lopiano, L., Fincati, E., Guidi, M., Marini, P., Stocchi, F., Onofrj, M., Toni, V., Tinazzi, M., Fabbrini, G., Lamberti, P., Vanacore, N., Meco, G., Leitner, P., Uitti, R. J., Wszolek, Z. K., Gasser, T., Simons, E. J., Breedveld, G. J., Goldwurm, S., Pezzoli, G., Sampaio, C., Barbosa, E., Martignoni, E., Oostra, B. A., Bonifati, V., and Network, I. P. G. (2006a). Comprehensive analysis of the lrrk2 gene in sixty families with parkinson's disease. *Eur J Hum Genet*, 14(3):322–331.

Di Fonzo, A., Wu-Chou, Y.-H., Lu, C.-S., van Doeselaar, M., Simons, E. J., Roh, C. F., Chang, H.-C., Chen, R.-S., Weng, Y.-H., Vanacore, N., Breedveld, G. J., Oostra, B. A., and Bonifati, V. (2006b). A common missense variant in the lrrk2 gene, gly2385arg, associated with parkinson's disease risk in taiwan. *Neurogenetics*, 7(3):133–138.

Dodson, M. W., Zhang, T., Jiang, C., Chen, S., and Guo, M. (2012). Roles of the drosophila lrrk2 homolog in rab7-dependent lysosomal positioning. *Hum Mol Genet*, 21(6):1350–1363.

Donaldson, I. M. L. (2015). James parkinson's essay on the shaking palsy. *J R Coll Physicians Edinb*, 45(1):84–86.

Dubochet, J., Adrian, M., Chang, J. J., Homo, J. C., Lepault, J., McDowall, A. W., and Schultz, P. (1988). Cryo-electron microscopy of vitrified specimens. *Q Rev Biophys*, 21(2):129–228.

Dusonchet, J., Kochubey, O., Stafa, K., Young, S. M., Zufferey, R., Moore, D. J., Schneider, B. L., and Aebischer, P. (2011). A rat model of progressive nigral neurodegeneration induced by the parkinson's disease-associated g2019s mutation in lrrk2. *J Neurosci*, 31(3):907–912.

Dusonchet, J., Li, H., Guillily, M., Liu, M., Stafa, K., Derada Troletti, C., Boon, J. Y., Saha, S., Glauser, L., Mamais, A., Citro, A., Youmans, K. L., Liu, L., Schneider, B. L., Aebischer, P., Yue, Z., Bandopadhyay, R., Glicksman, M. A., Moore, D. J., Collins, J. J., and Wolozin, B. (2014). A parkinson's disease gene regulatory network identifies the signaling protein rgs2 as a modulator of lrrk2 activity and neuronal toxicity. *Hum Mol Genet*, 23(18):4887–4905.

Dzamko, N., Deak, M., Hentati, F., Reith, A. D., Prescott, A. R., Alessi, D. R., and Nichols, R. J. (2010). Inhibition of lrrk2 kinase activity leads to dephosphorylation of ser(910)/ser(935), disruption of 14-3-3 binding and altered cytoplasmic localization. *Biochem J*, 430(3):405–413.

Dzamko, N. and Halliday, G. M. (2012). An emerging role for lrrk2 in the immune system. *Biochem Soc Trans*, 40(5):1134–1139.

Dchsel, J. C., Ross, O. A., Mata, I. F., Kachergus, J., Toft, M., Cannon, A., Baker, M., Adamson, J., Hutton, M., Dickson, D. W., and Farrer, M. J. (2007). Lrrk2 g2019s substitution in frontotemporal lobar degeneration with ubiquitin-immunoreactive neuronal inclusions. *Acta Neuropathol*, 113(5):601–606.

Egelman, E. H. (2016). The current revolution in cryo-em. *Biophys J*, 110(5):1008–1012.

Elbaz, A., Levecque, C., Clavel, J., Vidal, J.-S., Richard, F., Corrze, J.-R., Delemotte, B., Amouyel, P., Alprovitch, A., Chartier-Harlin, M.-C., and Tzourio, C. (2003). S18y polymorphism in the uch-l1 gene and parkinson's disease: evidence for an age-dependent relationship. *Mov Disord*, 18(2):130–137.

Fagerberg, L., Jonasson, K., von Heijne, G., Uhln, M., and Berglund, L. (2010). Prediction of the human membrane proteome. *Proteomics*, 10(6):1141–1149.

Faini, M., Prinz, S., Beck, R., Schorb, M., Riches, J. D., Bacia, K., Brgger, B., Wieland, F. T., and Briggs, J. A. G. (2012). The structures of copi-coated vesicles reveal alternate coatomer conformations and interactions. *Science*, 336(6087):1451–1454.

Farrer, M., Wavrant-De Vrieze, F., Crook, R., Boles, L., Perez-Tur, J., Hardy, J., Johnson, W. G., Steele, J., Maraganore, D., Gwinn, K., and Lynch, T. (1998). Low frequency of alpha-synuclein mutations in familial parkinson's disease. *Ann Neurol*, 43(3):394–397.

Forno, L. S. (1996). Neuropathology of parkinson's disease. *J Neuropathol Exp Neurol*, 55(3):259–272.

Forsayeth, J., Bankiewicz, K. S., and Aminoff, M. J. (2010). Gene therapy for parkinson's disease: where are we now and where are we going? *Expert Rev Neurother*, 10(12):1839–1845.

Frank, G., Shukla, S., Rao, P., Borgnia, M. J., Bartesaghi, A., Merk, A., Mobin, A., Esser, L., Earl, L. A., Gottesman, M. M., Xia, D., Ambudkar, S. V., and Subramaniam, S. (2016). Cryo-em analysis of the conformational landscape of human p-glycoprotein (abcb1) during its catalytic cycle. *Mol Pharmacol*.

Frank, J., Verschoor, A., and Boublik, M. (1981). Computer averaging of electron micrographs of 40s ribosomal subunits. *Science*, 214(4527):1353–1355.

Frank, M. J. (2005). Dynamic dopamine modulation in the basal ganglia: a neurocomputational account of cognitive deficits in medicated and nonmedicated parkinsonism. *J Cogn Neurosci*, 17(1):51–72.

Freedom, T. (2007). Sleep and parkinson's disease. *Dis Mon*, 53(5):275–290.

Funayama, M., Hasegawa, K., Kowa, H., Saito, M., Tsuji, S., and Obata, F. (2002). A new locus for parkinson's disease (park8) maps to chromosome 12p11.2-q13.1. *Ann Neurol*, 51(3):296–301.

Funayama, M., Hasegawa, K., Ohta, E., Kawashima, N., Komiyama, M., Kowa, H., Tsuji, S., and Obata, F. (2005). An lrrk2 mutation as a cause for the parkinsonism in the original park8 family. *Ann Neurol*, 57(6):918–921.

Fung, H.-C., Chen, C.-M., Hardy, J., Hernandez, D., Singleton, A., and Wu, Y.-R. (2006a). Lack of g2019s lrrk2 mutation in a cohort of taiwanese with sporadic parkinson's disease. *Mov Disord*, 21(6):880–881.

Fung, H.-C., Chen, C.-M., Hardy, J., Singleton, A. B., and Wu, Y.-R. (2006b). A common genetic factor for parkinson disease in ethnic chinese population in taiwan. *BMC Neurol*, 6:47.

Galter, D., Westerlund, M., Belin, A. C., and Olson, L. (2007). Dj-1 and uch-l1 gene activity patterns in the brains of controls, parkinson and schizophrenia patients and in rodents. *Physiol Behav*, 92(1-2):46–53.

Galter, D., Westerlund, M., Carmine, A., Lindqvist, E., Sydow, O., and Olson, L. (2006). Lrrk2 expression linked to dopamine-innervated areas. *Ann Neurol*, 59(4):714–719.

Gandhi, S., Muqit, M. M. K., Stanyer, L., Healy, D. G., Abou-Sleiman, P. M., Hargreaves, I., Heales, S., Ganguly, M., Parsons, L., Lees, A. J., Latchman, D. S., Holton, J. L., Wood, N. W., and Revesz, T. (2006). Pink1 protein in normal human brain and parkinson's disease. *Brain*, 129(Pt 7):1720–1731.

Gasper, R., Meyer, S., Gotthardt, K., Sirajuddin, M., and Wittinghofer, A. (2009). It takes two to tango: regulation of g proteins by dimerization. *Nat Rev Mol Cell Biol*, 10(6):423–429.

Gelb, D. J., Oliver, E., and Gilman, S. (1999). Diagnostic criteria for parkinson disease. *Arch Neurol*, 56(1):33–39.

Giasson, B. I., Duda, J. E., Murray, I. V., Chen, Q., Souza, J. M., Hurtig, H. I., Ischiropoulos, H., Trojanowski, J. Q., and Lee, V. M. (2000). Oxidative damage linked to neurodegeneration by selective alpha-synuclein nitration in synucleinopathy lesions. *Science*, 290(5493):985–989.

Gibb, W. R. and Lees, A. J. (1988). The relevance of the lewy body to the pathogenesis of idiopathic parkinson's disease. *J Neurol Neurosurg Psychiatr*, 51(6):745–752.

Giesert, F., Hofmann, A., Brger, A., Zerle, J., Kloos, K., Hafen, U., Ernst, L., Zhang, J., Vogt-Weisenhorn, D. M., and Wurst, W. (2013). Expression analysis of lrrk1, lrrk2 and lrrk2 splice variants in mice. *PLoS ONE*, 8(5):e63778.

Gilsbach, B. K., Ho, F. Y., Vetter, I. R., van Haastert, P. J. M., Wittinghofer, A., and Kortholt, A. (2012). Roco kinase structures give insights into the mechanism of parkinson disease-related leucine-rich-repeat kinase 2 mutations. *Proc Natl Acad Sci U S A*, 109(26):10322–10327.

Gilsbach, B. K. and Kortholt, A. (2014). Structural biology of the lrrk2 gtpase and kinase domains: implications for regulation. *Front Mol Neurosci*, 7:32.

Glaeser, R. M. (2016). How good can cryo-em become? *Nat Methods*, 13(1):28–32.

Gloeckner, C. J., Kinkl, N., Schumacher, A., Braun, R. J., O'Neill, E., Meitinger, T., Kolch, W., Prokisch, H., and Ueffing, M. (2006). The parkinson disease causing lrrk2 mutation i2020t is associated with increased kinase activity. *Hum Mol Genet*, 15(2):223–232.

Goetz, C. G. (2006). What's new? clinical progression and staging of parkinson's disease. *J Neural Transm Suppl*, (70):305–308.

Goldwurm, S., Zini, M., Mariani, L., Tesei, S., Miceli, R., Sironi, F., Clementi, M., Bonifati, V., and Pezzoli, G. (2007). Evaluation of lrrk2 g2019s penetrance: relevance for genetic counseling in parkinson disease. *Neurology*, 68(14):1141–1143.

Gotthardt, K., Weyand, M., Kortholt, A., Van Haastert, P. J. M., and Wittinghofer, A. (2008). Structure of the roc-cor domain tandem of c. tepidum, a prokaryotic homologue of the human lrrk2 parkinson kinase. *EMBO J*, 27(16):2239–2249.

Grammatikakis, N., Lin, J. H., Grammatikakis, A., Tsichlis, P. N., and Cochran, B. H. (1999). p50(cdc37) acting in concert with hsp90 is required for raf-1 function. *Mol Cell Biol*, 19(3):1661–1672.

Greggio, E. and Cookson, M. R. (2009). Leucine-rich repeat kinase 2 mutations and parkinson's disease: three questions. *ASN Neuro*, 1(1).

Greggio, E., Jain, S., Kingsbury, A., Bandopadhyay, R., Lewis, P., Kaganovich, A., van der Brug, M. P., Beilina, A., Blackinton, J., Thomas, K. J., Ahmad, R., Miller, D. W., Kesavapany, S., Singleton, A., Lees, A., Harvey, R. J., Harvey, K., and Cookson, M. R. (2006). Kinase activity is required for the toxic effects of mutant lrrk2/dardarin. *Neurobiol Dis*, 23(2):329–341.

Greggio, E., Lewis, P. A., van der Brug, M. P., Ahmad, R., Kaganovich, A., Ding, J., Beilina, A., Baker, A. K., and Cookson, M. R. (2007). Mutations in lrrk2/dardarin associated with parkinson disease are more toxic than equivalent mutations in the homologous kinase lrrk1. *J Neurochem*, 102(1):93–102.

Greggio, E., Zambrano, I., Kaganovich, A., Beilina, A., Taymans, J.-M., Danils, V., Lewis, P., Jain, S., Ding, J., Syed, A., Thomas, K. J., Baekelandt, V., and Cookson, M. R. (2008). The parkinson disease-associated leucine-rich repeat kinase 2 (lrrk2) is a dimer that undergoes intramolecular autophosphorylation. *J Biol Chem*, 283(24):16906–16914.

Guo, L., Gandhi, P. N., Wang, W., Petersen, R. B., Wilson-Delfosse, A. L., and Chen, S. G. (2007). The parkinson's disease-associated protein, leucine-rich repeat kinase 2 (lrrk2), is an authentic gtpase that stimulates kinase activity. *Exp Cell Res*, 313(16):3658–3670.

Guo, L., Wang, W., and Chen, S. G. (2006). Leucine-rich repeat kinase 2: relevance to parkinson's disease. *Int J Biochem Cell Biol*, 38(9):1469–1475.

Gmez-Suaga, P., Luzn-Toro, B., Churamani, D., Zhang, L., Bloor-Young, D., Patel, S., Woodman, P. G., Churchill, G. C., and Hilfiker, S. (2012). Leucine-rich repeat kinase 2 regulates autophagy through a calcium-dependent pathway involving naadp. *Hum Mol Genet*, 21(3):511–525.

Gring, S., Taymans, J.-M., Baekelandt, V., and Schmidt, B. (2014). Indolinone based lrrk2 kinase inhibitors with a key hydrogen bond. *Bioorg Med Chem Lett*, 24(19):4630–4637.

Hammerstad, J. and Hogarth, P. (2001). Parkinson's disease: surgical options. *Curr Neurol Neurosci Rep*, 1(4):313–319.

Hanafusa, H., Ishikawa, K., Kedashiro, S., Saigo, T., Iemura, S.-I., Natsume, T., Komada, M., Shibuya, H., Nara, A., and Matsumoto, K. (2011). Leucine-rich repeat kinase lrrk1 regulates endosomal trafficking of the egf receptor. *Nat Commun*, 2:158.

Hely, M. A., Morris, J. G. L., Reid, W. G. J., and Trafficante, R. (2005). Sydney multicenter study of parkinson's disease: non-l-dopa-responsive problems dominate at 15 years. *Mov Disord*, 20(2):190–199.

Henderson, R. (2015). Overview and future of single particle electron cryomicroscopy. *Arch Biochem Biophys*, 581:19–24.

Henderson, R., Baldwin, J. M., Ceska, T. A., Zemlin, F., Beckmann, E., and Downing, K. H. (1990). Model for the structure of bacteriorhodopsin based on high-resolution electron cryo-microscopy. *J Mol Biol*, 213(4):899–929.

Henderson, R. and Unwin, P. N. (1975). Three-dimensional model of purple membrane obtained by electron microscopy. *Nature*, 257(5521):28–32.

Hernandez, D. G., Reed, X., and Singleton, A. B. (2016). Genetics in parkinson disease: Mendelian versus non-mendelian inheritance. *J Neurochem*.

Herzig, M. C., Kolly, C., Persohn, E., Theil, D., Schweizer, T., Hafner, T., Stemmelen, C., Troxler, T. J., Schmid, P., Danner, S., Schnell, C. R., Mueller, M., Kinzel, B., Grevot, A., Bolognani, F., Stirn, M., Kuhn, R. R., Kaupmann, K., van der Putten, P. H., Rovelli, G., and Shimshek, D. R. (2011). Lrrk2 protein levels are determined by kinase function and are crucial for kidney and lung homeostasis in mice. *Hum Mol Genet*, 20(21):4209–4223.

Higashi, S., Moore, D. J., Colebrooke, R. E., Biskup, S., Dawson, V. L., Arai, H., Dawson, T. M., and Emson, P. C. (2007). Expression and localization of parkinson's disease-associated leucine-rich repeat kinase 2 in the mouse brain. *J Neurochem*, 100(2):368–381.

Hindle, J. V. (2010). Ageing, neurodegeneration and parkinson's disease. *Age Ageing*, 39(2):156–161.

Imai, Y., Gehrke, S., Wang, H.-Q., Takahashi, R., Hasegawa, K., Oota, E., and Lu, B. (2008). Phosphorylation of 4e-bp by lrrk2 affects the maintenance of dopaminergic neurons in drosophila. *EMBO J*, 27(18):2432–2443.

Ishikawa, K., Nara, A., Matsumoto, K., and Hanafusa, H. (2012). Egfr-dependent phosphorylation of leucine-rich repeat kinase lrrk1 is important for proper endosomal trafficking of egfr. *Mol Biol Cell*, 23(7):1294–1306.

Ishizawa, T., Mattila, P., Davies, P., Wang, D., and Dickson, D. W. (2003). Colocalization of tau and alpha-synuclein epitopes in lewy bodies. *J Neuropathol Exp Neurol*, 62(4):389–397.

Ito, G. and Iwatsubo, T. (2012). Re-examination of the dimerization state of leucine-rich repeat kinase 2: predominance of the monomeric form. *Biochem J*, 441(3):987–994.

Ito, G., Okai, T., Fujino, G., Takeda, K., Ichijo, H., Katada, T., and Iwatsubo, T. (2007). Gtp binding is essential to the protein kinase activity of lrrk2, a causative gene product for familial parkinson's disease. *Biochemistry*, 46(5):1380–1388.

Jahan, I., Hauser, R. A., Sullivan, K. L., Miller, A., and Zesiewicz, T. A. (2009). Sleep disorders in parkinson's disease. *Neuropsychiatr Dis Treat*, 5:535–540.

Jaleel, M., Nichols, R. J., Deak, M., Campbell, D. G., Gillardon, F., Knebel, A., and Alessi, D. R. (2007). Lrrk2 phosphorylates moesin at threonine-558: characterization of how parkinson's disease mutants affect kinase activity. *Biochem J*, 405(2):307–317.

Janda, L., Tich, P., Spzek, J., and Petrcek, M. (1996). A deduced thermomonospora curvata protein containing serine/threonine protein kinase and wd-repeat domains. *J Bacteriol*, 178(5):1487–1489.

Jang, H., Boltz, D., Sturm-Ramirez, K., Shepherd, K. R., Jiao, Y., Webster, R., and Smeyne, R. J. (2009). Highly pathogenic h5n1 influenza virus can enter the central nervous system and induce neuroinflammation and neurodegeneration. *Proc Natl Acad Sci U S A*, 106(33):14063–14068.

Jankovic, J. (2008). Parkinson's disease: clinical features and diagnosis. *J Neurol Neurosurg Psychiatr*, 79(4):368–376.

Kachergus, J., Mata, I. F., Hulihan, M., Taylor, J. P., Lincoln, S., Aasly, J., Gibson, J. M., Ross, O. A., Lynch, T., Wiley, J., Payami, H., Nutt, J., Maraganore, D. M., Czyzewski, K., Styczynska, M., Wszolek, Z. K., Farrer, M. J., and Toft, M. (2005). Identification of a novel lrrk2 mutation linked to autosomal dominant parkinsonism: evidence of a common founder across european populations. *Am J Hum Genet*, 76(4):672–680.

Kamikawaji, S., Ito, G., and Iwatsubo, T. (2009). Identification of the autophosphorylation sites of lrrk2. *Biochemistry*, 48(46):10963–10975.

Kanao, T., Venderova, K., Park, D. S., Unterman, T., Lu, B., and Imai, Y. (2010). Activation of foxo by lrrk2 induces expression of proapoptotic proteins and alters survival of postmitotic dopaminergic neuron in drosophila. *Hum Mol Genet*, 19(19):3747–3758.

Kedashiro, S., Pastuhov, S. I., Nishioka, T., Watanabe, T., Kaibuchi, K., Matsumoto, K., and Hanafusa, H. (2015). Lrrk1-phosphorylated clip-170 regulates egfr trafficking by recruiting p150glued to microtubule plus ends. *J Cell Sci*, 128(2):385–396.

Kern, D. S. and Kumar, R. (2007). Deep brain stimulation. *Neurologist*, 13(5):237–252.

Kitada, T., Asakawa, S., Hattori, N., Matsumine, H., Yamamura, Y., Minoshima, S., Yokochi, M., Mizuno, Y., and Shimizu, N. (1998). Mutations in the parkin gene cause autosomal recessive juvenile parkinsonism. *Nature*, 392(6676):605–608.

Klein, C. and Schlossmacher, M. G. (2006). The genetics of parkinson disease: Implications for neurological care. *Nat Clin Pract Neurol*, 2(3):136–146.

Klein, C. L., Rovelli, G., Springer, W., Schall, C., Gasser, T., and Kahle, P. J. (2009). Homo- and heterodimerization of roco kinases: Lrrk2 kinase inhibition by the lrrk2 roco fragment. *J Neurochem*, 111(3):703–715.

Kobe, B. and Kajava, A. V. (2001). The leucine-rich repeat as a protein recognition motif. *Curr Opin Struct Biol*, 11(6):725–732.

Koller, W. C. and Rueda, M. G. (1998). Mechanism of action of dopaminergic agents in parkinson's disease. *Neurology*, 50(6 Suppl 6):S11–4; discussion S44.

Korr, D., Toschi, L., Donner, P., Pohlenz, H.-D., Kreft, B., and Weiss, B. (2006). Lrrk1 protein kinase activity is stimulated upon binding of gtp to its roc domain. *Cell Signal*, 18(6):910–920.

Kowal, J., Chami, M., Baumgartner, P., Arheit, M., Chiu, P.-L., Rangl, M., Scheuring, S., Schrder, G. F., Nimigean, C. M., and Stahlberg, H. (2014). Ligand-induced structural changes in the cyclic nucleotide-modulated potassium channel mlok1. *Nat Commun*, 5:3106.

Krger, R., Kuhn, W., Mller, T., Woitalla, D., Graeber, M., Ksel, S., Przuntek, H., Epplen, J. T., Schls, L., and Riess, O. (1998). Ala30pro mutation in the gene encoding alpha-synuclein in parkinson's disease. *Nat Genet*, 18(2):106–108.

Lang, A. E. and Lozano, A. M. (1998). Parkinson's disease. first of two parts. *N Engl J Med*, 339(15):1044–1053.

Langston, J. W., Ballard, P., Tetrud, J. W., and Irwin, I. (1983). Chronic parkinsonism in humans due to a product of meperidine-analog synthesis. *Science*, 219(4587):979–980.

Lazzarini, A. M., Myers, R. H., Zimmerman, T. R., Mark, M. H., Golbe, L. I., Sage, J. I., Johnson, W. G., and Duvoisin, R. C. (1994). A clinical genetic study of parkinson's disease: evidence for dominant transmission. *Neurology*, 44(3 Pt 1):499–506.

Lee, B. D., Dawson, V. L., and Dawson, T. M. (2012). Leucine-rich repeat kinase 2 (lrrk2) as a potential therapeutic target in parkinson's disease. *Trends Pharmacol Sci*, 33(7):365–373.

Lee, B. D., Shin, J.-H., VanKampen, J., Petrucelli, L., West, A. B., Ko, H. S., Lee, Y.-I., Maguire-Zeiss, K. A., Bowers, W. J., Federoff, H. J., Dawson, V. L., and Dawson, T. M. (2010a). Inhibitors of leucine-rich repeat kinase-2 protect against models of parkinson's disease. *Nat Med*, 16(9):998–1000.

Lee, S., Liu, H.-P., Lin, W.-Y., Guo, H., and Lu, B. (2010b). Lrrk2 kinase regulates synaptic morphology through distinct substrates at the presynaptic and postsynaptic compartments of the drosophila neuromuscular junction. *J Neurosci*, 30(50):16959–16969.

Lee, S. B., Kim, W., Lee, S., and Chung, J. (2007). Loss of lrrk2/park8 induces degeneration of dopaminergic neurons in drosophila. *Biochem Biophys Res Commun*, 358(2):534–539.

Leentjens, A. F. G. (2004). Depression in parkinson's disease: conceptual issues and clinical challenges. *J Geriatr Psychiatry Neurol*, 17(3):120–126.

Lees, A. J., Hardy, J., and Revesz, T. (2009). Parkinson's disease. *Lancet*, 373(9680):2055–2066.

Leroy, E., Boyer, R., Auburger, G., Leube, B., Ulm, G., Mezey, E., Harta, G., Brownstein, M. J., Jonnalagada, S., Chernova, T., Dehejia, A., Lavedan, C., Gasser, T., Steinbach, P. J., Wilkinson, K. D., and Polymeropoulos, M. H. (1998). The ubiquitin pathway in parkinson's disease. *Nature*, 395(6701):451–452.

Lesage, S. and Brice, A. (2009). Parkinson's disease: from monogenic forms to genetic susceptibility factors. *Hum Mol Genet*, 18(R1):R48–R59.

Lesage, S., Drr, A., Tazir, M., Lohmann, E., Leutenegger, A.-L., Janin, S., Pollak, P., Brice, A., and Group, F. P. D. G. S. (2006). Lrrk2 g2019s as a cause of parkinson's disease in north african arabs. *N Engl J Med*, 354(4):422–423.

Levin, B. E. and Katzen, H. L. (2005). Early cognitive changes and nondementing behavioral abnormalities in parkinson's disease. *Adv Neurol*, 96:84–94.

Lewis, P. A. (2012). Assaying the kinase activity of lrrk2 in vitro. *J Vis Exp*, (59).

Lewis, P. A., Greggio, E., Beilina, A., Jain, S., Baker, A., and Cookson, M. R. (2007). The r1441c mutation of lrrk2 disrupts gtp hydrolysis. *Biochem Biophys Res Commun*, 357(3):668–671.

Li, X., Patel, J. C., Wang, J., Avshalumov, M. V., Nicholson, C., Buxbaum, J. D., Elder, G. A., Rice, M. E., and Yue, Z. (2010). Enhanced striatal dopamine transmission and motor performance with lrrk2 overexpression in mice is eliminated by familial parkinson's disease mutation g2019s. *J Neurosci*, 30(5):1788–1797.

Li, X., Tan, Y.-C., Poulose, S., Olanow, C. W., Huang, X.-Y., and Yue, Z. (2007). Leucine-rich repeat kinase 2 (lrrk2)/park8 possesses gtpase activity that is altered in familial parkinson's disease r1441c/g mutants. *J Neurochem*, 103(1):238–247.

Li, Y., Liu, W., Oo, T. F., Wang, L., Tang, Y., Jackson-Lewis, V., Zhou, C., Geghman, K., Bogdanov, M., Przedborski, S., Beal, M. F., Burke, R. E., and Li, C. (2009). Mutant lrrk2(r1441g) bac transgenic mice recapitulate cardinal features of parkinson's disease. *Nat Neurosci*, 12(7):826–828.

Lichtenberg, M., Mansilla, A., Zecchini, V. R., Fleming, A., and Rubinsztein, D. C. (2011). The parkinson's disease protein lrrk2 impairs proteasome substrate clearance without affecting proteasome catalytic activity. *Cell Death Dis*, 2:e196.

Lieberman, A. (2006). Depression in parkinson's disease – a review. *Acta Neurol Scand*, 113(1):1–8.

Lin, C.-H., Tsai, P.-I., Wu, R.-M., and Chien, C.-T. (2010). Lrrk2 g2019s mutation induces dendrite degeneration through mislocalization and phosphorylation of tau by recruiting autoactivated gsk3. *J Neurosci*, 30(39):13138–13149.

Lin, X., Parisiadou, L., Gu, X.-L., Wang, L., Shim, H., Sun, L., Xie, C., Long, C.-X., Yang, W.-J., Ding, J., Chen, Z. Z., Gallant, P. E., Tao-Cheng, J.-H., Rudow, G., Troncoso, J. C., Liu, Z., Li, Z., and Cai, H. (2009). Leucine-rich repeat kinase 2 regulates the progression of neuropathology induced by parkinson's-disease-related mutant alpha-synuclein. *Neuron*, 64(6):807–827.

Liu, Z., Galemmo, R. A., Fraser, K. B., Moehle, M. S., Sen, S., Volpicelli-Daley, L. A., DeLucas, L. J., Ross, L. J., Valiyaveettil, J., Moukha-Chafiq, O., Pathak, A. K., Ananthan, S., Kezar, H., White, E. L., Gupta, V., Maddry, J. A., Suto, M. J., and West, A. B. (2014). Unique functional and structural properties of the lrrk2 protein atp-binding pocket. *J Biol Chem*, 289(47):32937–32951.

Liu, Z., Hamamichi, S., Lee, B. D., Yang, D., Ray, A., Caldwell, G. A., Caldwell, K. A., Dawson, T. M., Smith, W. W., and Dawson, V. L. (2011a). Inhibitors of lrrk2 kinase attenuate neurodegeneration and parkinson-like phenotypes in caenorhabditis elegans and drosophila parkinson's disease models. *Hum Mol Genet*, 20(20):3933–3942.

Liu, Z., Lee, J., Krummey, S., Lu, W., Cai, H., and Lenardo, M. J. (2011b). The kinase lrrk2 is a regulator of the transcription factor nfat that modulates the severity of inflammatory bowel disease. *Nat Immunol*, 12(11):1063–1070.

Liu, Z., Wang, X., Yu, Y., Li, X., Wang, T., Jiang, H., Ren, Q., Jiao, Y., Sawa, A., Moran, T., Ross, C. A., Montell, C., and Smith, W. W. (2008). A drosophila model for lrrk2-linked parkinsonism. *Proc Natl Acad Sci U S A*, 105(7):2693–2698.

Lounnas, V., Ritschel, T., Kelder, J., McGuire, R., Bywater, R. P., and Foloppe, N. (2013). Current progress in structure-based rational drug design marks a new mindset in drug discovery. *Comput Struct Biotechnol J*, 5:e201302011.

Lowe, J., McDermott, H., Kenward, N., Landon, M., Mayer, R. J., Bruce, M., McBride, P., Somerville, R. A., and Hope, J. (1990). Ubiquitin conjugate immunoreactivity in the brains of scrapie infected mice. *J Pathol*, 162(1):61–66.

Lu, C.-S., Simons, E. J., Wu-Chou, Y.-H., Fonzo, A. D., Chang, H.-C., Chen, R.-S., Weng, Y.-H., Roh, C. F., Breedveld, G. J., Hattori, N., Gasser, T., Oostra, B. A., and Bonifati, V. (2005). The lrrk2 i2012t, g2019s, and i2020t mutations are rare in taiwanese patients with sporadic parkinson's disease. *Parkinsonism Relat Disord*, 11(8):521–522.

Luzn-Toro, B., Rubio de la Torre, E., Delgado, A., Prez-Tur, J., and Hilfiker, S. (2007). Mechanistic insight into the dominant mode of the parkinson's disease-associated g2019s lrrk2 mutation. *Hum Mol Genet*, 16(17):2031–2039.

Lcking, C. B., Drr, A., Bonifati, V., Vaughan, J., De Michele, G., Gasser, T., Harhangi, B. S., Meco, G., Denfle, P., Wood, N. W., Agid, Y., Brice, A., Group, F. P. D. G. S., and on Genetic Susceptibility in Parkinson's Disease, E. C. (2000). Association between early-onset parkinson's disease and mutations in the parkin gene. *N Engl J Med*, 342(21):1560–1567.

MacLeod, D., Dowman, J., Hammond, R., Leete, T., Inoue, K., and Abeliovich, A. (2006). The familial parkinsonism gene lrrk2 regulates neurite process morphology. *Neuron*, 52(4):587–593.

Manning, G., Whyte, D. B., Martinez, R., Hunter, T., and Sudarsanam, S. (2002). The protein kinase complement of the human genome. *Science*, 298(5600):1912–1934.

Marder, K., Tang, M. X., Mejia, H., Alfaro, B., Ct, L., Louis, E., Groves, J., and Mayeux, R. (1996). Risk of parkinson's disease among first-degree relatives: A community-based study. *Neurology*, 47(1):155–160.

Marsden, C. D. (1983). Neuromelanin and parkinson's disease. *J Neural Transm Suppl*, 19:121–141.

Marn, I. (2006). The parkinson disease gene lrrk2: evolutionary and structural insights. *Mol Biol Evol*, 23(12):2423–2433.

Marn, I., van Egmond, W. N., and van Haastert, P. J. M. (2008). The roco protein family: a functional perspective. *FASEB J*, 22(9):3103–3110.

Mata, I. F., Wedemeyer, W. J., Farrer, M. J., Taylor, J. P., and Gallo, K. A. (2006). Lrrk2 in parkinson's disease: protein domains and functional insights. *Trends Neurosci*, 29(5):286–293.

Matison, R., Mayeux, R., Rosen, J., and Fahn, S. (1982). "tip-of-the-tongue" phenomenon in parkinson disease. *Neurology*, 32(5):567–570.

Melrose, H., Lincoln, S., Tyndall, G., Dickson, D., and Farrer, M. (2006). Anatomical localization of leucine-rich repeat kinase 2 in mouse brain. *Neuroscience*, 139(3):791–794.

Melrose, H. L., Dchsel, J. C., Behrouz, B., Lincoln, S. J., Yue, M., Hinkle, K. M., Kent, C. B., Korvatska, E., Taylor, J. P., Witten, L., Liang, Y.-Q., Beevers, J. E., Boules, M., Dugger, B. N., Serna, V. A., Gaukhman, A., Yu, X., Castanedes-Casey, M., Braithwaite, A. T., Ogholikhan, S., Yu, N., Bass, D., Tyndall, G., Schellenberg, G. D., Dickson, D. W., Janus, C., and Farrer, M. J. (2010). Impaired dopaminergic neurotransmission and microtubule-associated protein tau alterations in human lrrk2 transgenic mice. *Neurobiol Dis*, 40(3):503–517.

Meylan, E. and Tschopp, J. (2005). The rip kinases: crucial integrators of cellular stress. *Trends Biochem Sci*, 30(3):151–159.

Mills, R. D., Mulhern, T. D., Cheng, H.-C., and Culvenor, J. G. (2012). Analysis of lrrk2 accessory repeat domains: prediction of repeat length, number and sites of parkinson's disease mutations. *Biochem Soc Trans*, 40(5):1086–1089.

Mills, R. D., Mulhern, T. D., Liu, F., Culvenor, J. G., and Cheng, H.-C. (2014). Prediction of the repeat domain structures and impact of parkinsonism-associated variations on structure and function of all functional domains of leucine-rich repeat kinase 2 (lrrk2). *Hum Mutat*, 35(4):395–412.

Mortiboys, H., Johansen, K. K., Aasly, J. O., and Bandmann, O. (2010). Mitochondrial impairment in patients with parkinson disease with the g2019s mutation in lrrk2. *Neurology*, 75(22):2017–2020.

Mosavi, L. K., Cammett, T. J., Desrosiers, D. C., and Peng, Z.-Y. (2004). The ankyrin repeat as molecular architecture for protein recognition. *Protein Sci*, 13(6):1435–1448.

Mueller, J. C., Fuchs, J., Hofer, A., Zimprich, A., Lichtner, P., Illig, T., Berg, D., Wllner, U., Meitinger, T., and Gasser, T. (2005). Multiple regions of alpha-synuclein are associated with parkinson's disease. *Ann Neurol*, 57(4):535–541.

Narendra, D., Tanaka, A., Suen, D.-F., and Youle, R. J. (2008). Parkin is recruited selectively to impaired mitochondria and promotes their autophagy. *J Cell Biol*, 183(5):795–803.

Neumann, M., Adler, S., Schlter, O., Kremmer, E., Benecke, R., and Kretzschmar, H. A. (2000). Alpha-synuclein accumulation in a case of neurodegeneration with brain iron accumulation type 1 (nbia-1, formerly hallervorden-spatz syndrome) with widespread cortical and brainstem-type lewy bodies. *Acta Neuropathol*, 100(5):568–574.

Ng, C.-H., Mok, S. Z. S., Koh, C., Ouyang, X., Fivaz, M. L., Tan, E.-K., Dawson, V. L., Dawson, T. M., Yu, F., and Lim, K.-L. (2009). Parkin protects against lrrk2 g2019s mutant-induced dopaminergic neurodegeneration in drosophila. *J Neurosci*, 29(36):11257–11262.

Nichols, R. J., Dzamko, N., Morrice, N. A., Campbell, D. G., Deak, M., Ordureau, A., Macartney, T., Tong, Y., Shen, J., Prescott, A. R., and Alessi, D. R. (2010). 14-3-3 binding to lrrk2 is disrupted by multiple parkinson's disease-associated mutations and regulates cytoplasmic localization. *Biochem J*, 430(3):393–404.

Niu, J., Yu, M., Wang, C., and Xu, Z. (2012). Leucine-rich repeat kinase 2 disturbs mitochondrial dynamics via dynamin-like protein. *J Neurochem*, 122(3):650–658.

Nogales, E. (2016). The development of cryo-em into a mainstream structural biology technique. *Nat Methods*, 13(1):24–27.

Nolen, B., Taylor, S., and Ghosh, G. (2004). Regulation of protein kinases; controlling activity through activation segment conformation. *Mol Cell*, 15(5):661–675.

Nuti, A., Ceravolo, R., Piccinni, A., Dell'Agnello, G., Bellini, G., Gambaccini, G., Rossi, C., Logi, C., Dell'Osso, L., and Bonuccelli, U. (2004). Psychiatric comorbidity in a population of parkinson's disease patients. *Eur J Neurol*, 11(5):315–320.

Olanow, C. W., Perl, D. P., DeMartino, G. N., and McNaught, K. S. P. (2004). Lewy-body formation is an aggresome-related process: a hypothesis. *Lancet Neurol*, 3(8):496–503.

Paisn-Ruz, C., Senz, A., Lpez de Munain, A., Mart, I., Martnez Gil, A., Mart-Mass, J. F., and Prez-Tur, J. (2005). Familial parkinson's disease: clinical and genetic analysis of four basque families. *Ann Neurol*, 57(3):365–372.

Paisn-Ruz, C., Jain, S., Evans, E. W., Gilks, W. P., Simn, J., van der Brug, M., Lpez de Munain, A., Aparicio, S., Gil, A. M., Khan, N., Johnson, J., Martinez, J. R., Nicholl, D., Carrera, I. M., Pena, A. S., de Silva, R., Lees, A., Mart-Mass, J. F., Prez-Tur, J., Wood, N. W., and Singleton, A. B. (2004). Cloning of the gene containing mutations that cause park8-linked parkinson's disease. *Neuron*, 44(4):595–600.

Pandey, A., Shin, K., Patterson, R. E., Liu, X.-Q., and Rainey, J. K. (2016). Current strategies for protein production and purification enabling membrane protein structural biology. *Biochem Cell Biol*, pages 1–21.

Pettersen, E. F., Goddard, T. D., Huang, C. C., Couch, G. S., Greenblatt, D. M., Meng, E. C., and Ferrin, T. E. (2004). Ucsf chimera–a visualization system for exploratory research and analysis. *J Comput Chem*, 25(13):1605–1612.

Piccini, P., Burn, D. J., Ceravolo, R., Maraganore, D., and Brooks, D. J. (1999). The role of inheritance in sporadic parkinson's disease: evidence from a longitudinal study of dopaminergic function in twins. *Ann Neurol*, 45(5):577–582.

Plaha, P., Ben-Shlomo, Y., Patel, N. K., and Gill, S. S. (2006). Stimulation of the caudal zona incerta is superior to stimulation of the subthalamic nucleus in improving contralateral parkinsonism. *Brain*, 129(Pt 7):1732–1747.

Plazzi, G., Corsini, R., Provini, F., Pierangeli, G., Martinelli, P., Montagna, P., Lugaresi, E., and Cortelli, P. (1997). Rem sleep behavior disorders in multiple system atrophy. *Neurology*, 48(4):1094–1097.

Pollak, P., Tison, F., Rascol, O., Deste, A., Pr, J. J., Senard, J. M., Durif, F., and Bourdeix, I. (2004). Clozapine in drug induced psychosis in parkinson's disease: a randomised, placebo controlled study with open follow up. *J Neurol Neurosurg Psychiatr*, 75(5):689–695.

Polymeropoulos, M. H., Lavedan, C., Leroy, E., Ide, S. E., Dehejia, A., Dutra, A., Pike, B., Root, H., Rubenstein, J., Boyer, R., Stenroos, E. S., Chandrasekharappa, S., Athanassiadou, A., Papapetropoulos, T., Johnson, W. G., Lazzarini, A. M., Duvoisin, R. C., Di Iorio, G., Golbe, L. I., and Nussbaum, R. L. (1997). Mutation in the alpha-synuclein gene identified in families with parkinson's disease. *Science*, 276(5321):2045–2047.

Price, K. S., Farley, I. J., and Hornykiewicz, O. (1978). Neurochemistry of parkinson's disease: relation between striatal and limbic dopamine. *Adv Biochem Psychopharmacol*, 19:293–300.

Punia, S., Behari, M., Govindappa, S. T., Swaminath, P. V., Jayaram, S., Goyal, V., Muthane, U. B., Juyal, R. C., and Thelma, B. K. (2006). Absence/rarity of commonly

reported lrrk2 mutations in indian parkinson's disease patients. *Neurosci Lett*, 409(2):83–88.

Radad, K., Gille, G., and Rausch, W.-D. (2005). Short review on dopamine agonists: insight into clinical and research studies relevant to parkinson's disease. *Pharmacol Rep*, 57(6):701–712.

Ramonet, D., Daher, J. P. L., Lin, B. M., Stafa, K., Kim, J., Banerjee, R., Westerlund, M., Pletnikova, O., Glauser, L., Yang, L., Liu, Y., Swing, D. A., Beal, M. F., Troncoso, J. C., McCaffery, J. M., Jenkins, N. A., Copeland, N. G., Galter, D., Thomas, B., Lee, M. K., Dawson, T. M., Dawson, V. L., and Moore, D. J. (2011). Dopaminergic neuronal loss, reduced neurite complexity and autophagic abnormalities in transgenic mice expressing g2019s mutant lrrk2. *PLoS ONE*, 6(4):e18568.

Reinhard, L., Mayerhofer, H., Geerlof, A., Mueller-Dieckmann, J., and Weiss, M. S. (2013). Optimization of protein buffer cocktails using thermofluor. *Acta Crystallogr Sect F Struct Biol Cryst Commun*, 69(Pt 2):209–214.

Ren, G., Xin, S., Li, S., Zhong, H., and Lin, S. (2011). Disruption of lrrk2 does not cause specific loss of dopaminergic neurons in zebrafish. *PLoS ONE*, 6(6):e20630.

Reyniers, L., Del Giudice, M. G., Civiero, L., Belluzzi, E., Lobbestael, E., Beilina, A., Arrigoni, G., Derua, R., Waelkens, E., Li, Y., Crosio, C., Iaccarino, C., Cookson, M. R., Baekelandt, V., Greggio, E., and Taymans, J.-M. (2014). Differential protein-protein interactions of lrrk1 and lrrk2 indicate roles in distinct cellular signaling pathways. *J Neurochem*, 131(2):239–250.

Rodriguez-Viciana, P., Warne, P. H., Khwaja, A., Marte, B. M., Pappin, D., Das, P., Waterfield, M. D., Ridley, A., and Downward, J. (1997). Role of phosphoinositide 3-oh kinase in cell transformation and control of the actin cytoskeleton by ras. *Cell*, 89(3):457–467.

Rudi, K., Ho, F. Y., Gilsbach, B. K., Pots, H., Wittinghofer, A., Kortholt, A., and Klare, J. P. (2015). Conformational heterogeneity of the roc domains in c. tepidum roc-cor and implications for human lrrk2 parkinson mutations. *Biosci Rep*, 35(5).

Saha, S., Guillily, M. D., Ferree, A., Lanceta, J., Chan, D., Ghosh, J., Hsu, C. H., Segal, L., Raghavan, K., Matsumoto, K., Hisamoto, N., Kuwahara, T., Iwatsubo, T., Moore, L., Goldstein, L., Cookson, M., and Wolozin, B. (2009). Lrrk2 modulates vulnerability to mitochondrial dysfunction in caenorhabditis elegans. *J Neurosci*, 29(29):9210–9218.

Sakaguchi-Nakashima, A., Meir, J. Y., Jin, Y., Matsumoto, K., and Hisamoto, N. (2007). Lrk-1, a c. elegans park8-related kinase, regulates axonal-dendritic polarity of sv proteins. *Curr Biol*, 17(7):592–598.

Samii, A., Nutt, J. G., and Ransom, B. R. (2004). Parkinson's disease. *Lancet*, 363(9423):1783–1793.

Satake, W., Nakabayashi, Y., Mizuta, I., Hirota, Y., Ito, C., Kubo, M., Kawaguchi, T., Tsunoda, T., Watanabe, M., Takeda, A., Tomiyama, H., Nakashima, K., Hasegawa, K., Obata, F., Yoshikawa, T., Kawakami, H., Sakoda, S., Yamamoto, M., Hattori, N., Murata, M., Nakamura, Y., and Toda, T. (2009). Genome-wide association study identifies common variants at four loci as genetic risk factors for parkinson's disease. *Nat Genet*, 41(12):1303–1307.

Schapansky, J., Nardozzi, J. D., Felizia, F., and LaVoie, M. J. (2014). Membrane recruitment of endogenous lrrk2 precedes its potent regulation of autophagy. *Hum Mol Genet*, 23(16):4201–4214.

Schenck, C. H., Bundlie, S. R., and Mahowald, M. W. (1996). Delayed emergence of a parkinsonian disorder in 38% of 29 older men initially diagnosed with idiopathic rapid eye movement sleep behaviour disorder. *Neurology*, 46(2):388–393.

Scherer, S., Arheit, M., Kowal, J., Zeng, X., and Stahlberg, H. (2014). Single particle 3d reconstruction for 2d crystal images of membrane proteins. *J Struct Biol*, 185(3):267–277.

Scheres, S. H. W. (2012). Relion: implementation of a bayesian approach to cryo-em structure determination. *J Struct Biol*, 180(3):519–530.

Schlossmacher, M. G., Frosch, M. P., Gai, W. P., Medina, M., Sharma, N., Forno, L., Ochiishi, T., Shimura, H., Sharon, R., Hattori, N., Langston, J. W., Mizuno, Y., Hyman, B. T., Selkoe, D. J., and Kosik, K. S. (2002). Parkin localizes to the lewy bodies of parkinson disease and dementia with lewy bodies. *Am J Pathol*, 160(5):1655–1667.

Schlossmacher, M. G. and Shimura, H. (2005). Parkinson's disease: assays for the ubiquitin ligase activity of neural parkin. *Methods Mol Biol*, 301:351–369.

Schulte, E. C., Ellwanger, D. C., Dihanich, S., Manzoni, C., Stangl, K., Schormair, B., Graf, E., Eck, S., Mollenhauer, B., Haubenberger, D., Pirker, W., Zimprich, A., Brcke, T., Lichtner, P., Peters, A., Gieger, C., Trenkwalder, C., Mewes, H.-W., Meitinger, T., Lewis, P. A., Klnemann, H. H., and Winkelmann, J. (2014). Rare variants in lrrk1 and parkinson's disease. *Neurogenetics*, 15(1):49–57.

Schur, F. K. M., Hagen, W. J. H., de Marco, A., and Briggs, J. A. G. (2013). Determination of protein structure at 8.5 resolution using cryo-electron tomography and sub-tomogram averaging. *J Struct Biol*, 184(3):394–400.

Semchuk, K. M., Love, E. J., and Lee, R. G. (1993). Parkinson's disease: a test of the multifactorial etiologic hypothesis. *Neurology*, 43(6):1173–1180.

Sen, S., Webber, P. J., and West, A. B. (2009). Dependence of leucine-rich repeat kinase 2 (lrrk2) kinase activity on dimerization. *J Biol Chem*, 284(52):36346–36356.

Shen, J. (2004). Protein kinases linked to the pathogenesis of parkinson's disease. *Neuron*, 44(4):575–577.

Sheng, D., Qu, D., Kwok, K. H. H., Ng, S. S., Lim, A. Y. M., Aw, S. S., Lee, C. W. H., Sung, W. K., Tan, E. K., Lufkin, T., Jesuthasan, S., Sinnakaruppan, M., and Liu, J. (2010). Deletion of the wd40 domain of lrrk2 in zebrafish causes parkinsonism-like loss of neurons and locomotive defect. *PLoS Genet*, 6(4):e1000914.

Shulman, L. M. (2007). Gender differences in parkinson's disease. *Gend Med*, 4(1):8–18.

Silvestri, L., Caputo, V., Bellacchio, E., Atorino, L., Dallapiccola, B., Valente, E. M., and Casari, G. (2005). Mitochondrial import and enzymatic activity of pink1 mutants associated to recessive parkinsonism. *Hum Mol Genet*, 14(22):3477–3492.

Simon, D. K., Lin, M. T., and Pascual-Leone, A. (2002). "nature versus nurture" and incompletely penetrant mutations. *J Neurol Neurosurg Psychiatr*, 72(6):686–689.

Smith, T. F., Gaitatzes, C., Saxena, K., and Neer, E. J. (1999). The wd repeat: a common architecture for diverse functions. *Trends Biochem Sci*, 24(5):181–185.

Smith, W. W., Pei, Z., Jiang, H., Dawson, V. L., Dawson, T. M., and Ross, C. A. (2006). Kinase activity of mutant lrrk2 mediates neuronal toxicity. *Nat Neurosci*, 9(10):1231–1233.

Smith, W. W., Pei, Z., Jiang, H., Moore, D. J., Liang, Y., West, A. B., Dawson, V. L., Dawson, T. M., and Ross, C. A. (2005). Leucine-rich repeat kinase 2 (lrrk2) interacts with parkin, and mutant lrrk2 induces neuronal degeneration. *Proc Natl Acad Sci U S A*, 102(51):18676–18681.

Solano, S. M., Miller, D. W., Augood, S. J., Young, A. B., and Penney, J. B. (2000). Expression of alpha-synuclein, parkin, and ubiquitin carboxy-terminal hydrolase l1 mrna in human brain: genes associated with familial parkinson's disease. *Ann Neurol*, 47(2):201–210.

Spillantini, M. G., Crowther, R. A., Jakes, R., Hasegawa, M., and Goedert, M. (1998). alpha-synuclein in filamentous inclusions of lewy bodies from parkinson's disease and dementia with lewy bodies. *Proc Natl Acad Sci U S A*, 95(11):6469–6473.

Stafa, K., Tsika, E., Moser, R., Musso, A., Glauser, L., Jones, A., Biskup, S., Xiong, Y., Bandopadhyay, R., Dawson, V. L., Dawson, T. M., and Moore, D. J. (2014). Functional interaction of parkinson's disease-associated lrrk2 with members of the dynamin gtpase superfamily. *Hum Mol Genet*, 23(8):2055–2077.

Stenmark, H. and Olkkonen, V. M. (2001). The rab gtpase family. *Genome Biol*, 2(5):REVIEWS3007.

Su, Y.-C. and Qi, X. (2013). Inhibition of excessive mitochondrial fission reduced aberrant autophagy and neuronal damage caused by lrrk2 g2019s mutation. *Hum Mol Genet*, 22(22):4545–4561.

Smann, J., Hegermann, J., von Gromoff, E., Eimer, S., Baumeister, R., and Schmidt, E. (2009). Caenorhabditits elegans lrk-1 and pink-1 act antagonistically in stress response and neurite outgrowth. *J Biol Chem*, 284(24):16482–16491.

Tain, L. S., Mortiboys, H., Tao, R. N., Ziviani, E., Bandmann, O., and Whitworth, A. J. (2009). Rapamycin activation of 4e-bp prevents parkinsonian dopaminergic neuron loss. *Nat Neurosci*, 12(9):1129–1135.

Takai, Y., Sasaki, T., and Matozaki, T. (2001). Small gtp-binding proteins. *Physiol Rev*, 81(1):153–208.

Talpade, D. J., Greene, J. G., Higgins, D. S., and Greenamyre, J. T. (2000). In vivo labeling of mitochondrial complex i (nadh:ubiquinone oxidoreductase) in rat brain using [(3)h]dihydrorotenone. *J Neurochem*, 75(6):2611–2621.

Tan, E. K., Shen, H., Tan, L. C. S., Farrer, M., Yew, K., Chua, E., Jamora, R. D., Puvan, K., Puong, K. Y., Zhao, Y., Pavanni, R., Wong, M. C., Yih, Y., Skipper, L., and Liu, J.-J. (2005). The g2019s lrrk2 mutation is uncommon in an asian cohort of parkinson's disease patients. *Neurosci Lett*, 384(3):327–329.

Tan, E.-K., Zhao, Y., Tan, L., Lim, H.-Q., Lee, J., Yuen, Y., Pavanni, R., Wong, M.-C., Fook-Chong, S., and Liu, J.-J. (2007). Analysis of lrrk2 gly2385arg genetic variant in non-chinese asians. *Mov Disord*, 22(12):1816–1818.

Tang, G., Peng, L., Baldwin, P. R., Mann, D. S., Jiang, W., Rees, I., and Ludtke, S. J. (2007). Eman2: an extensible image processing suite for electron microscopy. *J Struct Biol*, 157(1):38–46.

Taylor, J. P., Hulihan, M. M., Kachergus, J. M., Melrose, H. L., Lincoln, S. J., Hinkle, K. M., Stone, J. T., Ross, O. A., Hauser, R., Aasly, J., Gasser, T., Payami, H., Wszolek, Z. K., and Farrer, M. J. (2007). Leucine-rich repeat kinase 1: a paralog of lrrk2 and a candidate gene for parkinson's disease. *Neurogenetics*, 8(2):95–102.

Taylor, K. A. and Glaeser, R. M. (1974). Electron diffraction of frozen, hydrated protein crystals. *Science*, 186(4168):1036–1037.

Taymans, J.-M. (2012). The gtpase function of lrrk2. *Biochem Soc Trans*, 40(5):1063–1069.

Taymans, J.-M. and Cookson, M. R. (2010). Mechanisms in dominant parkinsonism: The toxic triangle of lrrk2, alpha-synuclein, and tau. *Bioessays*, 32(3):227–235.

Taymans, J.-M., Van den Haute, C., and Baekelandt, V. (2006). Distribution of pink1 and lrrk2 in rat and mouse brain. *J Neurochem*, 98(3):951–961.

Teismann, P. and Ferger, B. (2001). Inhibition of the cyclooxygenase isoenzymes cox-1 and cox-2 provide neuroprotection in the mptp-mouse model of parkinson's disease. *Synapse*, 39(2):167–174.

Terheyden, S., Ho, F. Y., Gilsbach, B. K., Wittinghofer, A., and Kortholt, A. (2015). Revisiting the roco g-protein cycle. *Biochem J*, 465(1):139–147.

Tewari, R., Bailes, E., Bunting, K. A., and Coates, J. C. (2010). Armadillo-repeat protein functions: questions for little creatures. *Trends Cell Biol*, 20(8):470–481.

Tomiyama, H., Li, Y., Funayama, M., Hasegawa, K., Yoshino, H., Kubo, S.-I., Sato, K., Hattori, T., Lu, C.-S., Inzelberg, R., Djaldetti, R., Melamed, E., Amouri, R., Gouider-Khouja, N., Hentati, F., Hatano, Y., Wang, M., Imamichi, Y., Mizoguchi, K., Miyajima, H., Obata, F., Toda, T., Farrer, M. J., Mizuno, Y., and Hattori, N. (2006). Clinicogenetic study of mutations in lrrk2 exon 41 in parkinson's disease patients from 18 countries. *Mov Disord*, 21(8):1102–1108.

Tong, Y., Pisani, A., Martella, G., Karouani, M., Yamaguchi, H., Pothos, E. N., and Shen, J. (2009). R1441c mutation in lrrk2 impairs dopaminergic neurotransmission in mice. *Proc Natl Acad Sci U S A*, 106(34):14622–14627.

Tong, Y., Yamaguchi, H., Giaime, E., Boyle, S., Kopan, R., Kelleher, R. J., and Shen, J. (2010). Loss of leucine-rich repeat kinase 2 causes impairment of protein degradation pathways, accumulation of alpha-synuclein, and apoptotic cell death in aged mice. *Proc Natl Acad Sci U S A*, 107(21):9879–9884.

Uhl, G. R., Javitch, J. A., and Snyder, S. H. (1985). Normal mptp binding in parkinsonian substantial nigra: evidence for extraneuronal toxin conversion in human brain. *Lancet*, 1(8435):956–957.

Unwin, N. (1995). Acetylcholine receptor channel imaged in the open state. *Nature*, 373(6509):37–43.

Valente, E. M., Abou-Sleiman, P. M., Caputo, V., Muqit, M. M. K., Harvey, K., Gispert, S., Ali, Z., Del Turco, D., Bentivoglio, A. R., Healy, D. G., Albanese, A., Nussbaum, R., Gonzlez-Maldonado, R., Deller, T., Salvi, S., Cortelli, P., Gilks, W. P., Latchman, D. S., Harvey, R. J., Dallapiccola, B., Auburger, G., and Wood, N. W. (2004). Hereditary early-onset parkinson's disease caused by mutations in pink1. *Science*, 304(5674):1158–1160.

Van Den Eeden, S. K., Tanner, C. M., Bernstein, A. L., Fross, R. D., Leimpeter, A., Bloch, D. A., and Nelson, L. M. (2003). Incidence of parkinson's disease: variation by age, gender, and race/ethnicity. *Am J Epidemiol*, 157(11):1015–1022.

Vancraenenbroeck, R., Lobbestael, E., Weeks, S. D., Strelkov, S. V., Baekelandt, V., Taymans, J.-M., and De Maeyer, M. (2012). Expression, purification and preliminary biochemical and structural characterization of the leucine rich repeat namesake domain of leucine rich repeat kinase 2. *Biochim Biophys Acta*, 1824(3):450–460.

Venderova, K., Kabbach, G., Abdel-Messih, E., Zhang, Y., Parks, R. J., Imai, Y., Gehrke, S., Ngsee, J., Lavoie, M. J., Slack, R. S., Rao, Y., Zhang, Z., Lu, B., Haque, M. E., and Park, D. S. (2009). Leucine-rich repeat kinase 2 interacts with parkin, dj-1 and pink-1 in a drosophila melanogaster model of parkinson's disease. *Hum Mol Genet*, 18(22):4390–4404.

Wang, C., Tan, J. M. M., Ho, M. W. L., Zaiden, N., Wong, S. H., Chew, C. L. C., Eng, P. W., Lim, T. M., Dawson, T. M., and Lim, K. L. (2005). Alterations in the solubility and intracellular localization of parkin by several familial parkinson's disease-linked point mutations. *J Neurochem*, 93(2):422–431.

Wang, L., Xie, C., Greggio, E., Parisiadou, L., Shim, H., Sun, L., Chandran, J., Lin, X., Lai, C., Yang, W.-J., Moore, D. J., Dawson, T. M., Dawson, V. L., Chiosis, G., Cookson, M. R., and Cai, H. (2008). The chaperone activity of heat shock protein 90 is critical for maintaining the stability of leucine-rich repeat kinase 2. *J Neurosci*, 28(13):3384–3391.

Wang, X., Winter, D., Ashrafi, G., Schlehe, J., Wong, Y. L., Selkoe, D., Rice, S., Steen, J., LaVoie, M. J., and Schwarz, T. L. (2011). Pink1 and parkin target miro for phosphorylation and degradation to arrest mitochondrial motility. *Cell*, 147(4):893–906.

Wang, X., Yan, M. H., Fujioka, H., Liu, J., Wilson-Delfosse, A., Chen, S. G., Perry, G., Casadesus, G., and Zhu, X. (2012). Lrrk2 regulates mitochondrial dynamics and function through direct interaction with dlp1. *Hum Mol Genet*, 21(9):1931–1944.

Webber, P. J., Smith, A. D., Sen, S., Renfrow, M. B., Mobley, J. A., and West, A. B. (2011). Autophosphorylation in the leucine-rich repeat kinase 2 (lrrk2) gtpase domain modifies kinase and gtp-binding activities. *J Mol Biol*, 412(1):94–110.

Weiss, W., Weiland, F., and Grg, A. (2009). Protein detection and quantitation technologies for gel-based proteome analysis. *Methods Mol Biol*, 564:59–82.

West, A. B., Moore, D. J., Biskup, S., Bugayenko, A., Smith, W. W., Ross, C. A., Dawson, V. L., and Dawson, T. M. (2005). Parkinson's disease-associated mutations in leucine-rich repeat kinase 2 augment kinase activity. *Proc Natl Acad Sci U S A*, 102(46):16842–16847.

West, A. B., Moore, D. J., Choi, C., Andrabi, S. A., Li, X., Dikeman, D., Biskup, S., Zhang, Z., Lim, K.-L., Dawson, V. L., and Dawson, T. M. (2007). Parkinson's disease-associated mutations in lrrk2 link enhanced gtp-binding and kinase activities to neuronal toxicity. *Hum Mol Genet*, 16(2):223–232.

Wilkinson, K. D., Lee, K. M., Deshpande, S., Duerksen-Hughes, P., Boss, J. M., and Pohl, J. (1989). The neuron-specific protein pgp 9.5 is a ubiquitin carboxyl-terminal hydrolase. *Science*, 246(4930):670–673.

Wirdefeldt, K., Gatz, M., Schalling, M., and Pedersen, N. L. (2004). No evidence for heritability of parkinson disease in swedish twins. *Neurology*, 63(2):305–311.

Wolozin, B., Saha, S., Guillily, M., Ferree, A., and Riley, M. (2008). Investigating convergent actions of genes linked to familial parkinson's disease. *Neurodegener Dis*, 5(3-4):182–185.

Yao, C., El Khoury, R., Wang, W., Byrd, T. A., Pehek, E. A., Thacker, C., Zhu, X., Smith, M. A., Wilson-Delfosse, A. L., and Chen, S. G. (2010). Lrrk2-mediated neurodegeneration and dysfunction of dopaminergic neurons in a caenorhabditis elegans model of parkinson's disease. *Neurobiol Dis*, 40(1):73–81.

Yuan, Y., Cao, P., Smith, M. A., Kramp, K., Huang, Y., Hisamoto, N., Matsumoto, K., Hatzoglou, M., Jin, H., and Feng, Z. (2011). Dysregulated lrrk2 signaling in response to endoplasmic reticulum stress leads to dopaminergic neuron degeneration in c. elegans. *PLoS ONE*, 6(8):e22354.

Zhang, H., Wu, W., Du, Y., Santos, S. J., Conrad, S. E., Watson, J. T., Grammatikakis, N., and Gallo, K. A. (2004). Hsp90/p50cdc37 is required for mixed-lineage kinase (mlk) 3 signaling. *J Biol Chem*, 279(19):19457–19463.

Zhu, X., Babar, A., Siedlak, S. L., Yang, Q., Ito, G., Iwatsubo, T., Smith, M. A., Perry, G., and Chen, S. G. (2006a). Lrrk2 in parkinson's disease and dementia with lewy bodies. *Mol Neurodegener*, 1:17.

Zhu, X., Siedlak, S. L., Smith, M. A., Perry, G., and Chen, S. G. (2006b). Lrrk2 protein is a component of lewy bodies. *Ann Neurol*, 60(5):617–8; author reply 618.

Zimprich, A., Biskup, S., Leitner, P., Lichtner, P., Farrer, M., Lincoln, S., Kachergus, J., Hulihan, M., Uitti, R. J., Calne, D. B., Stoessl, A. J., Pfeiffer, R. F., Patenge, N., Carbajal, I. C., Vieregge, P., Asmus, F., Mller-Myhsok, B., Dickson, D. W., Meitinger, T., Strom, T. M., Wszolek, Z. K., and Gasser, T. (2004). Mutations in lrrk2 cause autosomal-dominant parkinsonism with pleomorphic pathology. *Neuron*, 44(4):601–607.